# Doctoral thesis

# Orogenic type gold mineralization in the North Khentei gold belt, Central Northern Mongolia

## ( 北モンゴル中央部北ケンテイ金鉱床帯における造山帯型金鉱化作用)

## Chinbat Khishgee

Department of Geoscience

Faculty of Science and Engineering

Graduate School of Shimane University

Nishikawatsu-cho 1060,

Matsue 690, Japan

July 2015

# CONTENTS

4

# LIST OF TABLES

# LIST OF FIGURES

# ABSTRACT

The representative gold and copper deposits in the North Khentei gold belt of Mongolia were investigated to characterize their mineralization and genetic evolution, based on the ore occurrence, mineralogy, hydrothermal alteration, fluid inclusion and age dating studies.

The gold mineralization in representative Gatsuurt, Boroo and Ulaanbulag deposits occurs as two and three ore types: I) disseminated and stockwork ores in granitoid, volcanic and metasedimentary rocks; II) quartz vein ores, auriferous quartz vein ores and siliceous ores; and III) silicified zone ores only in the Gatsuurt deposit. The ore grades of each type are about 1 to 3, 5 to 10 and more than 10 g/t Au grades, respectively. The main sulfide minerals in the ores of gold deposits are pyrite and arsenopyrite, both of which are divisible into two different generations (pyrite-I and pyrite-II; arsenopyrite-I and arsenopyrite-II). Sphalerite, galena, chalcopyrite, and tetrahedrite are minor associated minerals, with trace amounts of bournonite, boulangerite, geerite, alloclasite, native gold, and electrum. The ore minerals in the three types of ores are variable in distribution, abundance and grain size. Four modes of gold occurrences are recognized in these three deposits: 1) invisible gold in pyrite and arsenopyrite in the disseminated and stockwork ores and the auriferous quartz vein ores; 2) microscopic native gold with 3 to 100 μm in diameter that occurs as a filling phase or interstitial phases in sulfides in the three ores types; 3) visible native gold, up to 1 cm in diameter, in the disseminated and stockwork ores of the Gatsuurt and Boroo deposits; and 4) electrum in the auriferous quartz vein ores of the Boroo deposit.

The Khadat copper deposit occurs as the vein type mineralization in the intrusive stocks or dikes and metasedimentary rocks. The main copper bearing ore mineral is chalcopyrite, and minor amounts of pyrite, arsenopyrite, pyrrhotite, sphalerite and galena

are recognized. However, assemblages of minor minerals are varied depending on depth of the deposit.

The disseminated and stockwork mineralization in the Gatsuurt, Boroo and Ulaanbulag deposits is composed of four distinct stages characterized by crystallization of (i) pyrite-I + arsenopyrite-I, (ii) pyrite-II + arsenopyrite-II, (iii) galena + tetrahedrite + sphalerite + chalcopyrite + jamesonite + bournonite + scheelite, and (iv) boulangerite + native gold for the Gatsuurt deposit; (i) pyrite-I + arsenopyrite-I, (ii) pyrite-II + arsenopyrite-II, (iii) sphalerite + galena + chalcopyrite + tetrahedrite + bournonite + boulangerite + alloclasite + native gold, and (iv) native gold for the Boroo deposit; and (i) pyrite-I + arsenopyrite-I, (ii) pyrite-II + arsenopyrite-II, (iii) chalcopyrite + sphalerite + galena, and (iv) native gold for the Ulaanbulag deposit. The quartz vein ores and auriferous quartz vein ores in the Gatsuurt and Boroo, and the siliceous ores of the Ulaanbulag deposit consists of four, five and four mineralization stages characterized by crystallization of (i) pyrite-I, (ii) pyrite-II + arsenopyrite + galena + Ag-rich tetrahedrite-tennantite + sphalerite + chalcopyrite + bournonite, (iii) geocronite + geerite + native gold, and (iv) native gold for the Gatsuurt deposit; (i) pyrite-I, (ii) pyrite-II + arsenopyrite, (iii) sphalerite + galena + chalcopyrite, (iv) Ag-rich tetrahedrite-tennantite + bournonite + geerite + native gold, and (v) electrum for the Boroo deposit; and (i) pyrite-I + arsenopyrite, (ii) pyrite-II + arsenopyrite, (iii) chalcopyrite + sphalerite + galena + bournonite + boulangerite, and (iv) native gold for the Ulaanbulag deposit. The silicified zone ores in the Gatsuurt deposit is characterized by two mineralization stages: (i) pyrite + arsenopyrite + tetrahedrite + chalcopyrite; and (ii) galena + sphalerite + native gold. Both ore types are associated with sericitic and siliceous alterations. The As-Au relations in pyrite-II and arsenopyrite in the

gold deposits suggest gold detected as invisible gold is mostly attributed to $Au^{+1}$ in those minerals.

In the copper deposit, five crystallization stages are recognized: (i) pyrite-I, (ii) pyrite-II + arsenopyrite-I, (iii) pyrite-III + arsenopyrite-II, (iv) pyrrhotite + sphalerite + galena + chalcopyrite, and (v) chalcopyrite.

In the Gatsuurt and Boroo deposits, both ore types contain coexisting $CO_2$-rich and aqueous fluid inclusions. The inclusions in quartz of the disseminated and stockwork ores homogenized at temperatures between 254–362ºC, whereas inclusions in the auriferous quartz vein ores of the Boroo homogenized at 237–305ºC. Fluid salinities in both ore types range from 3–6 wt% (NaCl equiv.).

The U-Pb age of zircons from the Boroo host granites of 472.5 ± 6.9 Ma is much older than previously defined alteration minerals ages (ca. 210 Ma). U-Pb age of zircons in host granodiorite of the Khadat deposit presents 274.2 ± 1.7 Ma.

By applying arsenopyrite geothermometer to arsenopyrite-II in the type-II ores of gold deposits and arsenopyrite in copper deposit, crystallization temperature and $\log f_{S_2}$ are estimated to be 300-365ºC and -7.5 to -10.1, and 400-495ºC and -5 to -6.8, respectively. The results indicate that these gold deposits were developed in two stages. The disseminated and stockwork ores were formed at early stage by hydrothermal metasomatic mineralization process, and the quartz vein ores, auriferous quartz vein ores, siliceous ores and silicified type ores are later stage products, mineralized from the hydrothermal fluids with decreasing fluid temperature.

According to the paragenetic sequences in the Gatsuurt, Boroo and Ulaanbulag deposits, gold mineralization can be formed from the same source of the hydrothermal activity in this region. Thus, the gold deposits can be classified as contiguous orogenic type

mineralization. The Khadat copper deposit could be expected to be one of the porphyry systems in this orogenic gold belt, in terms of geologic setting, mineral assemblages and high temperatures of ore mineral crystallization.

# Chapter I

## 1. INTRODUCTION

The North Khentei gold belt (NKGB) is situated in central northern Mongolia, which forms part of the Central Asian Orogenic Belt (CAOB). The CAOB has considerable economic potential. Central Asia contains major orogenic gold provinces that formed during multistage collisional tectonism during the late Proterozoic to late Mesozoic, due to interaction between the Asian continent and oceanic arcs (Goldfarb et al., 2013). One of these orogenic gold provinces is considered to have formed by granitoid activity in late Triassic to early Jurassic times (Sengör & Natal'in 1996). This activity was created during collision and the final closure of the 2500 km long Mongol-Okhotsk oceanic basin, which stretched from central Mongolia to the northeast, near the present-day Okhotsk sea (Khanchuk, 2006) (Fig. 1). The orogenic activity led to formation of the Mongol-Transbaikalia arc in North and Central Asia (Zorin, 1999). Gold deposition in the central Transbaikal region of Russia and adjacent parts of Mongolia, including the study area, is associated with the formation of orogenic type, epithermal and porphyry deposits (Goldfarb et al., 2013). The NKGB contains numerous lode gold deposits (Fig. 1). These deposits are recognized as being intrusion-related vein-type gold mineralization (Dejidmaa, 1996). In recent studies, the lode gold deposits in the study area have been classified as both mesothermal and orogenic types (Goldfarb et al., 2013).
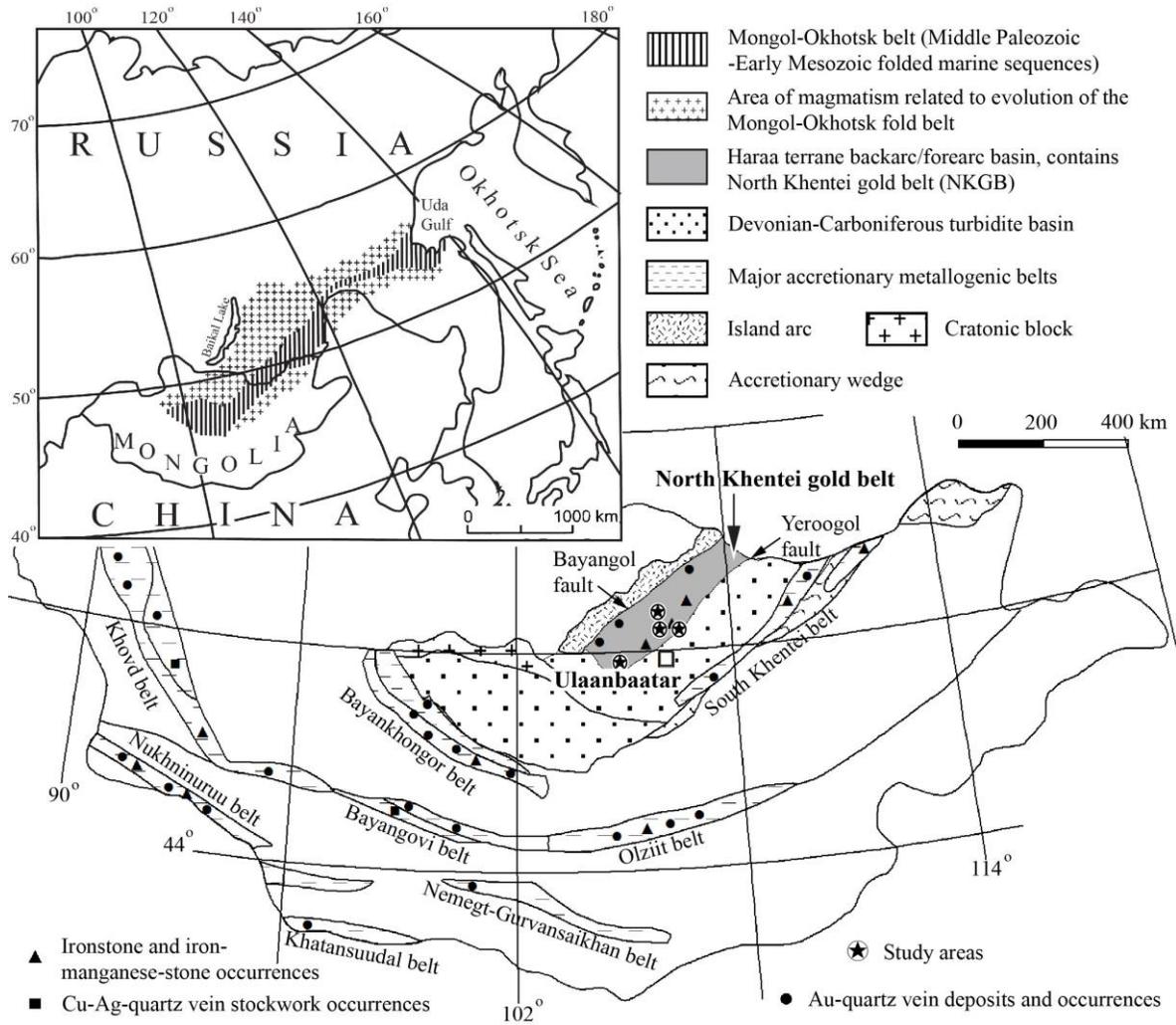
**Fig. 1** Simplified map showing the geotectonic setting of the North Khentei gold belt (NKGB) in central northern Mongolia, and location of the study area. Compiled from Dejidmaa and Badarch (1999), Zorin et al. (2001), and Badarch et al. (2002).

## 1.1 Exploration and mining history of the gold deposits in the North Khentei gold belt

The most gold occurrences in the NKGB were discovered in the beginning of the 20th century (1910) by Mongolor Company, which started industrial scale gold production on the Boroo, Tsagaan-Chuluut, Ereen and Sujigtei deposits, and other gold occurrences.

After that, probably until 1933, there were almost no geological or mining activities in the district. The exploration work for gold in the area was re-started in 1933 (Kolokol'nikov, 1933) and continued into 1941 (Alekseichik, 1943). Gold-bearing ore was probably mined from quartz veins in some gold deposits and occurrences in the district, but the mine had no data on reserves. Also, this belt has a long history of alluvial placer gold mining which includes well known gold reserves occurring in placer gold deposits. Extensive exploration in the gold belt was started in the late 70-s and continued in the 90-s.

The potential gold resources of both placer and lode gold deposits in the NKGB have been estimated to be as large as 250 tons (Gerel et al. 1999). However, a recent publication by Goldfarb et al. (2013), estimated placer gold resources alone at more than 600 tons. In the last few decades, most of the placer gold resources in the NKGB have been mined out, and gold exploration and mining activity have shifted to the lode gold deposits.

The reserves of gold deposits in the NKGB are as following: Boroo (> 54.1 Au tons), Gatsuurt (86 Au tons), Ulaanbulag (?), Bumbat (18 Au tons), Ereen (?), Baavgait (?), Narantolgoi (7.9 Au tons), and Sujigtei (2.9 Au tons), Kharganat (?) are the biggest bedrock gold deposits. The Zaamar (80 Au tons), Yeroo (701.6 Au kg), Kharaa (207 Au kg), Tolgoit (18.15 Au tons), Ikh Alt (2.99 Au tons), Sharingol district (total approximately 110 Au tones), Gatsuurt placer (3.77 Au tons) and Biluut (218 Au kg) placer gold deposits are in the district.

Gold potential and discovery of new deposit in the NKGB, which were investigated during last half of century, are still high (Kotlyar et al. 1999; Gerel et al. 1999). Gold placers are represented mainly by alluvial and diluvial types. Large placer districts are confined to erosion remains of Neogene depressions. Gold mineralization and prospects are located immediately to adjacent gold placers. Erosion of those deposits form two

16

distinct groups: 1) where placer reserves and grade decreases consistently and dramatically from the source of gold to lower part of the valley; and 2) where placer reserves and grade may increase in any part of the valley or repeatedly in the central and lower parts of the valley due to multiple sources of gold. The richer blocks in the placers, are coincident with gold-bearing bed rock or structures. Placer ore horizons appear not to be thicker than 1.0 meter, and are commonly confined to bedrock. In other words, the gold-bearing horizon is some cases include Au-bearing rocks.

Examination of bedrock gold occurrences along the NKGB suggests that occurrences of gold mineralization are associated with the bounding faults of the North Khentei tectonic belt, and its potential is determined by low-sulfide and moderate-sulfide mesothermal gold mineralization (Kotlyer et al., 1998). The two mineralized zones roughly parallel the northeast-southwest trend of the Bayangol and Yeroogol fault systems. One zone occurs within the southwestern part of the Bayangol fault where gold occurrences are hosted by granites of Boroo Complex and metasedimentary rocks of Kharaa formation. The second mineralization trends parallel to the Yeroogol fault system (Kotlyer et al., 1998). These deposits are located east of the deposits in the Boroo Complex granites. This zone is related to the Yeroogol fault system with gold occurrences consisting of vein, stockwork and silica altered host rocks. These deposits principally are located in Devonian volcanic and sedimentary rocks, and in some granite bodies. Deposits along this trend include the Sujigtei deposit, a newly discovered prospect in the central part of the North Khentei gold trend, and many smaller occurrences (Kotlyer et al., 1999).

These deposits and occurrences in the NKGB exhibit similar features, and can be classified as mesothermal quartz low-sulfide veins, veinlets or quartz stockwork in metasedimentary rocks and volcanic or granites. Rare examples of a moderate-sulfide

17

deposits occur in shear zones and are characterized by elevated contents of arsenic, base metal, and mercury. Low-sulfide Au-bearing quartz veins are well known in Mongolia, and were a major exploration target during the last thirty years, even though they usually have low potential in terms of profitable mining. The moderate-sulfide disseminated Au-sulfide mineralization (MSDM) was discovered during the last decades by Cascadia mining Inc. This mineralization is thought to have potential for economic scale bulk minable deposits. MSDM occurs in any type of rock, including metasedimentary rocks, acid intrusive and volcanic rocks. The last two are the most favorable environments. Prospects of MSDM are confined to regional deep-seated faults or second order faults, and shear zones (Kotlyer et al., 1999). Sericitic alteration (quartz+sericite+Fe carbonates) is a dominant alteration type. Propylitic alteration (chlorite or epidote, carbonate, and quartz) occurs in peripheral part of the mineralized systems. Potassic alteration (microcline) is recorded in the core and periphery of the prospect. Pyrite is a dominant sulfide of gold deposits in the region (Kotlyer et al., 1999).

A few deposits have pyrite and arsenopyrite, and galena, sphalerite, and chalcopyrite are common sulfides. Those sulfides accompany fine-grained native gold. Sulfides occur in clusters, stockwork, or as disseminated mineralization. Even though the MSDM prospects in the NKGB are classified as a mesothermal Au deposits, those are also characterized by some transitional or epithermal style features (Kotlyar et al. 1999). The latter include:

- Disseminated style of mineralization;

- Fine-grained gold (microns);

- Clay alteration;

- Comb and crustiform quartz and calcite textures, chalcedony like quartz;

- Occurrence of low-temperature minerals (stibnite); and anomalies of Hg and Sb.

18

These gold deposits and occurrences may be associated with a period of Triassic (Mesozoic) compression along the Yeroogol and Bayangol fault systems (Kotlyar et al. 1999).

## 1.2 Exploration and mining history of the copper deposit in the North Khentei gold belt

There is evidence that very old ancient mining was developed at the Khadat deposit area, especially within strong oxidized zones, and many ancient open pits were found. However, there is no detailed archeological studies have been done. Based on ancient stone imprint and tools, it can be believed in Bronze ages, which is about 3000 BC.

In the study area, between 1962 and 1963, geological mapping and detailed prospecting work with scale 1:50000 (within 120 km$^2$), and detailed geological mapping and local investigation works with scales 1:1000 and 1:2000 were carried out by Russian geological team. By this research work, they first found copper mineralization in the Khadat area by drilling (total meter of drill cores 3271.5 m) and trenching (total volume of trenches 9300 m$^3$).

From 1988 to 1989, the geological mapping with scale 1:50000 was done by Mongolian geological team. Their investigation generally were focused on gold exploration.
During the geological mapping with scale 1:50 000, thirty diamond drill holes (3271.5 m) were drilled, and eight drill holes were collared on the mineralized zone. Based on above drilling data, previous researchers were estimated ore resources around 630 000 tons with 0.4 % of Cu. However, the core samples from drilled holes were very low percentage (50-60 %) of total amount of samples (Data source from UNFM Company, unpublished report). By the recent exploration work in the Khadat deposit, UNFM Company found copper

mineralization in the deeper parts of the deposit, and they are re-estimated the copper reserve. However, there is no any published data and no any research works in this deposit.

## 1.3   Purpose of the doctoral study

To date, previous investigations have focused on the general geology and gold exploration works, and no detailed studies of the mineralogy of these deposits and their genesis have been made. Consequently, the ore forming processes and characteristics of the gold mineralization are poorly understood, the ore type of the gold deposits remains controversial, and the genetic processes involved are not well known. My study is aimed at characterizing the gold mineralization and genetic conditions, to reconstruct the evolution of the mineralization in this belt, and to provide a model for the gold genesis and primary mineralization. The significance of the research is to improve our understanding of the gold mineralization, its genesis, and the general features of gold systems in this paleo-collision zone. A refined genetic model can also contribute to exploration programs, and may lead to new approaches that can be used to discover new gold deposits in this belt. In order to achieve the goals of this research, I have selected four main primary gold and copper deposits that have already been identified in this belt, namely the Gatsuurt (Au), Boroo (Au), Ulaanbulag (Au) and Khadat (Cu) deposits. These deposits occur along a single trend, and represent similar mineralization, with low-grade bulk tonnage disseminated and quartz vein types occurring in differing host rocks. Therefore, studies of these deposits can contribute to better understanding of the gold mineralization and genetic evolution in the orogenic gold belt.

The objectives of my study are to characterize the gold mineralization processes and crystallization sequences of ore-forming minerals in representative deposits of the North

Khentei orogenic gold belt of Mongolia, in an effort to construct a genetic evolution model for the gold mineralization. This study is based on mineral assemblages, petrographic textural analysis, mineral compositions, hydrothermal alteration assemblages, fluid inclusion studies and age dating analysis.

# Chapter II

## 2. REGIONAL GEOLOGY OF THE NORTH KHENTEI GOLD BELT

Northern and eastern Mongolia is comprised of numerous terrains accreted onto the south-eastern edge of the Siberian Craton during the several Paleozoic orogenic pulses (Sengör and Natal'in 1996; Badarch et al. 2002). One of which is Haraa (Backarc/forearc basin) terrain, and it is located in the central northern part of Mongolia (Fig. 1). The north-east striking (~N45$^0$ E) Haraa terrain comprises the NKGB, and its bounded on the north by the Bayangol fault and on the south by the Yeroogol fault. These major faults continue for 100s km into Russia and may have 10s km of cumulative left-lateral (sinistral) displacement, and are generally considered major terrain bounding structures (Cluer et al. 2005).

The Haraa terrain is composed of four major litho-tectonic components (Tumur et al., 1995; Kotlyar et al., 1999; Cluer et al., 2005; Hendry et al., 2006) (Fig. 2):

1) Late Precambrian to Early Paleozoic flysch and subsequent plutonism. Miogeosynclinal flysch includes the Precambrian Yeroo Formation green schist grade metamorphic rocks adjacent to the north-west to the Yeroogol fault and the Lower Paleozoic Kharaa formation sandstone, shale, siltstone, conglomerate, phyllite, quartz-sericite and sericite-chlorite schist, and some intermediate tuffs. Early Paleozoic Boroogol Complex (520 Ma to 450 Ma; Kampe and Gottesmann 1966) biotite and biotite-hornblende granodiorite and granite have intruded into metasedimentary rocks of the Yeroo and Kharaa Formation.

2) Early Devonian (295±20 K-Ar age on whole-rock, Rb-Sr age of biotite 305±30 Ma; Kampe and Gottesmann, 1966) or Early Permian (K-Ar age on whole-rock 288.4±14 Ma; Baasandolgor et al., 2003) Zuunmod volcanic, granitic and sedimentary rocks lie unconformably on the Yeroo and Kharaa Formation and intrusive of the Boroogol Complex. They are spatially confined to the Yeroogol fault. Volcanic rocks consist of subvolcanic rhyolite porphyry, tuffaceous andesite lava and breccia. Granitic rocks consist of fine-grained granite and granodiorites. Sedimentary rocks consist of shale, sandstone, and conglomerate.

3) Late Triassic to early Jurassic Khazaar granite complex (Tumur et al., 1995).

4) Upper Mesozoic to Cretaceous terrigenous clastic facies sedimentary rocks (coal bearing) and Tertiary sedimentary rocks and conglomerates.
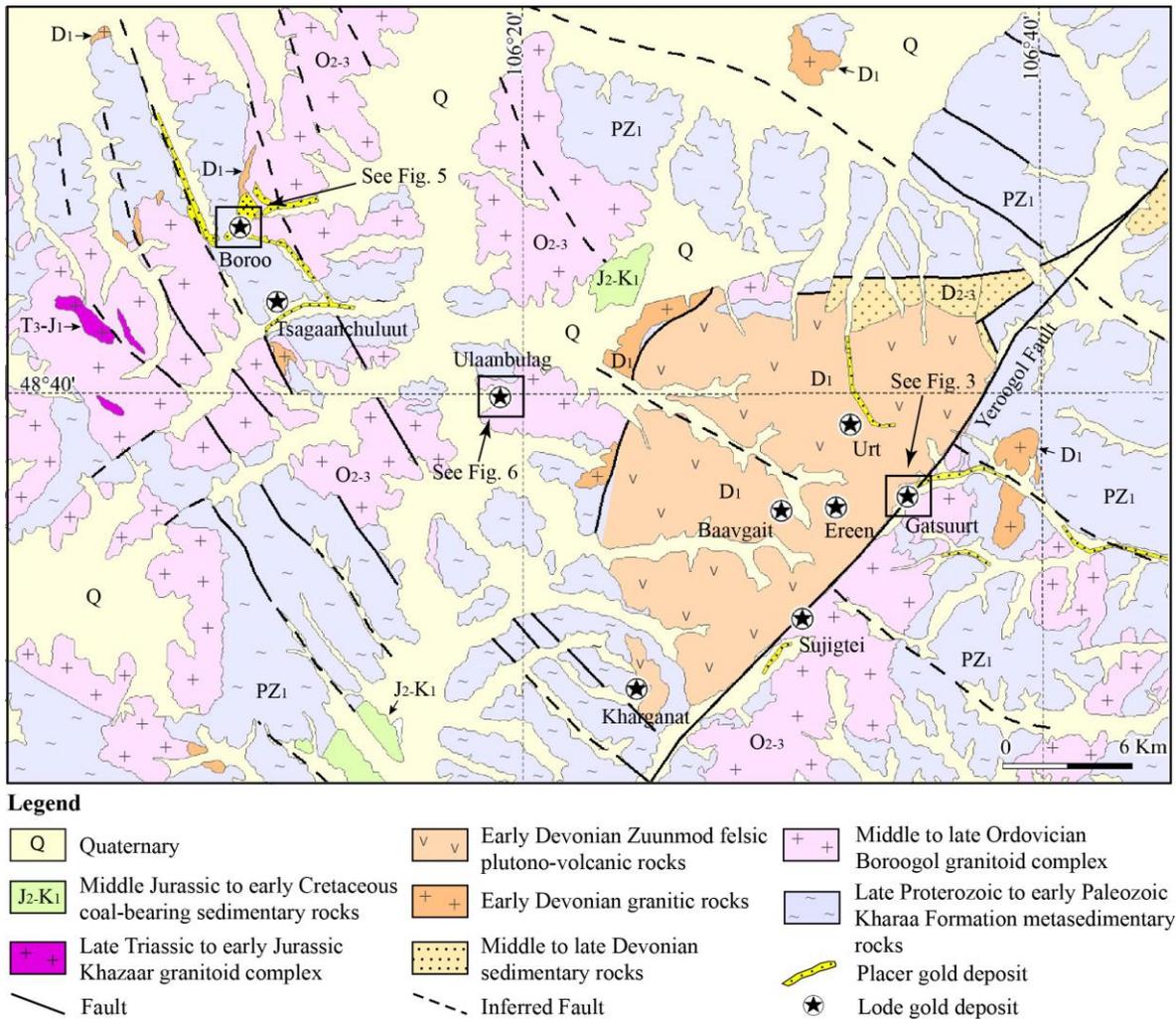
**Fig. 2** Regional geological map showing the geotectonic setting of the North Khentei gold belt (NKGB) in central northern Mongolia, and distribution of the lode and placer gold deposits. Modified after Tumur et al. (1995).

Kotlyar et al. (1998, 1999) summarized which general tectonic history of the Haraa terrain. As follows:

1) Development of a subduction zone along the Bayangol fault resulting in Late Precambrian through Early Paleozoic accretionary terrain and subsequent plutonism south and east of the Bayangol subduction zone.

2) Extension along the Yeroogol fault led to formation of the Yeroogol graben, which filled with Early Devonian or Early Permian volcanic rocks, breccia, tuff, agglomerates and conglomerates.

3) Compression and the emplacement of the late Triassic through early Jurassic Khazaar granite complex, where it intrudes metamorphosed Yeroo Formation and Lower Paleozoic and Silurian through Devonian sediments.

4) Intra continental extension led to formation of coal basins during Jurassic through Cretaceous time. Basalt dikes and flows are concentrated along the south to western end of the Yeroogol fault. Conglomerates are common along the north to eastern extension of the fault.

In this region, well developed structures that are north to west oriented (~$N30^0 W$) faults and fracture zones, intersect the Yeroogol fault and these intersections are considered favorable for gold mineralization (Cluer et al., 2005). The Gatsuurt, Boroo and Ulaanbulag deposits are situated in the part of tectonic setting along the Yeroogol fault.

# Chapter III

# 3. LOCAL GEOLOGY

## 3.1 Geology of the Gatsuurt deposit

The Gatsuurt deposit is underlain by early Permian Zuunmod volcanic rocks and the early Paleozoic Boroogol granitoid complex. These basement rocks are in fault contact with late Proterozoic to early Paleozoic Kharaa Formation metasedimentary rocks (Hendry et al., 2006). The Gatsuurt ore body is geographically divided into the Central and Main zones adjacent to the sub-vertical Sujigtei fault (Hendry et al., 2006) (Figs. 3, 4). The Central zone lies on the southeast hanging wall side of the Sujigtei fault, whereas the Main zone is on the northwest side of the fault, approximately 750 m southwest of the Central zone. The two zones initially formed as a single deposit, and were subsequently displaced by post-mineralization sinistral movement along the Sujigtei fault (Hendry et al., 2006).

The Central zone is hosted mostly within granites of the Boroogol complex, and lesser Kharaa Formation metasedimentary rocks, diorites and rhyolites. The Main zone is almost entirely hosted by Zuunmod volcanic rocks (porphyritic rhyolites and widespread microbrecciated rocks). The major fault strongly affected to granite in the Central zone, whereas rhyolite in the Main zone was less fractured, which is confirmed by the distribution and a large volume of quartz veins in granite in the Central zone and less volume of quartz veins and veinlets occurring in rhyolite in the Main zone (Hendry et al., 2006).

The Central zone mineralization has been traced over a strike length of 900 m and horizontal width of 100 m, and to a maximum depth of 360 m. The main mineralization

26

in the Central zone is characterized by disseminated and stockwork mineralization in granite, and Au grades exceed 1 g/t. Quartz veins are medium to coarse-grained, and range from a few cm to 2 m in thickness. They are locally superimposed on disseminated and stockwork mineralization. Sulfides in the quartz veins are low in volume, and occur randomly with variable amounts of coarse-grained native gold. Quartz vein type ores average 3 g/t, but grades are variable and increase dramatically when visible gold occurs. The silicified zone occurs only along the Sujigtei fault, and has the same strike and dip. The zone is linear, and can be traced for more than 800 m. Branches of the silicified zone intrude into fractures in granite which contain both disseminated and stockwork mineralization. The ores in this zone consist of very fine grained (<50 μm) quartz and dispersed sulfides. The ore zone is 3 to 7 m thick, shows massive texture, and is black or dark in appearance. Visible gold is rare in the silicified zone, but the Au grade is very high, averaging 5 g/t, and occasionally reaching 600 g/t. The metasedimentary rocks, diorites and rhyolites are barren.

The Main zone mineralization is traceable over a strike length of 600 m, with width of more than 70 m and vertical depth of 250 m (Hendry et al., 2006). The disseminated and stockwork mineralization in porphyritic rhyolite is rich in Au, with average grades of 2 to 2.5 g/t. The quartz veins in the Main zone are much less prevalent than the Central zone. Volumes of 0.1 to 2 cm thick quartz veinlets seldom exceed 5% in the Main zone (Hendry et al., 2006). Coarse-grained sulfides and native gold usually occur in quartz veins with centimeter scale width. Higher Au grade silicified zone mineralization also occurs along the fault.

The occurrences of ores in Central and Main zones are similar. As clarified by Hendry et al. (2006), ores of the Gatsuurt deposit are classified into three types: 1) low-

grade disseminated and stockwork ores; 2) moderate-grade quartz vein ores; 3) high-grade silicified ores. Their Au contents average about 1, 3 and 5 g/t, respectively. The Au-rich quartz vein and silicified zone are surrounded by or included in the disseminated and stockwork Au-mineralization region (Fig. 3). According to argon dating of alteration minerals formed by wall rock alteration, the ore mineralization occurred in early Mesozoic age (Gatsuurt deposit, ca. 178 Ma; Cluer et al., 2005).

**Fig. 3** Geological map of the Gatsuurt deposit, and localities of drill holes (modified from Hendry et al., 2006).
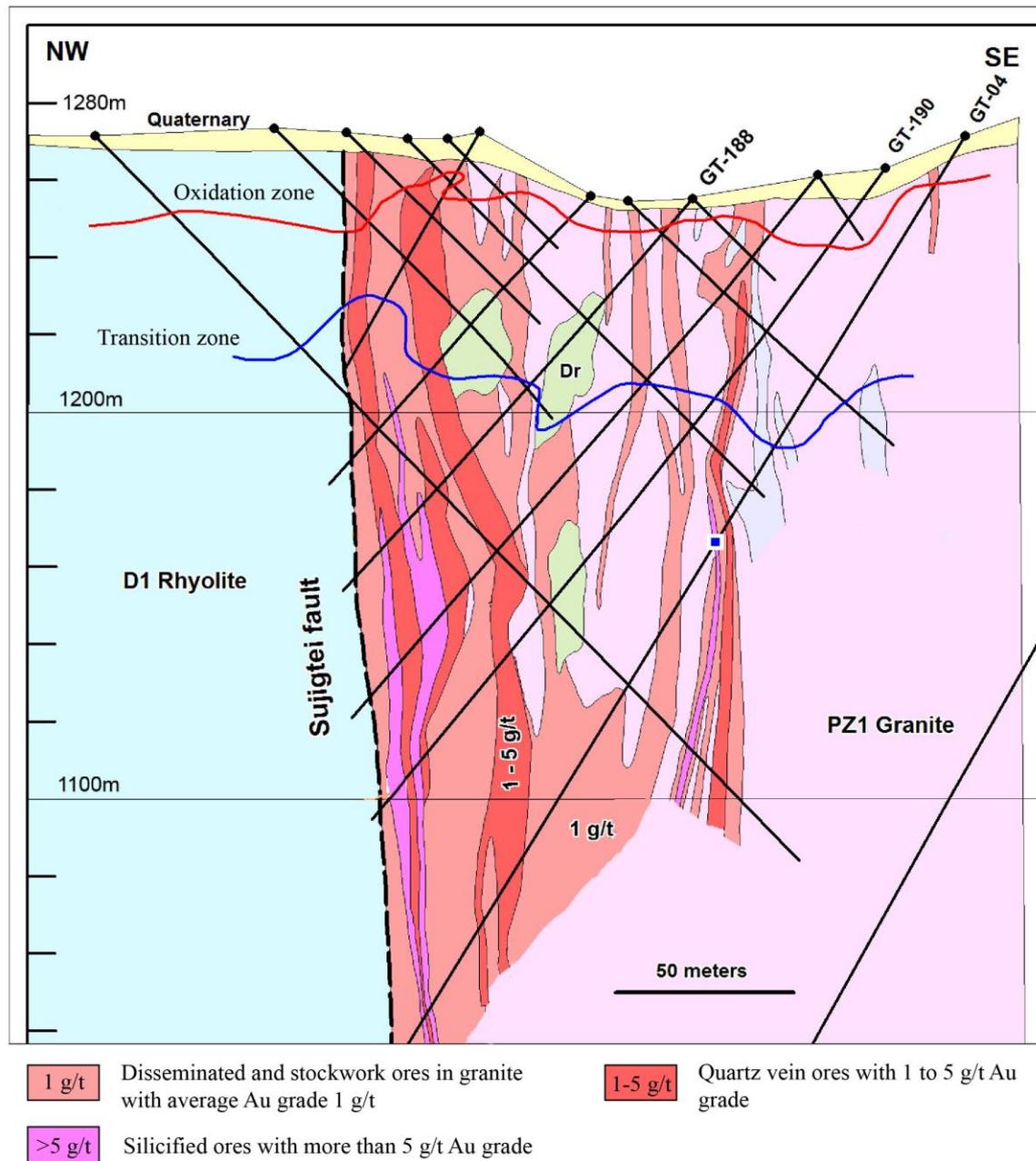
**Fig. 4** Geological cross section of Central Zone in the Gatsuurt deposit, and relationship of the disseminated and stockwork ores, quartz vein ores and silicified ores (Data source from Centerra Gold Mongolia Company).

## 3.2 Geology of the Boroo deposit

The Boroo deposit is situated along the NE-trending thrust fault structure with dips of 10 ˚NW. This structure is a branch of the Yeroogol fault (Kotlyar et al., 1999; Cluer et al., 2005), and is embedded in the metasedimentary rocks of the Kharaa Formation (Gerel et al., 1999) and granitoids of the Boroogol intrusive complex (Tumur et al., 1995). Those wall rocks are intruded by numerous late Paleozoic diorite dikes and granites (Cluer et al., 2005) (Figs. 2, 5).

Four main ore zones (named as Zones 2, 3, 5 and 6; Cluer et al., 2005) have been recognized in the Boroo deposit (Fig. 5). Those are elongated along the thrust fault structure (Fig. 5). Individual ore zones extend 1 km in length (Cluer et al., 2005), and the entire length of Au-rich ore zones carrying >0.8 g/t Au is around 2.5 km, with width of at least 400 m, and thickness reaching as much as 100 m locally. These ore zones contain Au-rich sub-zones exceeding 1 g/t Au on average. The thickness of these sub-zones varies from 20 to 30 m in Zones 2 and 3, and from 5 to 10 m in Zones 5 and 6 (Cluer et al., 2005).

Zones 2 and 3 occur in granites of the Boroogol intrusive complex and among lesser metasedimentary rock xenoliths present in the granite near the contact between the granite and the metasedimentary rocks (cross section A-A' in Fig. 5).

Zones 5 and 6 are hosted in highly deformed slates, siltstones and fine-grained sandstones of the Kharaa Formation. These lithotypes have been subjected to low-grade contact metamorphism that is characterized by the albite-epidote-hornfels facies (Cluer et al., 2005). Numerous diorite dikes several meters in thickness occur along the northwest trending vertical faults in Zones 5 and 6 (cross section B-B' in Fig. 5).

Gold mineralization consisting of disseminated and stockwork ores and auriferous quartz vein ores occurs in Zones 2, 3, 5 and 6. The disseminated and stockwork ores hosted in granite and metasedimentary rocks yielded the largest proportion of gold mineralization in the deposit, whereas in those in diorite dikes were lesser. All ore mineralization in the deposit has been subjected to intense quartz + sericite ± carbonate alteration. The disseminated and stockwork ores occurring in granite commonly contain fine-grained (micron scale) native gold, whereas the ores in the metasedimentary rocks and diorite dikes do not. The Au grades in the disseminated and stockwork ores hosted in the granite, metasedimentary rocks and diorite dikes range between 1 and 5 g/t.

The auriferous quartz vein ores are localized along the thrust fault structure which cut across the disseminated and stockwork ores. Thicknesses of the auriferous quartz veins reach 3 m, and their length is the same as the ore Zones. The auriferous quartz vein ores carry coarse-grained native gold (up to 1 cm), and minor amounts of sulfides. The Au grade is about 10 g/t, and rarely reaches 230 g/t.

In the Boroo deposit, $^{40}$Ar-$^{39}$Ar dating of hydrothermal minerals formed by wall rock alteration indicates that the ore mineralization occurred in early Mesozoic times (ca. 210-185 Ma, after Cluer et al., 2005).
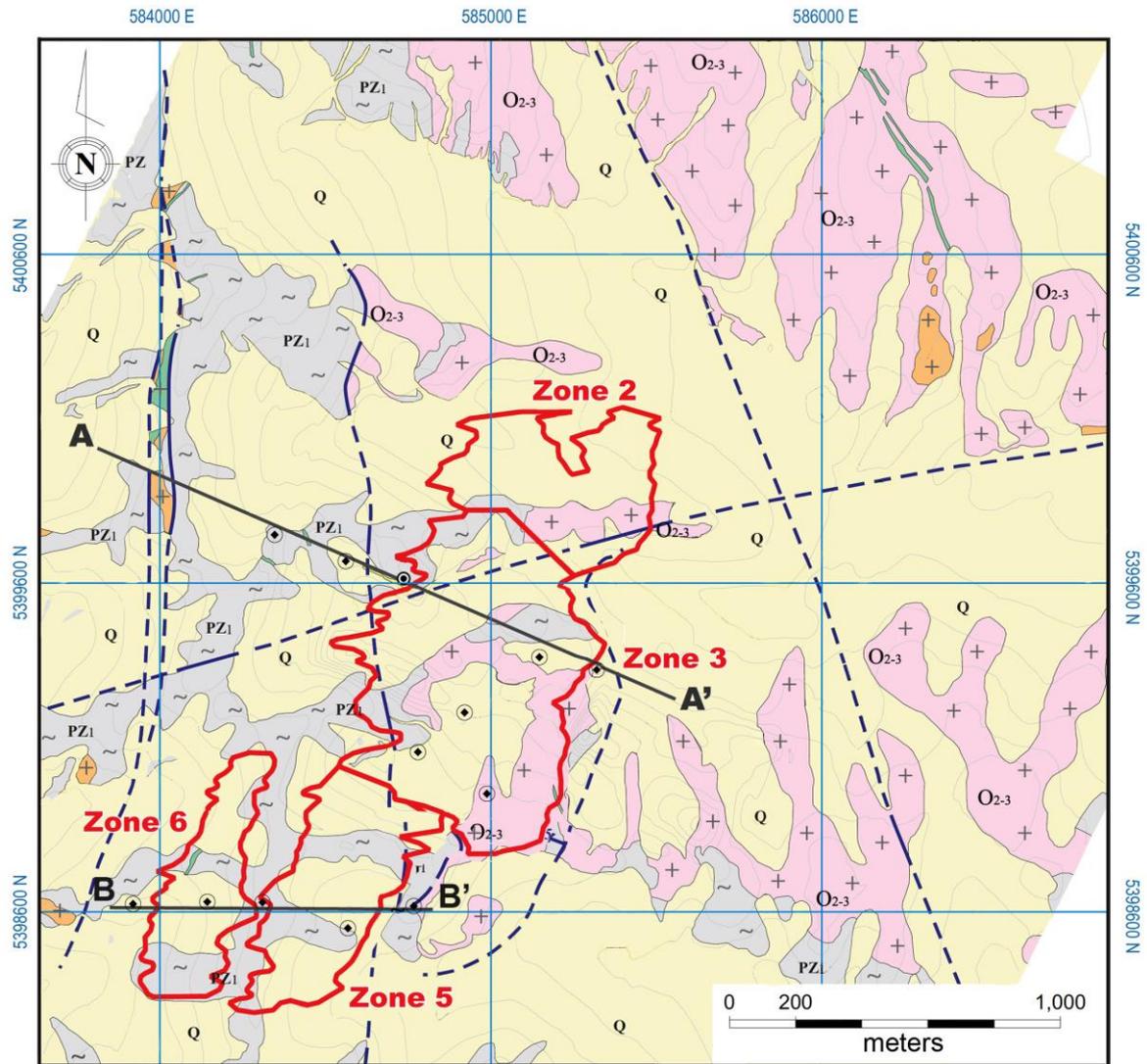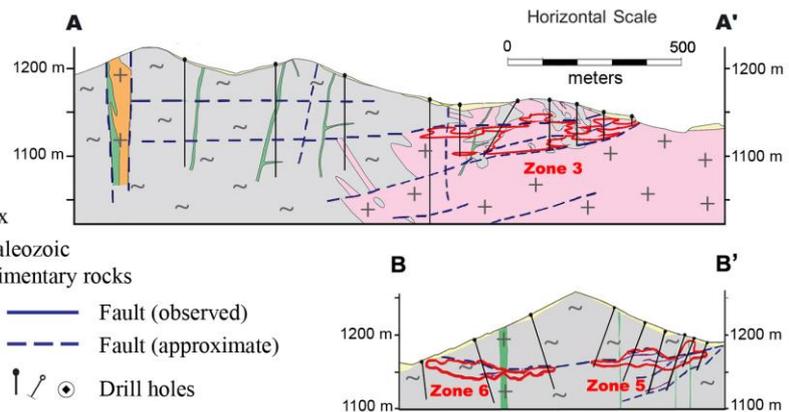
**Fig. 5** Geological map of the Boroo deposit, and its cross sections along A-A' and B-B' with localities of drill holes (modified from Raponi and Radmond, 2009).

## 3.3 Geology of the Ulaanbulag deposit

The Ulaanbulag deposit is hosted by granite and granodiorite of the Boroogol intrusive complex (Tumur et al., 1995) and overlying metasedimentary rocks of the Kharaa Formation (Gerel et al., 1999), and these rocks are commonly separated by flat lying thrust fault.

The ore body of the deposit is localized along the thrust fault structure as sub-horizontally near the surface (Fig. 6). The gold mineralization occurs in the surface more the 500 m in length and 100s m width, and its extend to the depth up to 250 m. The average Au grades ranging from 1 to 3 g/t Au.

Gold mineralization mainly occur as the disseminated and stockwork ores in granodiorite, and lesser as the siliceous ores in quartz veins or silicified zones. Both type ores do not show visible native gold.
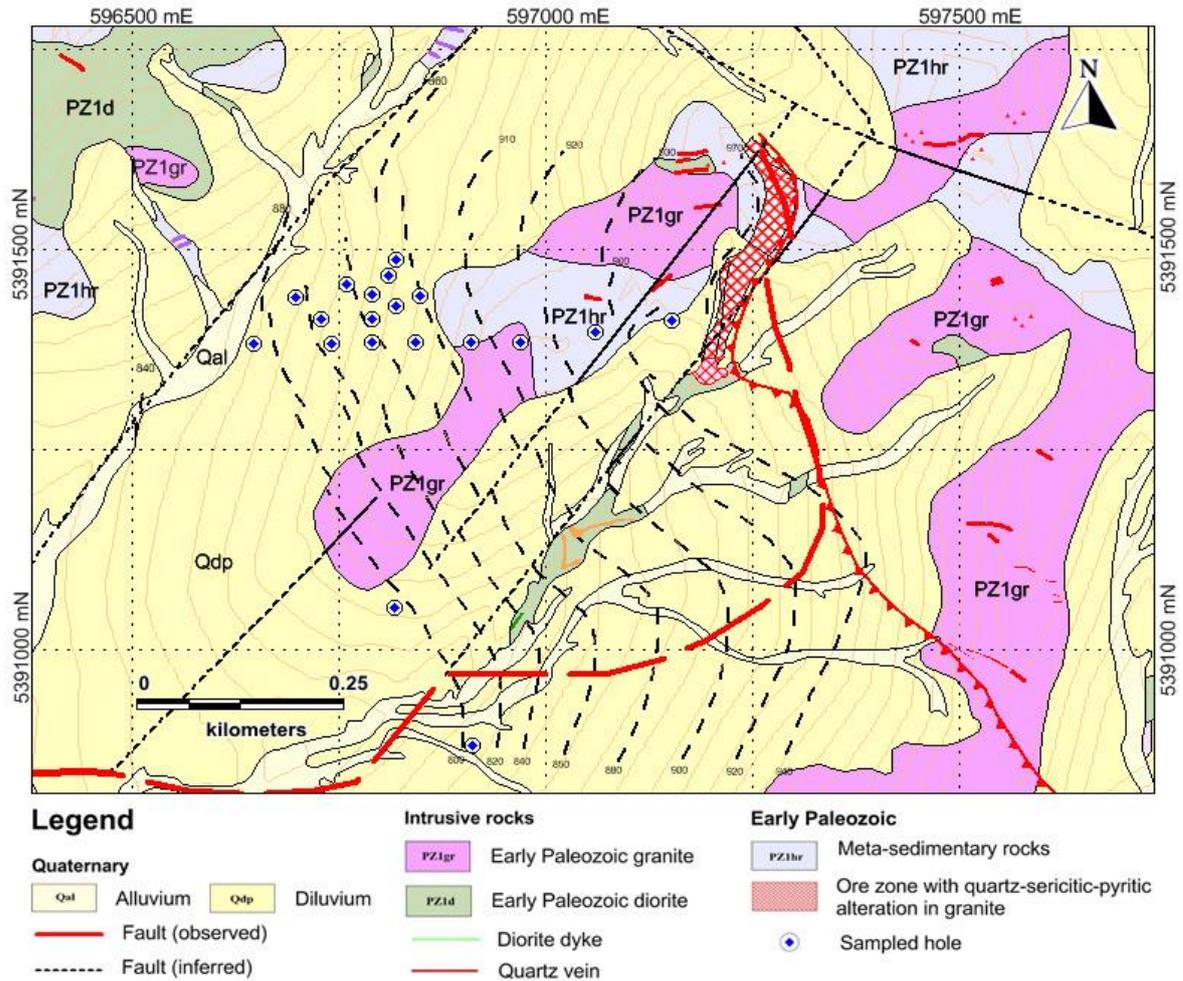
**Fig. 6** Geological map of the Ulaanbulag deposit, and localities of drill holes (Data source from Centerra Gold Company).

## 3.4 Geology of the Khadat deposit

The Khadat copper deposit is situated in the Bayantsogt Soum of Tuv province, Central northern Mongolia. The Khadat deposit area belongs to the Kharaa forearc or backarc basin terrane (Badarch et al., 2002), and the area lies on the south extension of the North Mongolian Copper-Molybdenite and Orogenic gold belt.

The deposit consists of Central, West and Between Zones which are hosted in Cambrian to Ordovician sedimentary rocks and Devonian intrusive stocks and dikes (Fig.

35

7). These intrusive stocks and dikes are intruded in sedimentary rocks as subvertical bodies with $75^0$ to $85^0$ dips (Nyamsuren & Altan-Erdene, 1991). However, the age of intrusive stocks is still not clear, because the age was considered differently by previous investigations. For example, on the report of 1:50 000 scale mapping at the Khadat deposit area in 1962 shows that age of sedimentary rocks is Devonian, and granodiorite porphyry stocks are Permian in age, whereas, in 1991, at 1:50 000 scale geological mapping report displays the age of sedimentary rock is Cambrian to Ordovician, and intrusive stocks are Devonian.

The copper mineralization occurs mainly as infilling of fractures, veinlets and porphyritic type, which are hosted in sandstone and granodiorite dikes.
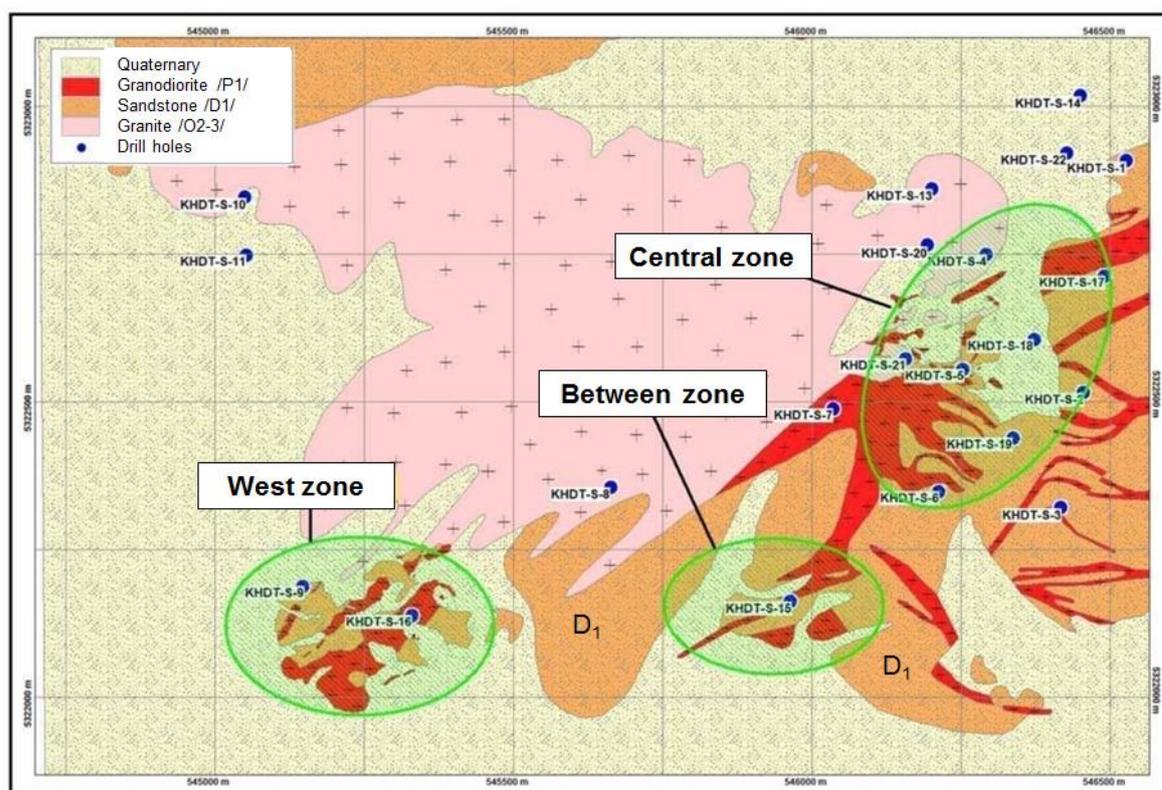


**Fig. 7** Geological map of the Khadat copper deposit, and localities of drill holes and mineralization zones (Map source from UNFM Company).

# Chapter IV

# 4. MATERIALS AND METHODS

## 4.1 Materials

### 4.1.1   Samples from the Gatsuurt deposit

Fifty-two samples were collected from drill cores taken in the Central and Main zones (Fig. 8). Representative samples were selected from all ore types, at depths ranging from 1315.77 m to 399.18 m in elevation. Representative samples of the disseminated and stockwork ores in granite of the Central zone, those in rhyolite of the Main zone, the quartz vein ores with native gold that associated coarse-grained sulfides, and silicified ores consisting of fine grains of quartz and dispersed sulfides are shown in Figs. 8(A), (B), (C) and (D), respectively. Fifty polished thin sections were prepared for petrological study.

For fluid inclusion study, samples were collected from volcanic rocks hosting a narrow sulfide-Au-bearing quartz vein (sample AM-7, vein thickness of 5 cm) in the Main zone, and from a narrow granite-hosted sulfide-bearing quartz vein (sample GT-172a, thickness 2 cm) in the Central zone.

**8A** | **Granite hosted ores (Central Zone)** ... **Sulfide-bearing stockwork**

Sulfide-bearing stockwork

Sulfide-bearing stockwork

Sulfides associated with sericite

**8B** | **Rhyolite hosted ores (Main Zone)**

Sulfide-bearing stockwork

Sulfide-bearing stockwork

**8C** | **Quartz vein ores**

Quartz

Granite

Native gold

Quartz

Native gold

**8D** | **Silicified ores**

Rhyolite

38
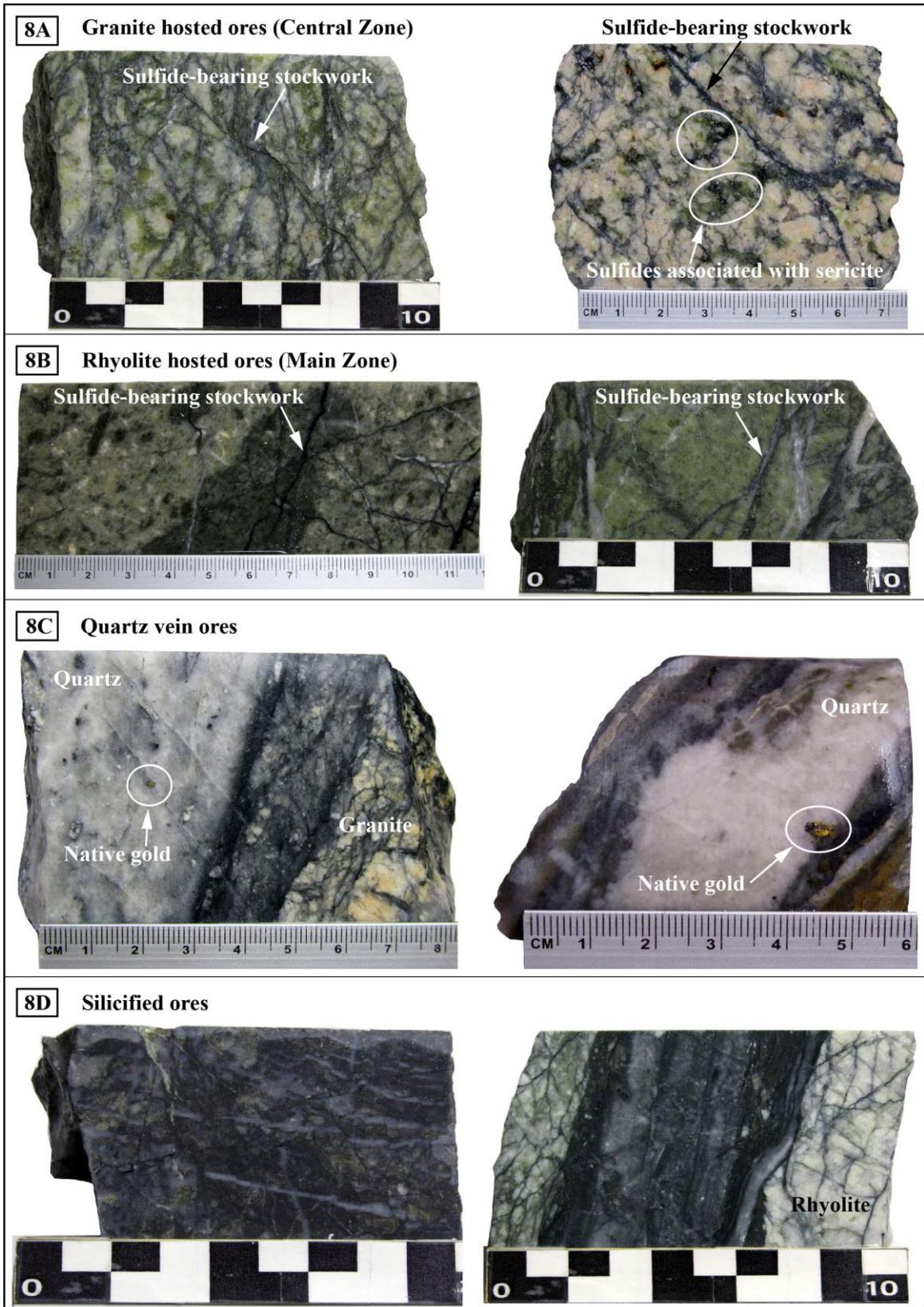
**Fig. 8** Samples of different ore types in the Gatsuurt deposit. (A) Disseminated and stockwork ores in granite in the Central zone. (B) Disseminated and stockwork ores in rhyolite in the Main zone. (C) Quartz vein ores with native gold and associated coarse-grained sulfides. (D) Silicified ore consisting of fine-grained quartz and dispersed sulfides.

### 4.1.2 Samples from the Boroo deposit

Ore samples for this study were taken from open-pits in the Zones 2, 3, 5 and 6, and also from drill cores (Figs. 5 and 9). Thirty-five disseminated and stockwork ores were hosted in granite, metasedimentary rocks and diorite dikes, and twenty-one auriferous quartz vein ores were collected at depths ranging from 1150 to 1040 m in elevation. Fifty polished thin sections were made for mineralogical study. Pyrite and arsenopyrite are the visible sulfides of the ores in granite. Coarse-grained sulfides mostly occur in the disseminated ores, whereas the fine-grained sulfides are present along the margins of stockwork veins (Fig. 9A). Disseminated euhedral pyrite and arsenopyrite of variable size occur in the metasedimentary rocks (Fig. 9B). Sulfides in the diorite dikes are also pyrite and arsenopyrite, and mostly appear as fine-grained crystals which are localized in the disseminated and stockwork ores (Fig. 9C). The auriferous quartz vein ores commonly contain coarse-grained tetrahedrite (Fig. 9D), and occasionally free native gold and sulfides.

For fluid inclusion study, samples were collected from granite that hosting a narrow sulfide-Au-bearing quartz veins (sample BR-07, 08, 11, and BDD-97 vein thickness of 2 cm) in the ore zone 3, and from the auriferous quartz vein ores (sample BR-12, 13, 14,

MDD-27 and BRD-18, thickness of quartz vein is around 50 cm to 1 meter) in the ore zone 3 and 5.

For age dating analysis, samples were collected from host granite of the ore zone 3, and from diorite dikes which occur in the ore zone 5. Each samples were taken from fresh outcrop rocks (non-altered), and their weight were around 4 to 5 kilograms.

**9A**   **Granite hosted ores**

Sulfide-bearing stockwork

Sulfides

Sulfide-bearing stockwork

**9B**   **Metasedimentary rock hosted ores**

Disseminated sulfides

Sandstone

Granite

Sulfides

**9C**   **Diorite dike hosted ores**

Sulfide-bearing stockwork

Sulfide-bearing stockwork

**9D**   **Auriferous quartz vein ores**

Tetrahedrite
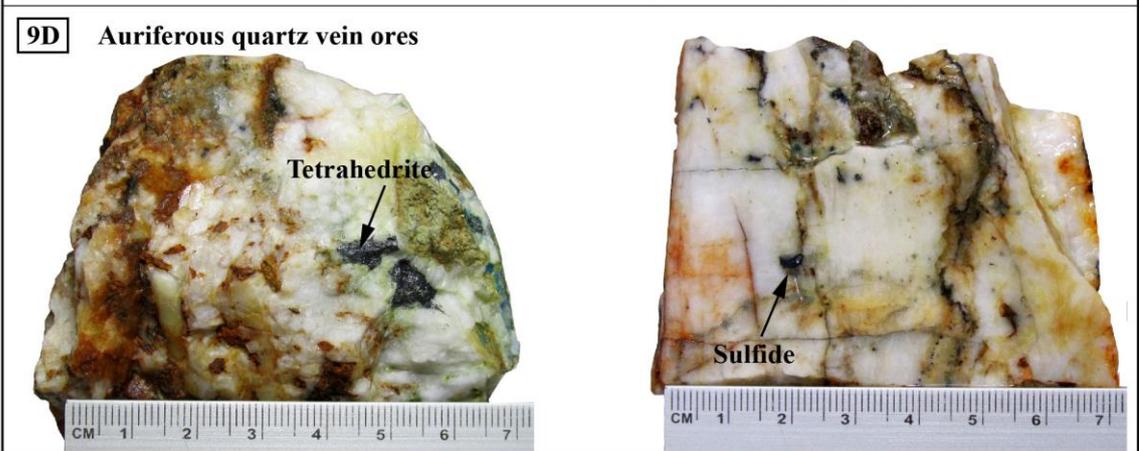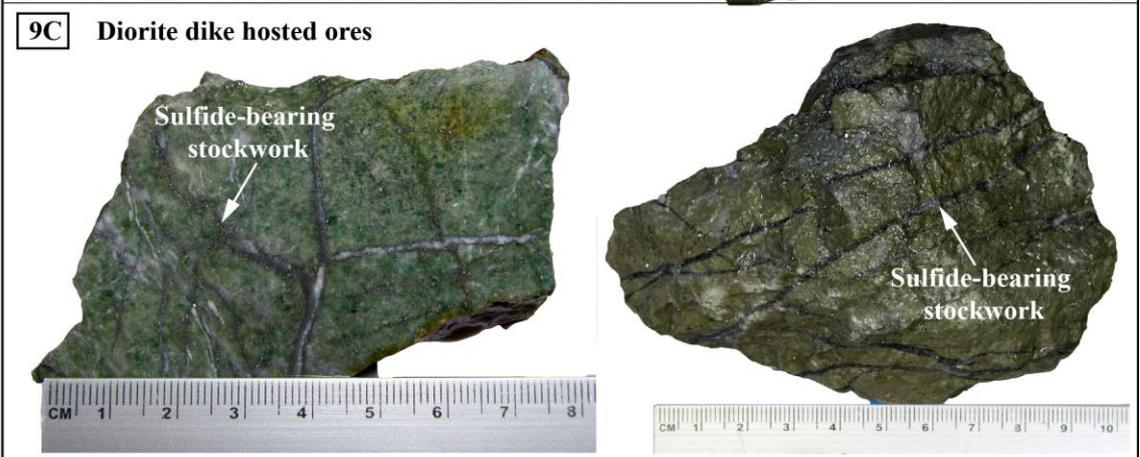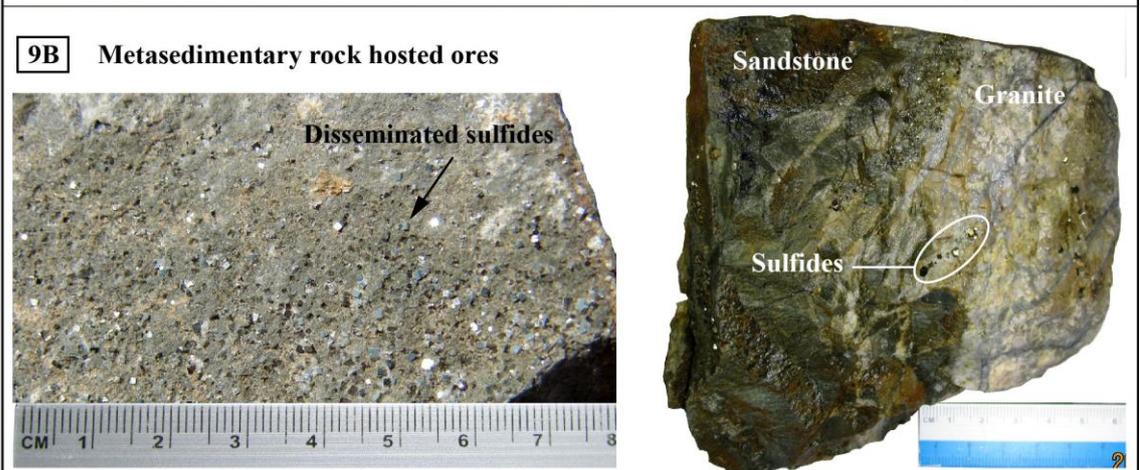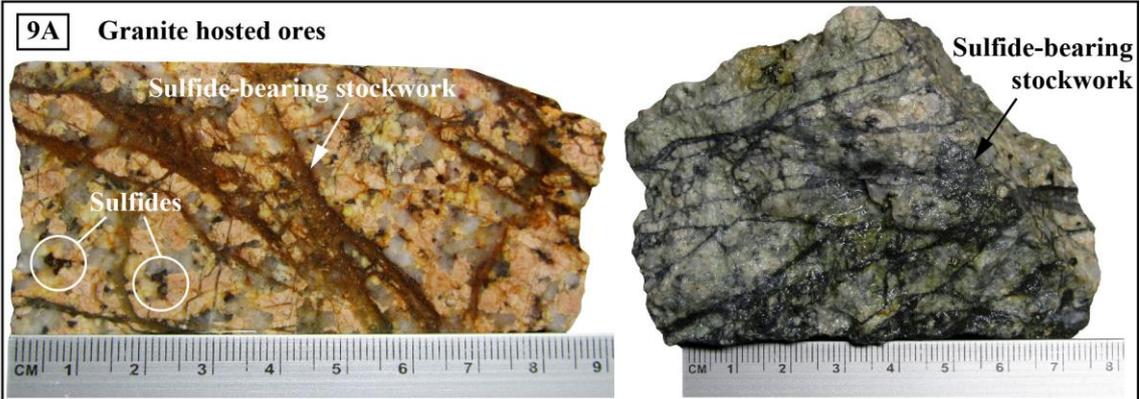
Sulfide

**Fig. 9** Samples of different ore types in the Boroo deposit. (A) Disseminated and stockwork ores in granite in ore Zone 3. The coarse-grained granite is yellowish due to oxidation and K-feldspar alteration. Sulfides occur as dissemination and sulfide-bearing stockwork. (B) Disseminated and stockwork ores in metasedimentary rock in ore Zone 5. Metasedimentary rocks are dark green, and weakly altered by silica. Fine-grained sulfides mostly occur as disseminations in the metasedimentary rocks. (C) Disseminated and stockwork ores in a diorite dike in ore Zone 6. Diorite dike is grayish-green due to the original fine-grained rock-forming minerals, and sulfides occur as disseminations and stockwork. (D) Auriferous quartz vein ore is massive, milky-white and smoky-gray, and commonly contains coarse-grained sulfides.

### 4.1.3  Samples from the Ulaanbulag deposit

Fifty-four samples were collected from drill cores in the deposit (Fig. 6). The among these samples, thirty-two representative samples of the disseminated and stockwork ores and twenty-two representative samples of the siliceous ores were collected at depths ranging from 1050 to 840 m in elevation. Twenty polished thin sections were made for mineralogical study. Pyrite and arsenopyrite are the visible sulfides in both the ore types. Coarse-grained sulfides mostly occur in the disseminated and stockwork ores (Fig. 10A), whereas the fine-grained sulfides are present as veinlets in the siliceous ores (Fig. 10B).
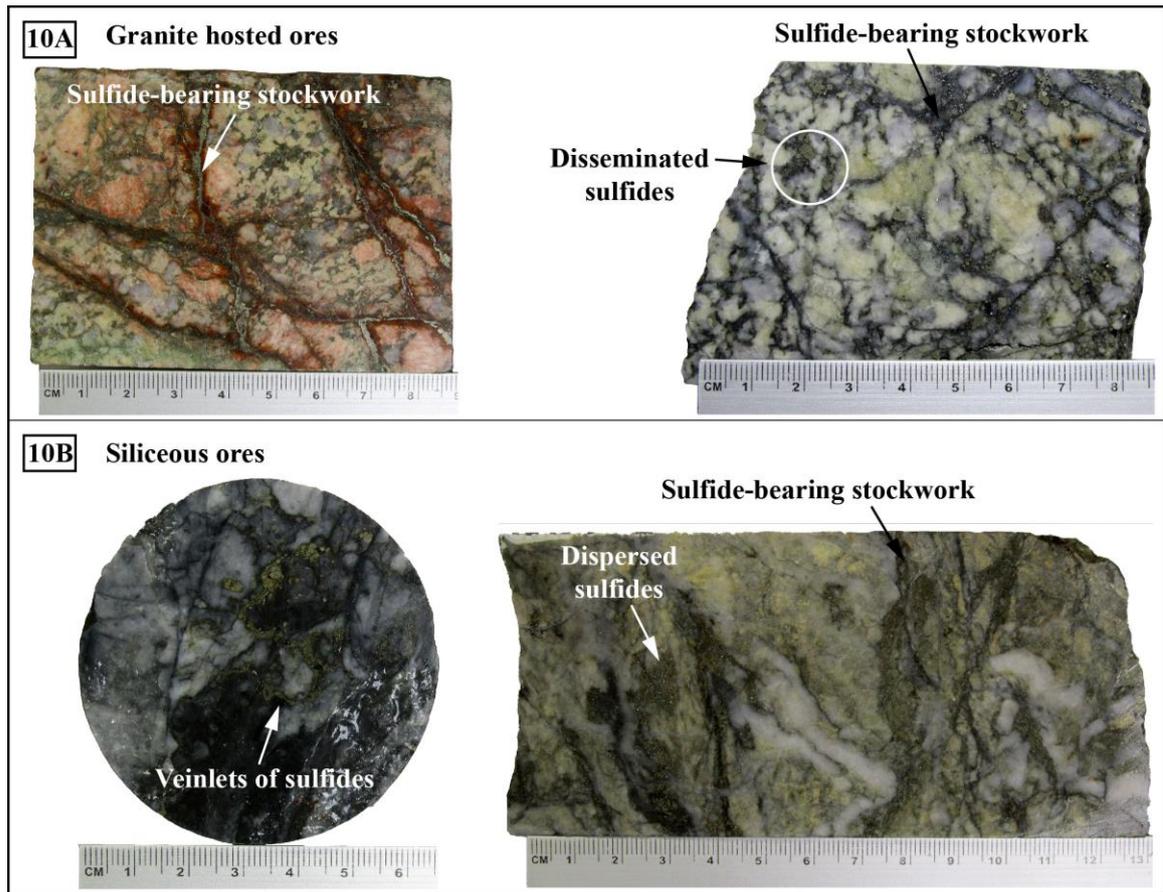
**Fig. 10** Samples of different ore types in the Ulaanbulag deposit. (A) Disseminated and stockwork ores in granite. The coarse-grained granite is altered by K-feldspar alteration, and shows pinkish color. Sulfides occur as dissemination and sulfide-bearing stockwork. (B) Siliceous ores with sulfide veinlets.

### 4.1.4  Samples from the Khadat deposit

Forty-nine samples were collected from drill cores in the Khadat copper deposit. Among the total samples, twenty-six representative ore samples were selected from surface to 100s meters in depth, and those are mostly oxidized, and show only chalcopyrite that occur as veins in fractures of metasedimentary rocks (Fig. 11A). Nineteen representative ore samples were taken from 100 to 200s meters in depth show more common assemblages of sphalerite, chalcopyrite and galena, and ores are hosted in both the granodiorite and metasedimentary rocks (Fig. 11B). Four representative ore samples were collected ranging from 200 to 250s meters in depth of the deposit. These samples present the disseminated and stockwork mineralization in the metasedimentary rocks (Fig. 11C), and here, mainly pyrite, arsenopyrite and chalcopyrite assemblages are observed.
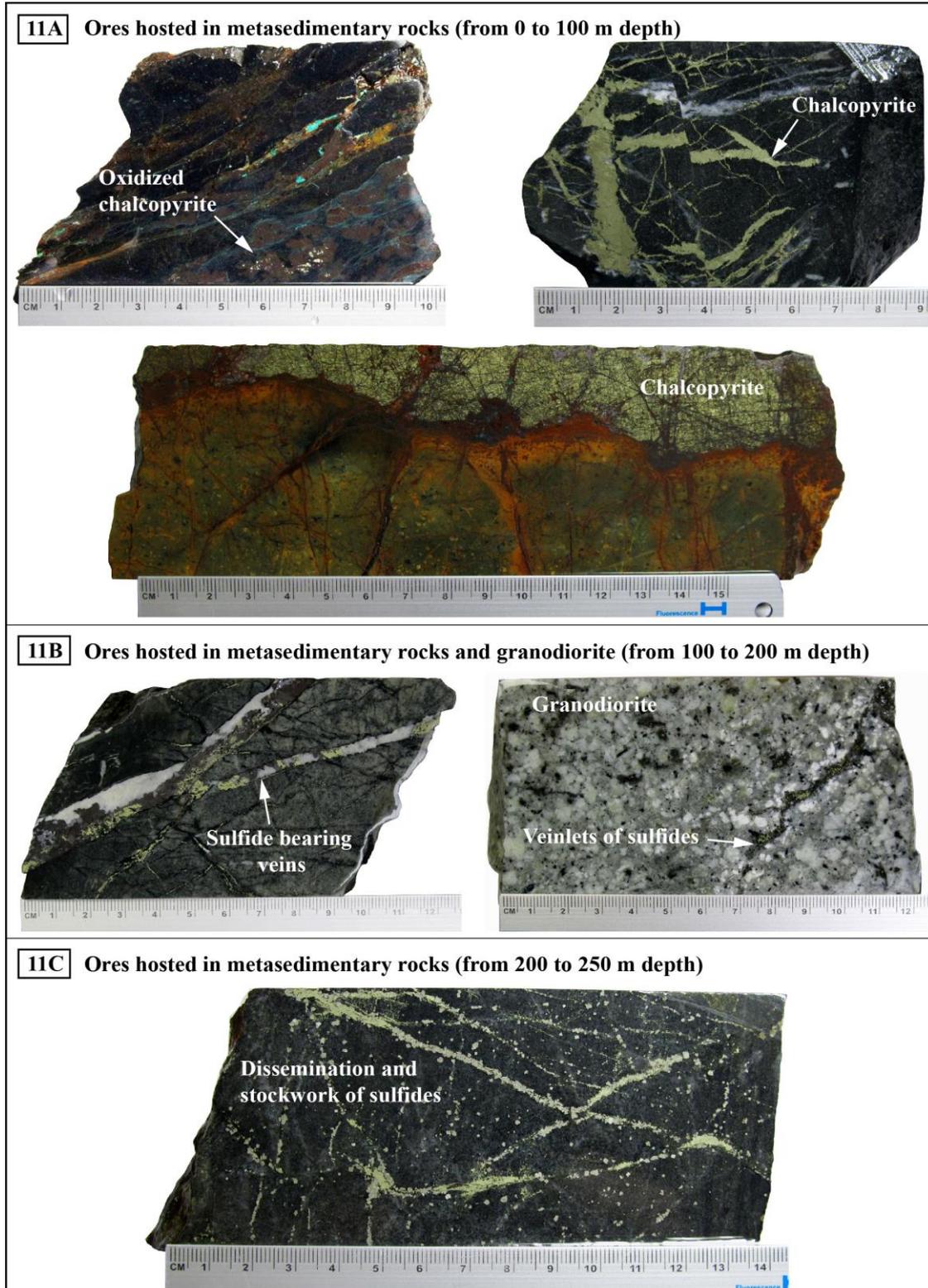
**Fig. 11** Ore samples from the Khadat copper deposit. (11A) samples showing oxidized and unoxidized ores. (11B) Sulfide-bearing veins in the metasedimentary rocks and granodiorite. (11C) Disseminated and stockwork ores in metasedimentary rocks.

## 4.2  Methods

### 4.2.1  Petrological study

Fifty, fifty and twenty polished thin sections are prepared for petrological study for the Gatsuurt, Boroo and Ulaanbulag deposits, respectively. The study of ore minerals in polished section used the polarizing reflected light microscope for the identification and characterization of the ore mineral phases in a sample and the textural relationships between them. Usually ore minerals textures are recognized high magnification (400X) and it was dependent on grain size of minerals.

### 4.2.2  Chemical analysis of minerals

Chemical compositions of ore minerals were determined using a JEOL JXA 8530F electron microprobe analyzer (EMPA) at Shimane University. The measurement conditions used for ore mineral analysis were 25 kV accelerating voltage, 20 nA beam current, and 2-3 μm probe diameter. Quantitative chemical analyses of ore minerals were processed using the ZAF correction method. Ore minerals were analyzed for Fe ($K\alpha$), S ($K\alpha$), As ($L\alpha$), Au ($M\alpha$), Sb ($L\alpha$), Ni ($K\alpha$), Te ($L\alpha$), Co ($K\alpha$), W ($L\alpha$), Mn ($K\alpha$), Pb ($M\alpha$), Cd ($L\alpha$), Cu ($K\alpha$), Zn ($K\alpha$), Bi ($L\alpha$) and Ag ($L\alpha$). Standard materials comprised compounds of $FeS_2$ (for Fe, S), MnS (Mn), CdS (Cd), GaAs (As), $Sb_2S_3$ (Sb), PbS (Pb), CoO (Co), and pure Au, Ag, Ni, W, Te, Zn, Bi and Cu metals.

### 4.2.3  X-ray powder diffraction analysis

Alteration minerals were carried out by X-ray powder diffractometer (XRD) and optical microscope. For this analysis the samples were powdered using agate mortar. XRD was carried out with Rigaku RAD-X and Rigaku Mini FLEX using random-orientation

method (constant orientation method for clay minerals), tube voltages and currents 30 kV × 20 mA, scan speed of 1°/min, scan step of 0.020° and scan range of 2 – 55°.

### 4.2.4   Fluid inclusion analysis

Fluid inclusions in quartz were first observed using a transmitted light binocular microscope, and inclusion size, shape and distribution were recorded. Detailed fluid inclusion petrography was conducted on polished plates prior to heating experiment. Fluid inclusions were located under low magnification, their origin, and textural relationship determined and their phase relationships were studied under high objectives of microscope. The primary and secondary inclusions have been identified following the criteria outlined by Roedder (1984). An Nikon microscope with 40X to 400X magnification and LINKAM LK-600+L600A heating and freezing stage were used for the microthermometric study. The accuracy of the measurement was ensured by calibrating the Linkam THM-600 with the triple point of $CO_2$ (–56.5°C), freezing of pure water (0°C), and melting points of different components. Precisions of the temperature measurement are within +1°C for heating.

### 4.2.5   U-Pb age dating in zircon by LA-ICP-MS analysis

Zircon grains separated from the rock samples or thin sections carrying zircon grains were embedded in epoxy for LA-ICP-MS analyses, together with grains of standard zircon. Zircon grains were separated by crushing rock chips into powder below 250 μm in size with a jaw crusher and stamp mill, followed by magnet and heavy liquid separation. Zircon grains were then handpicked, mounted in epoxy resin, and polished by diamond paste until they were thinned approximately to half of the original thickness. Before isotopic analysis, the internal zoning patterns of the crystals, mineral inclusion and cracks

were observed by back-scattered electron (BSE) and cathodoluminescence (CL) images at the Shimane University. Grains of zircon were analyzed for U–Th–Pb dating by a Laser Ablation Inductively Coupled Plasma Mass Spectrometry (LA-ICP-MS) at Hiroshima University. The spot size was about 15 μm, and seven scans through the critical mass ranges were made for data collection. Counts of $^{196}Zr_2O$, $^{204}Pb$, $^{206}Pb$, $^{207}Pb$, $^{208}Pb$, $^{238}U$, $^{248}UO$, $^{254}UO$ and background were measured seven times with a mass resolution of 5800 (M/ΔMat 1% of peak height). Two kinds of standard zircon, FC1 (1099Ma; Paces and Miller, 1993) and SL13 (572Ma, U concentration=238 ppm; Claoué-Long et al., 1995) were used for the U–Pb calibration and the calculation of U concentration in the samples, respectively. Common Pb was corrected by the measured $^{204}Pb$, based on the two-stage evolution model of Stacy and Kramers (1975). Isoplot/Ex 3.0 (Ludwig, 2003) was used for age calculations. Ages on single data points are quoted at 1δ level, whereas mean ages are given at 95% confidence level.

# Chapter V

## 5. RESULTS

### 5.1 Petrological study

#### 5.1.1 Petrography of the Gatsuurt deposit

Pyrite and arsenopyrite are abundant in the disseminated and stockwork, quartz vein and silicified ores (Figs. 12, 13, 14). These ores also contain moderate amounts of galena, tetrahedrite-tennantite, sphalerite and chalcopyrite, and minor amounts of other minerals including jamesonite, bournonite, boulangerite, geocronite, scheelite, geerite, native gold, and zircon. Abundances and grain sizes of the ore minerals vary in ores with differing host rock.

Pyrite is the most abundant sulfide in the disseminated and stockwork and silicified ores, and is common in the quartz vein ores. Pyrite is euhedral to subhedral in form, with a wide range of grain size, from 10 µm to 3 mm. Two generations of pyrite are recognized in the disseminated and stockwork and quartz vein ores (Fig. 12A; Fig. 13G). Small grains of early stage pyrite 20 µm in diameter (here termed pyrite-I) occur within later stage pyrites (pyrite-II). Aggregates of very fine (up to 50 µm) anhedral to subhedral pyrite and arsenopyrite form veinlets in the silicified ores (Fig. 14A).

Arsenopyrite is also a major sulfide in both the disseminated and stockwork ores and silicified ores, but is not common in the quartz vein ores. It occurs as euhedral rhombic, prismatic, or acicular crystals (Fig. 12B), and forms aggregates with pyrite. Two generations of arsenopyrite are recognized in the disseminated and stockwork ores (Fig. 12B): early stage arsenopyrite (arsenopyrite-I) occurs euhedral crystals up to 40 µm in

49

length, and is overgrown by later stage arsenopyrite-II, which forms euhedral crystals up to 0.2 mm long.

Galena is common in the quartz vein ores, and is occasionally observed in the disseminated and stockwork ores and silicified ores. In the disseminated and stockwork ores, it commonly occurs as inclusions in pyrite and arsenopyrite, and fills interstices in aggregates consisting of pyrite and arsenopyrite crystals (Figs. 12C, 12D). In the quartz vein ores, galena occurs as an interstitial mineral, along with tetrahedrite (Fig. 13A) and native gold (Fig. 13B).

Tetrahedrite occurs in the disseminated and stockwork ores and silicified ores as inclusions 5-30 µm in diameter or as fillings of fractures in pyrite and arsenopyrite (Figs. 12E, 12F, 14A, 14B). It rarely occurs with native gold in small cavities within medium-grained pyrite in the disseminated and stockwork ores. Large grains of anhedral tetrahedrite up to 2 mm in diameter occur in the quartz vein type, in which they coexist with or overgrow on galena, chalcopyrite, bournonite, and sphalerite (Figs. 13C, 13D). Tetrahedrite is occasionally overgrown by tennantite in the quartz vein ores.

Sphalerite occurs in the disseminated and stockwork ores as fine (5 to 40 µm) anhedral inclusions and as a fracture filling in pyrite and arsenopyrite (Fig. 12G). Sphalerite grains up to 3 mm across often occur in veinlets in the quartz vein ores, and are rimmed or replaced by geerite (Figs. 13A, 13C). In the silicified ores, sphalerite infrequently occurs with galena and native gold as inclusions in pyrite (Fig. 14C).

Chalcopyrite is found as inclusions around 10 µm in size in pyrite and tetrahedrite. It also occurs as anhedral single grains (up to 100 µm) in the disseminated and stockwork ores. Chalcopyrite is a common sulfide in the quartz vein ores, where larger grains (0.2

mm) are associated with pyrite, sphalerite, galena, tetrahedrite and native gold (Figs. 13D, 13E).
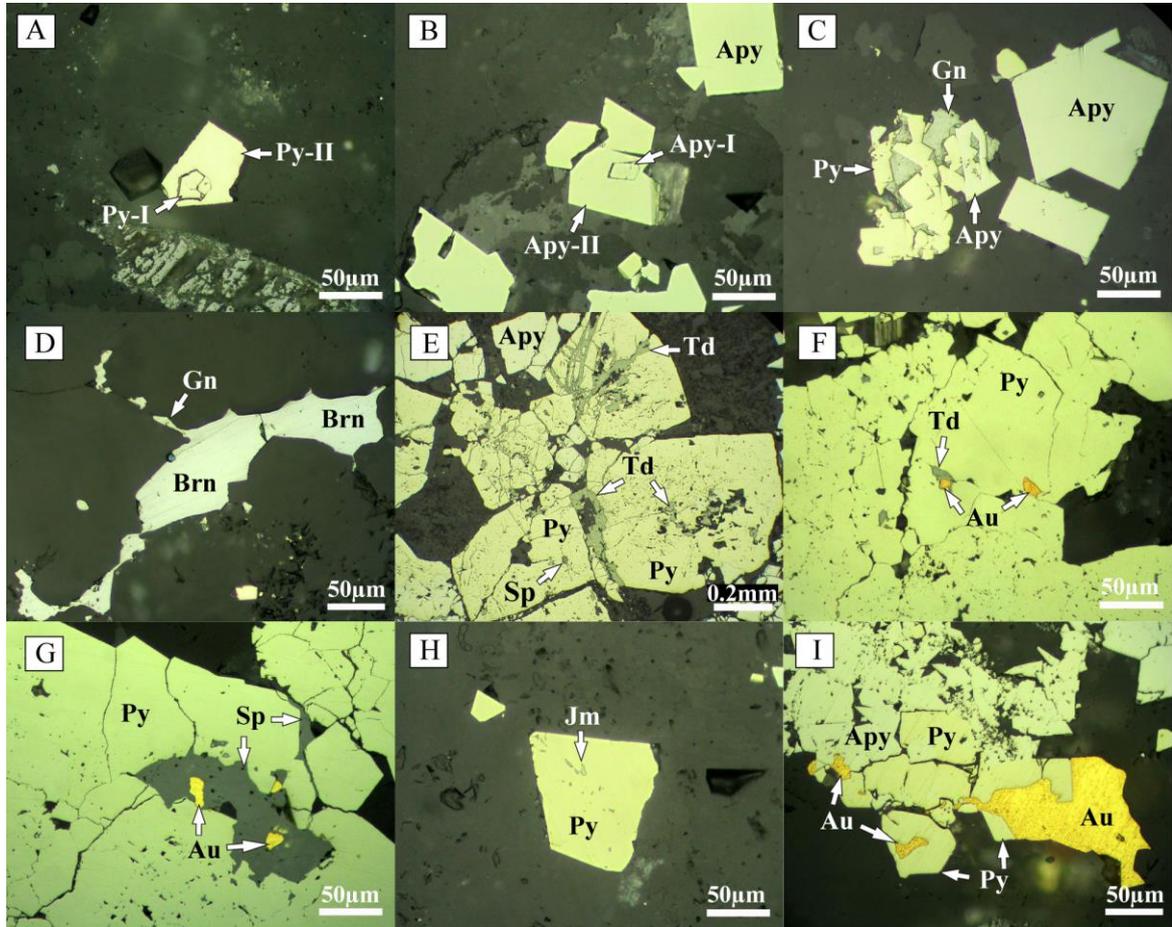


**Fig. 12** Photomicrographs of disseminated and stockwork ores from the Gatsuurt deposit. (A) Early stage pyrite (Py-I) within later stage pyrite (Py-II). (B) Early stage arsenopyrite (Apy-I) in later stage arsenopyrite (Apy-II). (C) Galena (Gn) filling interstices between pyrite and arsenopyrite. (D) Fine grained galena occurring with bournonite (Brn). (E) Tetrahedrite (Td) occurring along boundaries of arsenopyrite and fractured pyrites, and fine sphalerite (Sp) inclusions in pyrite. (F) Native gold (Au) occurring as inclusions within tetrahedrite and pyrite. (G) Native gold inclusions in sphalerite and in fractures in

pyrite. (H) Jamesonite (Jm) inclusions within a pyrite grain. (I) Native gold coating pyrite grain and fine grains occurring with pyrite and arsenopyrite.
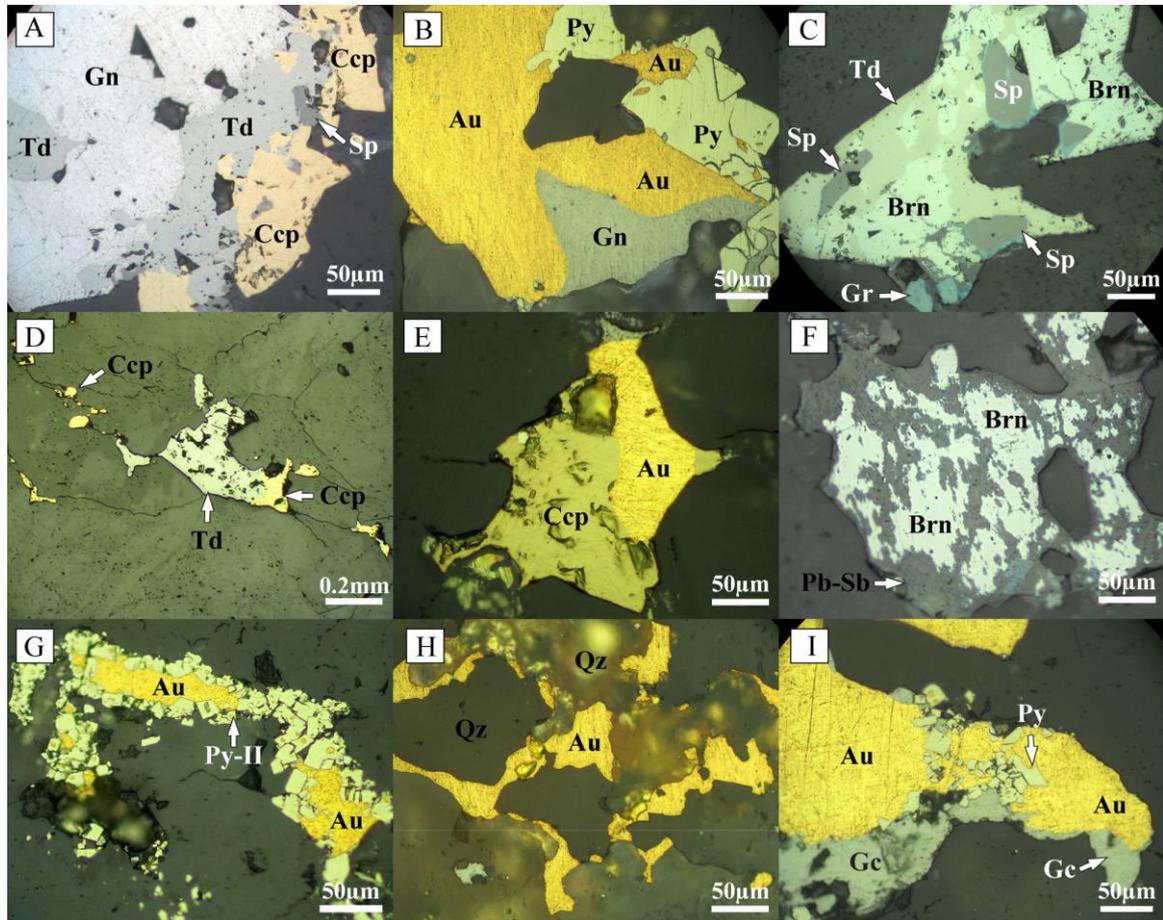


**Fig. 13** Photomicrographs of quartz vein ores from the Gatsuurt deposit. (A) Tetrahedrite in contact with galena, chalcopyrite and sphalerite. (B) Native gold, pyrite and galena. (C) Sphalerite rimmed by geerite (Gr), and its occurrence with tetrahedrite and bournonite. (D) Tetrahedrite and chalcopyrite occurring in a fracture in quartz (Qz). (E) Native gold and chalcopyrite (Ccp) filling interstices between quartz grains. (F) Bournonite replaced by a Pb-Sb-bearing mineral. (G) Native gold bordered by later stage pyrites. (H) Free native gold in quartz. (I) Pyrite, native gold and geocronite (Gc) filling interstices between quartz grains.
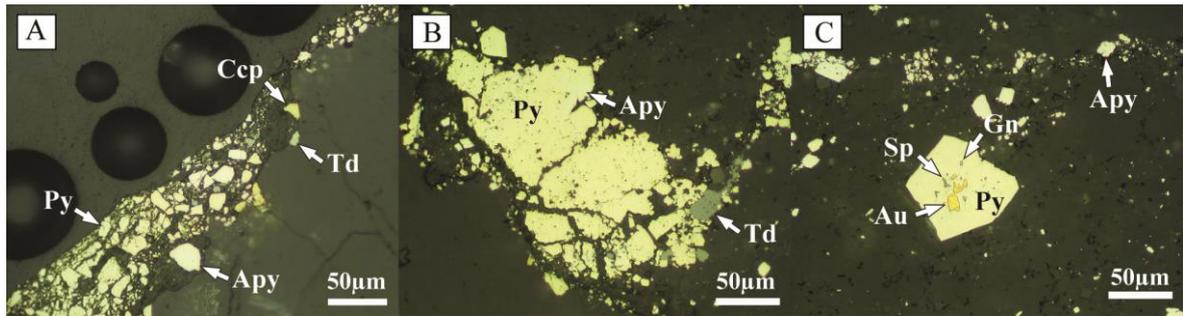
**Fig. 14** Photomicrographs of silicified ores from the Gatsuurt deposit. (A) Fine grained pyrite, arsenopyrite, chalcopyrite and tetrahedrite forming a vein. (B) Aggregates of pyrite and arsenopyrite, and associated tetrahedrite. (C) Native gold, sphalerite and galena inclusions in pyrite.

Native gold grains 5 to 50 μm in diameter occur in fractures in pyrite and arsenopyrite, and along crystal (or grain) boundaries of pyrite, arsenopyrite, and sphalerite in the disseminated and stockwork ores (Figs. 12F, 12G, 12I). Medium to large (up to 4 mm) grains of free visible native gold are found in the quartz vein type (Figs. 13B, 13E, 13G, 13H, 13I), whereas very fine grains of native gold (<30 μm) occur as inclusions in isolated pyrite crystals in the silicified ores (Fig. 14C).

Minor jamesonite, bournonite, boulangerite, geocronite, scheelite and geerite occur as anhedral grains of varying size. Bournonite fills the interstices of quartz aggregates in the disseminated and stockwork ores (Fig. 12D), and coexist with tetrahedrite in the quartz vein ores (Fig. 13C). A part of bournonite was altered and oxidized to secondary Pb-As-Sb oxide (Fig. 13F). Jamesonite occurs as inclusions and fracture fillings in pyrite and arsenopyrite in the disseminated and stockwork ores (Fig. 12H). Geocronite was observed in only one sample of the quartz vein ore, as a later phase than native gold and pyrite (Fig. 13I). Scheelite occurs in thin veinlets filling fractures of gangue minerals in

53

the disseminated and stockwork ores in the Main zone. Fine anhedral boulangerite occurs rarely within quartz in the disseminated and stockwork ores in the Main zone. Zircon crystals a few tens of microns in diameter occur as inclusions in pyrite in the disseminated and stockwork ores.

### 5.1.2 Petrography of the Boroo deposit

The disseminated and stockwork ores mainly contain pyrite and arsenopyrite, minor sphalerite, galena and tetrahedrite, and trace amounts of chalcopyrite, bournonite, boulangerite, alloclasite and native gold (Table 1). The ore minerals in the auriferous quartz vein ores are essentially the same as those of the disseminated and stockwork ores, but their abundances are different: pyrite, sphalerite, chalcopyrite, tetrahedrite and bournonite are more common than arsenopyrite and galena; coarse-grained native gold is characteristic; and arsenopyrite, geerite and electrum are present in trace amounts (Table 1).

Pyrite is the most abundant sulfide in the disseminated and stockwork ores. It is rather coarse-grained in the ores hosted in granite, whereas that in the ores hosted in diorite dikes and metasedimentary rocks is comparatively fine-grained. Two occurrences of pyrite were observed: small anhedral pyrite from few tens to hundreds of μm in size forming aggregates (Fig. 15A); euhedral crystals a few hundred μm to 5 mm in size (Fig. 15B). Pyrite shows compositional zoning due to As content, and two generations of pyrite were recognized (Fig. 15B). Early stage pyrite (hereafter pyrite-I) is characterized by anhedral form and indistinct internal structure, whereas later stage pyrite (pyrite-II) growing on pyrite-I shows euhedral to subhedral form and remarkable zoning. Pyrite is common in the auriferous quartz vein ores, occurring as subhedral grains up to 200 μm in

diameter. These pyrite grains are micro-fractured, and are commonly associated with arsenopyrite (Fig. 16A).

**Table 1** Distribution of ore minerals in the disseminated and stockwork ores and auriferous quartz vein ores of the Boroo deposit.

| | Ore mineral (abbreviation) | Disseminated and stockwork ores (A) | | | |
|---|---|---|---|---|---|
| | | abundance | shape | size (μm) | assemblage with |
| Main | Pyrite (Py) | ++++ | euhedral | <5000 | Apy, Sp, Gn, Ccp, Td, Au |
| | Arsenopyrite (Apy) | ++++ | euhedral | <1000 | Py, Gn, Td, Au |
| Minor | Sphalerite (Sp) | ++ | anhedral | <100 | Py, Apy, Gn, Au |
| | Galena (Gn) | ++ | anhedral | <400 | Py, Apy, Sp, Alc |
| | Tetrahedrite (Td) | ++ | anhedral | <100 | Ccp, Sp, Brn |
| Trace | Chalcopyrite (Ccp) | + | anhedral | <50 | Py, Td |
| | Bournonite (Brn) | + | anhedral | <10 | Gn |
| | Boulangerite (Bln) | + | anhedral | <10 | Gn |
| | Alloclasite (Alc) | + | anhedral | <10 | Py, Gn |
| | Native gold (Au) | + | anhedral | <500 | Py, Apy, Sp |

| | Ore mineral (abbreviation) | Auriferous quartz vein ores (B) | | | |
|---|---|---|---|---|---|
| | | abundance | shape | size (μm) | assemblage with |
| Main | Pyrite (Py) | +++ | subhedral | <300 | Apy, Sp, Gn, Ccp, Td, Au |
| | Sphalerite (Sp) | +++ | anhedral | <500 | Py, Gn, Ccp, Td, Au |
| | Chalcopyrite (Ccp) | +++ | anhedral | <500 | Td, Brn, Gr |
| | Tetrahedrite (Td) | +++ | anhedral | <1 cm | Brn |
| | Bournonite (Brn) | +++ | anhedral | <1000 | Td, Ccp, Gn |
| Minor | Galena (Gn) | ++ | anhedral | <800 | Py, Sp, Ccp, Td, Brn |
| | Native gold (Au) | ++ | anhedral | <1 cm | Py, Ccp, El |
| Trace | Arsenopyrite (Apy) | + | subhedral | <150 | Py, Td, Brn |
| | Geerite (Gr) | + | anhedral | <10 | Ccp, Brn, Td |
| | Electrum (El) | + | anhedral | <5 | Au |

++++ abundant, +++ common, ++ occasional, + rare

Pyrite in the auriferous quartz vein ores also exhibits varied compositional zoning due to As contents. The zoning patterns are complex, but are similar to those of pyrites in the disseminated and stockwork ores. Thus, two generations of pyrite are recognized in the auriferous quartz vein ores, namely early stage pyrite-I and later stage pyrite-II (Fig. 16A).

Arsenopyrite is also a major sulfide in the disseminated and stockwork ores. It occurs as euhedral rhombic crystals ranging between 50 μm and 1 mm in diameter, containing rare inclusions of pyrite, galena and native gold (Fig. 15C). In the auriferous quartz vein ores, arsenopyrite occurs as anhedral grains that are commonly cracked, and partially leached or corroded (Fig. 16A, B). Arsenopyrite in the disseminated and stockwork ores mostly presents zonal structure, and two generations of arsenopyrite are observed (Fig. 15D). Early stage arsenopyrite (hereafter arsenopyrite-I) is porous and anhedral in form, whereas the later stage arsenopyrite (arsenopyrite-II) is euhedral in form. However, arsenopyrite in the auriferous quartz vein ores shows only one generation. This is characterized by As-deficiency in arsenopyrite (0.79 atoms per formula unit) and lack of Fe-bearing primary minerals in the host quartz. Subhedral to anhedral arsenopyrite occurring in pyrite-II (Fig. 16A) suggests that arsenopyrite was dissolved, and arsenic released from the arsenopyrite was taken up in the crystallization of As-bearing pyrite-II.

Sphalerite occurs as a space-filling phase in pyrite and arsenopyrite in the disseminated and stockwork ores (Fig. 15E). Sphalerite is common in the auriferous quartz vein ores, and reaches 0.5 mm in size. It is often intruded and replaced by chalcopyrite (Fig. 16C), and replaces pyrite (Fig. 16D).

Galena occasionally appears in both the disseminated and stockwork ores and in the auriferous quartz vein ores. In the disseminated and stockwork ores, it occurs as a space-filling phase within pyrite and arsenopyrite, and fills interstices of pyrite and arsenopyrite

crystals (Fig. 15C, F). Galena in the auriferous quartz vein ores is anhedral in form, reaching 0.8 mm in size, and rarely exhibits cubic habit (Fig. 16E).

Chalcopyrite occurs as a filling phase within pyrite (Fig. 15F), or as anhedral grains associated with tetrahedrite in the disseminated and stockwork ores. Chalcopyrite is common in the auriferous quartz vein ores, and fills fractures in arsenopyrite (Fig. 16B), pyrite, sphalerite (Fig. 16C) and galena (Fig. 16E). This mineral is closely associated with tetrahedrite (Fig. 16F) and bournonite. Rims of significantly altered chalcopyrite grains are changed to geerite (Fig. 16B). In one sample of the auriferous quartz vein ores, chalcopyrite was observed in association with native gold (Fig. 16F).
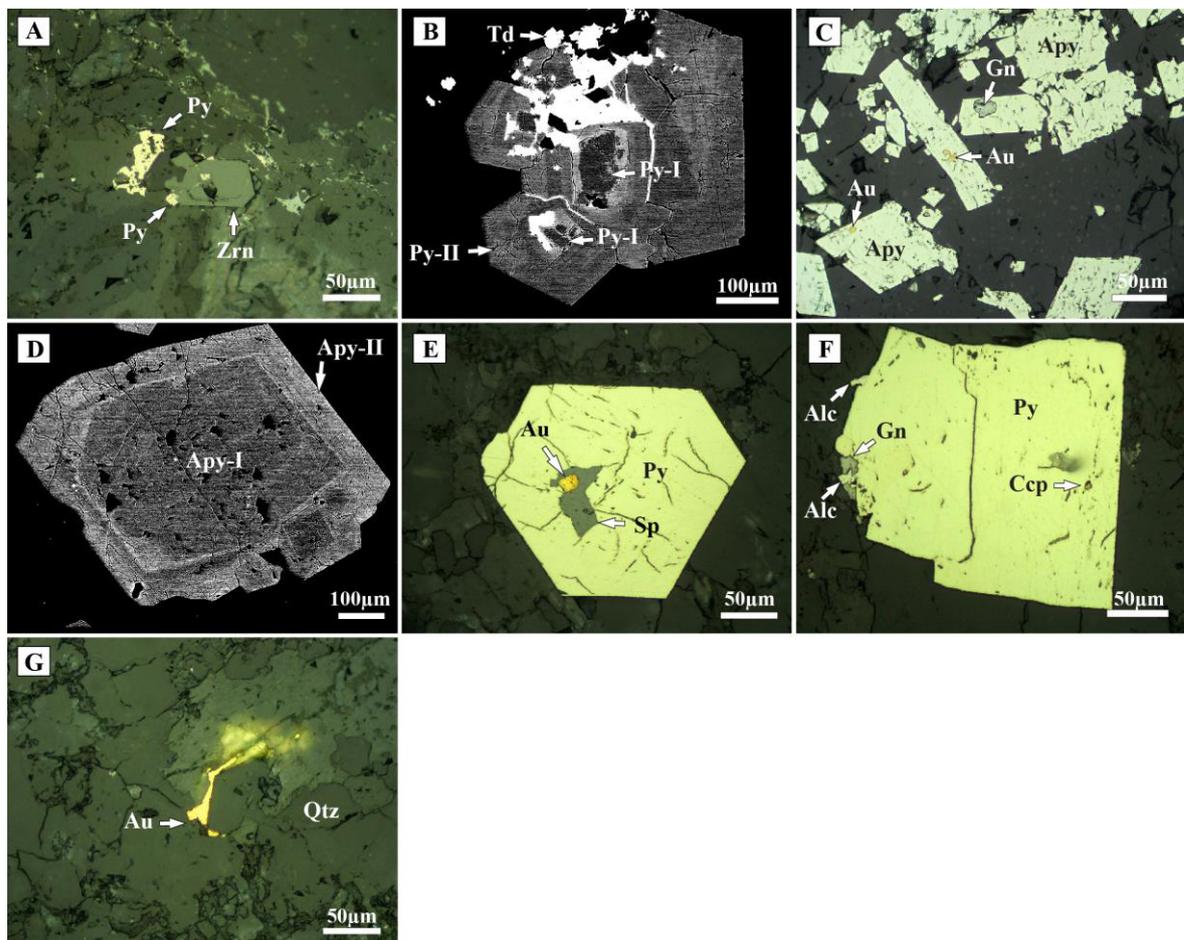


**Fig. 15** Photomicrographs of disseminated and stockwork ores from the Boroo deposit. (A) Pyrite (Py) filling interstices of gangue minerals and fractures of euhedral zircon

57

(Zrn). (B) Early stage pyrite (Py-I) within later stage pyrite (Py-II), and tetrahedrite (Td) filling interstices in pyrite. (C) Galena (Gn) and native gold (Au) occurring as fine grains within arsenopyrite (Apy). (D) Early stage arsenopyrite (Apy-I) and later stage arsenopyrite (Apy-II). (E) Native gold grains in sphalerite (Sp) filling fractures in euhedral pyrite. (F) Alloclasite (Alc) and galena occurring along rims of pyrite, and fine chalcopyrite (Ccp) grains in pyrite. (G) Native gold occurring as a filling phase in quartz aggregates.

Tetrahedrite occurs in the disseminated and stockwork ores as a filling of minute cavities and fractures in pyrite and arsenopyrite (Fig. 15B). Tetrahedrite in the auriferous quartz vein ores occurs as anhedral grains up to 1 cm (Fig. 9D). It replaces pyrite and arsenopyrite, and coexists with bournonite (Fig. 16G) and native gold.

Minor bournonite, boulangerite, geerite and alloclasite occur as anhedral grains of varying size. Bournonite in the disseminated and stockwork ores is rare, whereas in the auriferous quartz vein ores it is more common as an interstitial phase (Fig. 16G). Very small grains of boulangerite were found in a sample of the disseminated and stockwork ores. Geerite occurs only on the rim of chalcopyrite (Fig. 16B) and bournonite, and rarely tetrahedrite (Fig. 16G) in the auriferous quartz vein ores. Alloclasite occurs rarely in the disseminated and stockwork ores, as a filling phase less than 10 μm in size (Fig. 15F).

Native gold grains 5 to 40 μm in diameter occur rarely in fractures in pyrite and arsenopyrite (Fig. 15C, E), and along crystal or grain boundaries of ore and gangue minerals in the disseminated and stockwork ores (Fig. 15G). However, native gold was not observed in the disseminated and stockwork ores hosted in diorite dikes and metasedimentary rocks. Native gold in the auriferous quartz vein ores occurs as relatively

large free grains up to 1 cm in diameter, and as microscopic grains a few to 100 μm across (Fig. 16D, F).

In one auriferous quartz vein ore sample, electrum forms veinlets less than 5 μm in width within native gold (Fig. 16H).
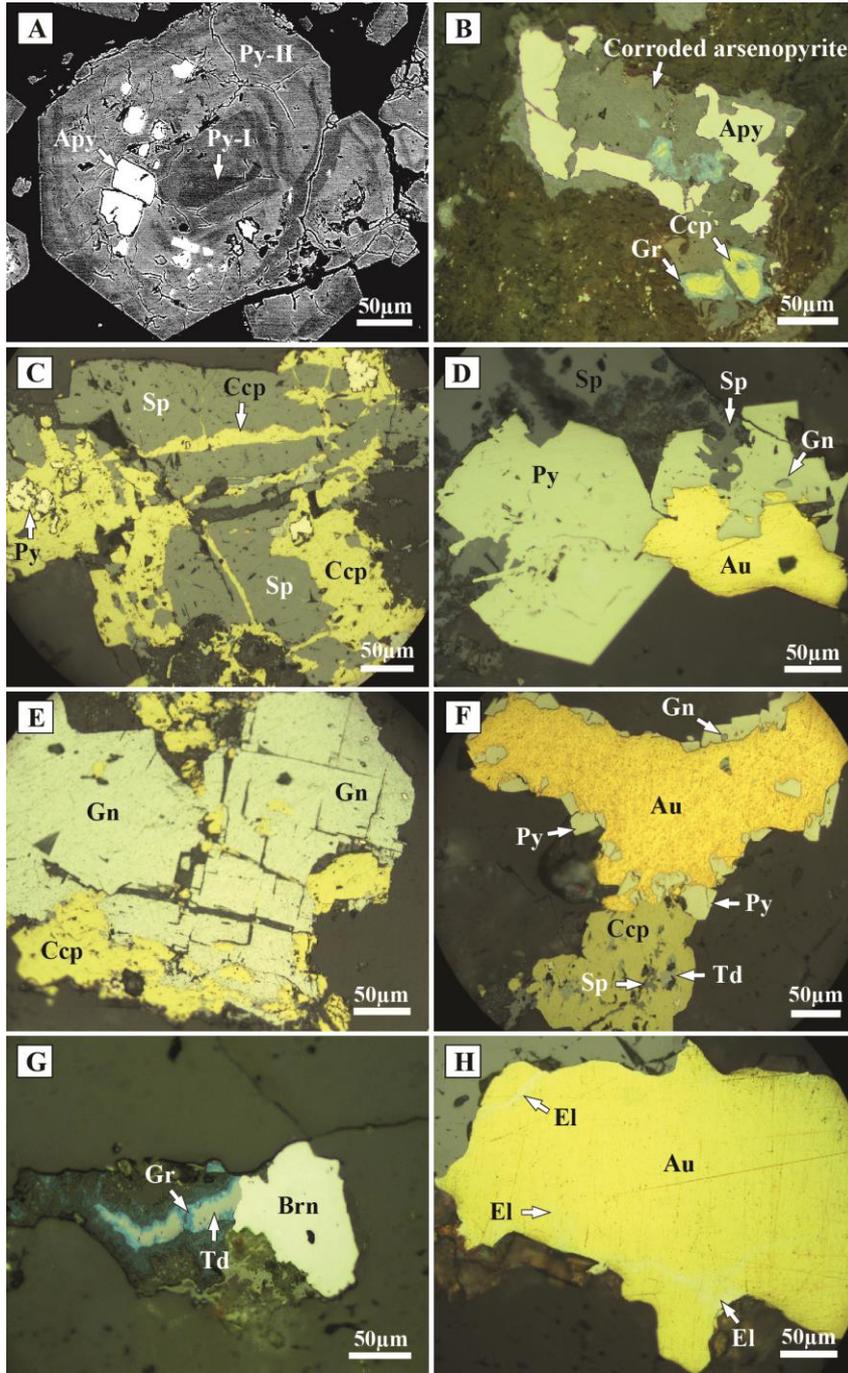
**Fig. 16** Photomicrographs of auriferous quartz vein ores from the Boroo deposit. (A) Early stage pyrite in the core and later stage pyrite in the rim, and associated arsenopyrite (B) Corroded arsenopyrite grain occurring with chalcopyrite and geerite (Gr). (C) Chalcopyrite in fractures in sphalerite. (D) Euhedral pyrite replaced by sphalerite, and covered by native gold. (E) Galena showing cubic habit, and chalcopyrite in fractures and

boundaries of galena. (F) Native gold associated with chalcopyrite and bordered by pyrite grains. (G) Tetrahedrite coexisting with bournonite (Brn) and rimmed by geerite. (H) Electrum (El) occurring as veinlets in coarse grained native gold.

### 5.1.3   Petrography of the Ulaanbulag deposit

The main ore minerals in the deposit are pyrite and arsenopyrite, and minor minerals are chalcopyrite, galena, sphalerite and tetrahedrite. Ore mineral abundances, localities and grain sizes are variable in the disseminated and stockwork ores and siliceous ore types.

Pyrite is the most abundant sulfide in both ores, and occurs in a wide range of grain sizes from 10 μm to 3 mm. It commonly occurs as subhedral to euhedral forms (Fig. 17), and two generations were recognized. Early stage pyrite occurs within later stage pyrite as small grains of 20 μm in diameter. Aggregates consisting of very fine grained anhedral to subhedral pyrite and arsenopyrite (up to 50 μm) form veinlets in the siliceous ores.

Arsenopyrite occurs as euhedral rhombic and prismatic crystals, and forms aggregates with pyrite (Fig. 17). Prismatic crystals of arsenopyrite are abundant in the disseminated and stockwork ores, and rarely form clusters. Two generations of arsenopyrite are recognized: early stage arsenopyrite within later stage ones is anhedral crystals up to 40 μm; later stage arsenopyrite is also euhedral crystals up to 0.2 mm.

Sphalerite is common in the disseminated and stockwork ores and siliceous ores, and grain sizes are variable in both ores. Sphalerite occurs as inclusions (~10 to 50 μm) and fracture filling phase in pyrite and arsenopyrite (Fig. 17).

Galena is not common in the disseminated and stockwork ores and siliceous ores. It usually occurs as a later stage phase than pyrite and arsenopyrite.

Chalcopyrite occurs as inclusions or as filling phase with about 30 μm in size in pyrite and galena. It also occurs as anhedral single grains (up to 100 μm) in the siliceous ores. Chalcopyrite does not show any textural relationship with native gold in the both ores.

Native gold in both the ore types occurs as microscopic native gold (5 to 50 μm) associated with sulfide minerals.
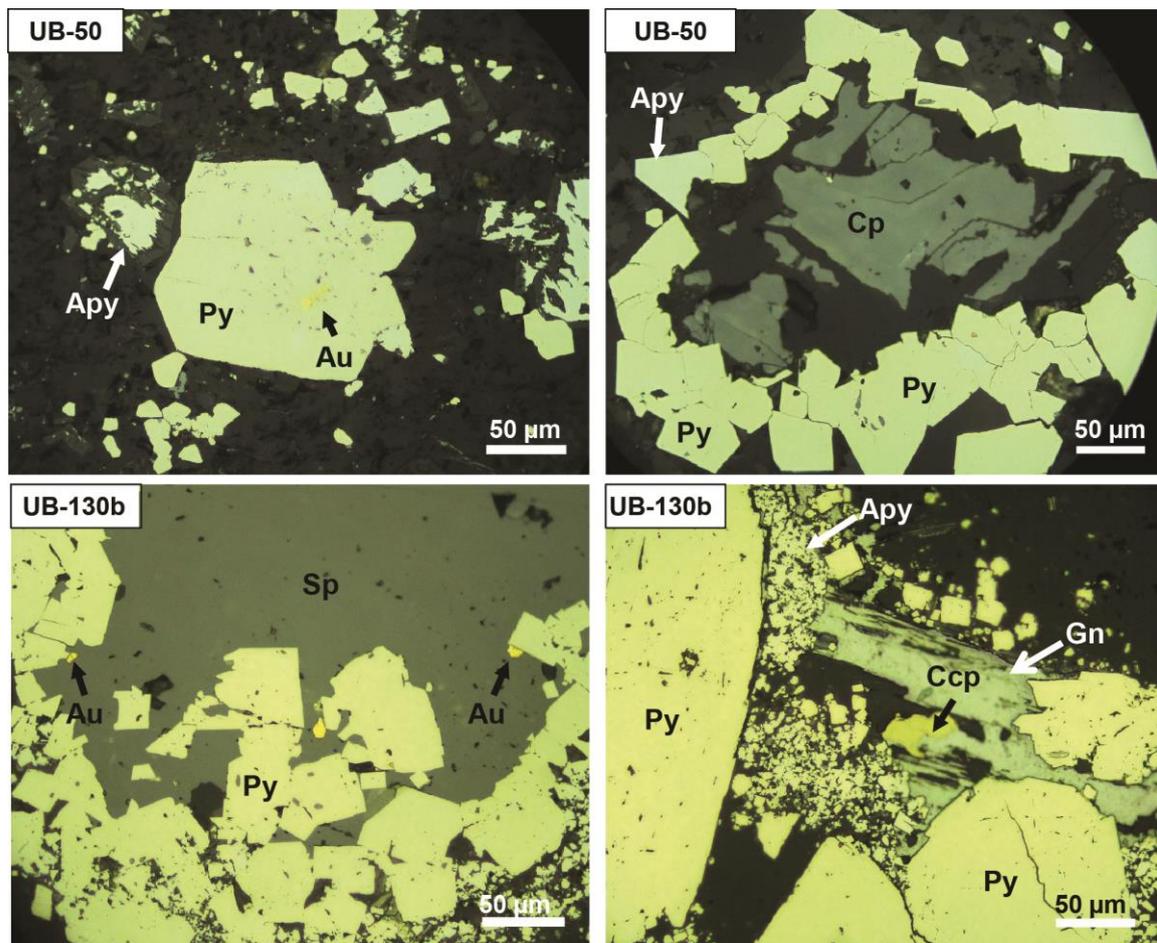


**Fig. 17** Photomicrographs of disseminated and stockwork ores and siliceous ores from the Ulaanbulag deposit. (UB-50) Native gold inclusion in pyrite. (Ub-50) Aggregates of pyrite and arsenopyrite, and associated with sphalerite. (UB-130b) Native gold inclusions in sphalerite, and association with pyrite. (UB-130b) Textural relationships of pyrite, arsenopyrite, chalcopyrite and galena.

### 5.1.4 Petrography of the Khadat deposit

The copper mineralization occurs as vein type ores in the metasedimentary rocks and granodiorite, and the mineral assemblages in ores are varied depending on depth of the deposit. The main ore mineral in the shallow parts of deposit, which from surface to 100s meters in depth, consists of chalcopyrite and its oxidized secondary minerals as malachite and azurite, and very rarely sphalerite and pyrite are observed (Fig. 11A). However, the ores in range from 100 to 200s meters of depth commonly show assemblages of chalcopyrite, sphalerite, galena, pyrite, arsenopyrite and rarely pyrrhotite. These mineral assemblages are formed as filling veins in fractures of the metasedimentary rocks and granodiorite (Fig. 11B), whereas, the ores occurring from 200 to 250s meters of depth represent the disseminated and stockwork mineralization in metasedimentary rocks. It mainly consists of the assemblages of chalcopyrite, pyrite and arsenopyrite (Fig. 11C).

Chalcopyrite is only found as copper-bearing sulfides in the ores. It occurs as large anhedral grains (Fig. 18A) or as massive sulfide with a wide range of size. Chalcopyrite is mostly oxidized in the ores of shallow parts, and is commonly produced secondary ore minerals (Fig. 18B). The occurrence of chalcopyrite in below 100s meters of depth shows common assemblage with pyrite, arsenopyrite, galena and sphalerite, and it is formed as fillings of fractures (Fig. 18D-G). Chalcopyrite also commonly occurs as inclusions and fillings of fissures in sphalerite crystals (Fig. 18C, E).

Pyrite is very rare sulfide in the ores from surface to 100s meters of depth, whereas, it is common sulfide below the 100s meters of depth. It occurs as euhedral to subhedral in forms, and grain size reaches up to 1.5 mm. Pyrite commonly shows textural assemblage with arsenopyrite. At least, three generations of pyrite are recognized in the ores from 200 to 250s meters in depth (Fig. 18H). Early stage, core part of pyrite-I, is crystallized as

euhedral, second stage pyrite-II is surrounded on early stage one, and third stage pyrite-III is rimmed on pyrite-II (Fig. 18H).

Arsenopyrite is another common sulfide in the ores. It occurs as euhedral grains with up to 1 mm in size. Two generations of arsenopyrite are also recognized: arsenopyrite-I is early stage of core part, and arsenopyrite-II is later stage rim parts of grain (Fig. 18I).

Pyrrhotite occurs rarely in the ores which is hosted in granodiorite. It occurs as inclusions or coexisting textures with arsenopyrite and chalcopyrite (Fig. 18D). The grain size of pyrrhotite is around 50 μm.

Sphalerite rarely occurs in the ores up to 100s meters in depth, and is oxidized (Fig. 18C), whereas, it is common sulfide in the ores ranging between 100 and 200s meters in depth. Sphalerite has anhedral forms, and its grain size is variable, largest grains extend up to 3 mm.

Galena commonly occurs in the ores from 100 to 200s meters in depth. It is formed as anhedral large grains, and mostly appears with sphalerite.
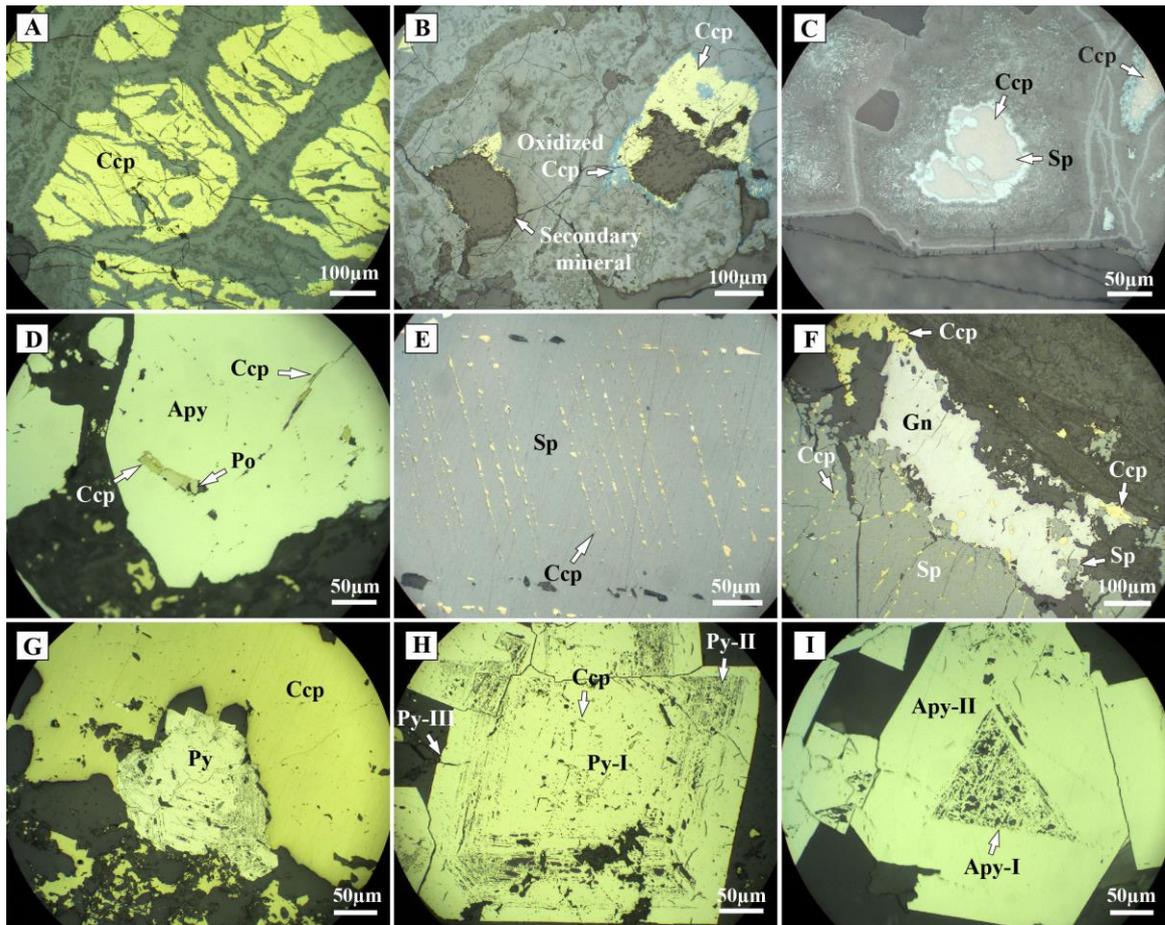
**Fig. 18** Photomicrographs of ores from the Khadat copper deposit. (A) Anhedral grains of chalcopyrite. (B) Oxidized chalcopyrite grains occurring in the shallow parts of ores. (C) Oxidized grains of sphalerite including as inclusions of chalcopyrite. (D) Coexisting texture of chalcopyrite and pyrrhotite in the fracture of arsenopyrite. (E) Chalcopyrite occurring as fillings in fissures of sphalerite crystals. (F) Galena showing coexisting texture with sphalerite, and they are included fine grains of chalcopyrite. (G) Large grain of chalcopyrite surrounding pyrite. (H) Core part pyrite-I including chalcopyrite inclusions, outer part pyrite-II showing some scratches in crystals, and pyrite-III occurring in rim. (I) Early stage arsenopyrite-I occurring with some pores in later stage arsenopyrite-II.

65

## 5.2 Mineral chemistry

### 5.2.1 Mineral chemistry of the Gatsuurt deposit

The chemical compositions of selected ore minerals from the disseminated and stockwork ores, quartz vein ores, and silicified ores are listed in Tables 2, 3 and 4, respectively.

Pyrite-I in the disseminated and stockwork ores has almost ideal composition. In contrast, pyrite-II in the disseminated and stockwork ores exhibits strong chemical zoning (sometimes oscillatory) due to As contents of up to 4.6 wt% (Fig. 19A), and Au up to 0.99 wt% (Table 2). In the quartz vein ores, pyrite-I has ideal composition, whereas pyrite-II contains trace amounts of Au and <0.94 wt% As, but chemical zoning is not remarkable. Pyrites in the silicified ores contain 1.10-4.64 wt% As and up to 0.19 wt% Au (Table 3). Such Au contents are attributed to the presence of so-called "invisible gold", because native gold is not found by ore microscope observation or by electron microprobe analyzer.

Arsenopyrites from the three ore types show significantly low As and high S contents relative to Fe (Tables 2, 3 and 4). Such negative correlation between As and S is explained by substitution of As by S in the arsenopyrite solid solution (Zachariáš et al., 2004). Arsenopyrite-I in the disseminated and stockwork ores shows no detectable chemical variation, whereas arsenopyrite-II exhibits weak chemical zonation due to varying As content, and the presence of some growth bands containing 0.11–0.25 wt% Bi and 0.1–0.23 wt% Pb (Fig. 19B). Arsenopyrite-II in the disseminated and stockwork ores and arsenopyrite in the silicified ores contain up to 0.74 wt% and 0.11 wt% Au, respectively, irrespective of the generation of arsenopyrite (Tables 2, 3). As in the case of pyrite, the Au contents of arsenopyrite is not attributable to the presence of visible gold.

Sphalerites in the disseminated and stockwork ores have Fe contents ranging from nil to 4.71 wt% (8 mol% FeS), whereas maximum Fe contents in those in the quartz vein and silicified ores reach only 2.2 wt% (4 mol% FeS) and 1.41 wt% (2 mol% FeS), respectively. In addition, sphalerite contains small amounts of Cu (0.50 wt%), Pb (0.27 wt%), Bi (0.37 wt%), Sb (0.14 wt%) and W (0.13 wt%), but their concentrations are not dependent on ore type.

Chalcopyrite in the disseminated and stockwork ores and quartz vein ores contain up to 0.2 wt% Au, which also cannot be attributed to the presence of visible native gold.

Tetrahedrite in the disseminated and stockwork ores has Ag, As and Te contents of up to 1.02, 3.03 and 0.25 wt%, respectively. Tetrahedrite and tennantite in the quartz vein ores contain variable amounts of Ag and As, and a small amount of Au (Table 4; Figs. 19C, 8D). The Ag content of tetrahedrite and tennantite reaches 6.34 and 11.95 wt%, respectively. Arsenic content reaches 0.75 wt% in tetrahedrite and 12.48 wt% in tennantite. Gold content reaches 0.33 wt%.

Native gold in the three ore types shows variable composition. That in the disseminated and stockwork ores is most auriferous, containing up to 97.97 wt% Au and 1.09 wt% Ag. Maximum Au content of native gold in the quartz vein ores is lower at 92.73 wt% Au, and 7.45 wt% Ag, and that in the silicified ores lower still at 90.88 wt% Au and 8.78 wt% Ag.

Boulangerite, jamesonite and bournonite in the disseminated and stockwork ores have chemical compositions almost identical with their ideal formulae of $Pb_5Sb_4S_{11}$, $Pb_4FeSb_6S_{14}$ and $PbCuSbS_3$, respectively, but all contain small to very small amount of As. Chemical compositions of bournonite, geocronite $Pb_{14}(Sb,As)_6S_{23}$ and geerite $Cu_8S_5$

in the quartz vein ores also are close to ideal chemical compositions. The Sb:As ratio of geocronite is about 4: 1 (Table 3).
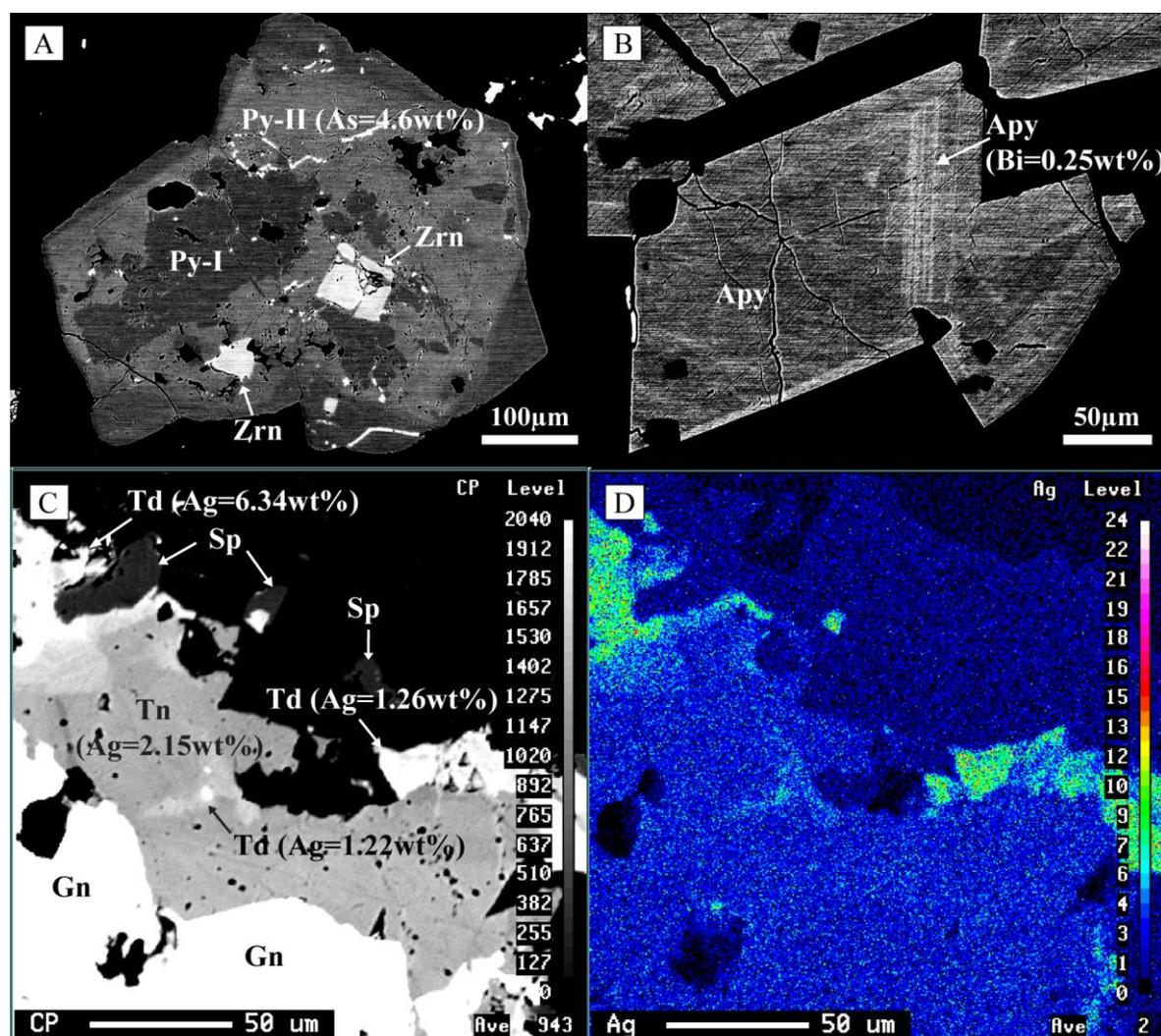


**Fig. 19** Backscattered electron(BSE) images showing compositional difference of pyrite and arsenopyrite in the disseminated and stockwork ores, and X-ray map showing Ag distribution in tetrahedrite-tennantite in the quartz vein ores. (A) Arsenic rich later stage pyrite and arsenic-free early stage pyrite zonations with inclusions of subhedral zircons. (B) Bi-Pb-bearing narrow growth zonation occurring in arsenopyrite crystal. (C) Tetrahedrite-tennantite textural relation with galena and sphalerite. (D) Ag distribution map of tetrahedrite-tennantite.

### 5.2.2  Mineral chemistry of the Boroo deposit

The chemical compositions of ore minerals from the disseminated and stockwork ores and auriferous quartz vein ores are listed in Tables 5 and 6, respectively.

Pyrite-I has almost ideal composition in both the disseminated and stockwork ores and auriferous quartz vein ores (Tables 5 and 6). However, it contains trace amounts of Au, Pb, Bi and Co in both ore types, with maximum values of 0.20, 0.69, 0.40 and 0.38 wt%, respectively. Pyrite-II in the disseminated and stockwork ores contains up to 4.50 wt% arsenic. Pyrite-II in the auriferous quartz vein ores contains 2.79 wt% As at maximum, and its As content is always less than that of pyrite-II in the disseminated and stockwork ores (Tables 5 and 6). A negative correlation exists between As and S in pyrite-II, indicating substitution of As for S in the pyrite structure (Fleet et al., 1993; Blanchard et al., 2007). Pyrite-II in both ore types contains small amounts of Au, Cu, Pb, Bi, Sb, Co, Cd and Ni, with maximum amounts of 0.19, 0.49, 0.44, 0.50, 0.98, 0.23, 0.07 and 0.87 wt%, respectively. However, detection of these elements detections in pyrite-II is variable. Very rarely fine-grained euhedral pyrite (generation is not recognized) in the auriferous quartz vein ores contains 0.16 to 2.48 wt% Co and up to 1.11 wt% Ni, and these contents of these metals show oscillatory zoning within pyrite (Fig. 20A, B, C).

Arsenopyrite-I is relatively poor in As with around 0.71 atoms per formula unit (apfu) per S = 1, whereas As content in arsenopyrite-II reaches 0.81 apfu, and only one analysis showed nearly ideal As content of 1.0 apfu. Arsenopyrite in the auriferous quartz vein ores does not show significant compositional difference, and is considered to have formed as a single generation phase. The As content of arsenopyrite in the auriferous quartz vein ores ranges between 0.79 and 0.90 apfu. Arsenopyrite contains commonly trace amounts of Au, Cu, Pb, Bi, Co and Ni, with maximum contents of 0.28, 1.10, 0.32,

0.62, 0.65 and 0.93 wt%, respectively. These contents of these metals are variable, and do not depend on the generation of arsenopyrite or ore type. However, Au contents of arsenopyrite usually increase with increasing As content in both ore types (Tables 5 and 6; Fig. 20D, E, F).

Sphalerite occurring as fine grains within pyrite and arsenopyrite contains up to 4.95 wt% Fe, and shows no compositional zoning in either ore type. Coarse-grained or single phase sphalerite in gangue mineral contains less than 1.30 wt% Fe. Pb, Bi, Mn, Cd and W were detected as trace metals in sphalerite, with maximum values of 0.35, 0.53, 0.04, 0.08 and 0.19 wt%, respectively.

Galena in both the ore types contains Bi in a range between 0.12 and 2.30 wt%, and small amounts of Ag and Cd.

Chalcopyrite in both ore types has almost ideal chemical composition of $Cu_{0.97}Fe_{1.02}S_2$. Although Bi, Pb and Au (up to 0.43, 0.27 and 0.19 wt%, respectively) were also detected in chalcopyrite, these may be attributed to the presence of nano-grains.

Tetrahedrite in the disseminated and stockwork ores shows chemical variation caused by substitutions of Ag for Cu and of As for Sb. However, the maximum Ag and As contents are only 0.78 and 1.52 wt%, respectively. Tetrahedrite in the auriferous quartz vein ores exhibits very strong internal textures due to significant compositional differences. Tetrahedrite in the veins is considerably enriched in Ag, with abundances reaching 5.29 wt% (Table 6; Fig. 20G, H), and also contains Bi and Cd (maximums of 1.05 and 0.17 wt%, respectively). Tennantite rarely occurs on the rim of tetrahedrite, but only in the auriferous quartz vein ores. This tennantite contains up to 6.94 wt% Ag (Table 6).
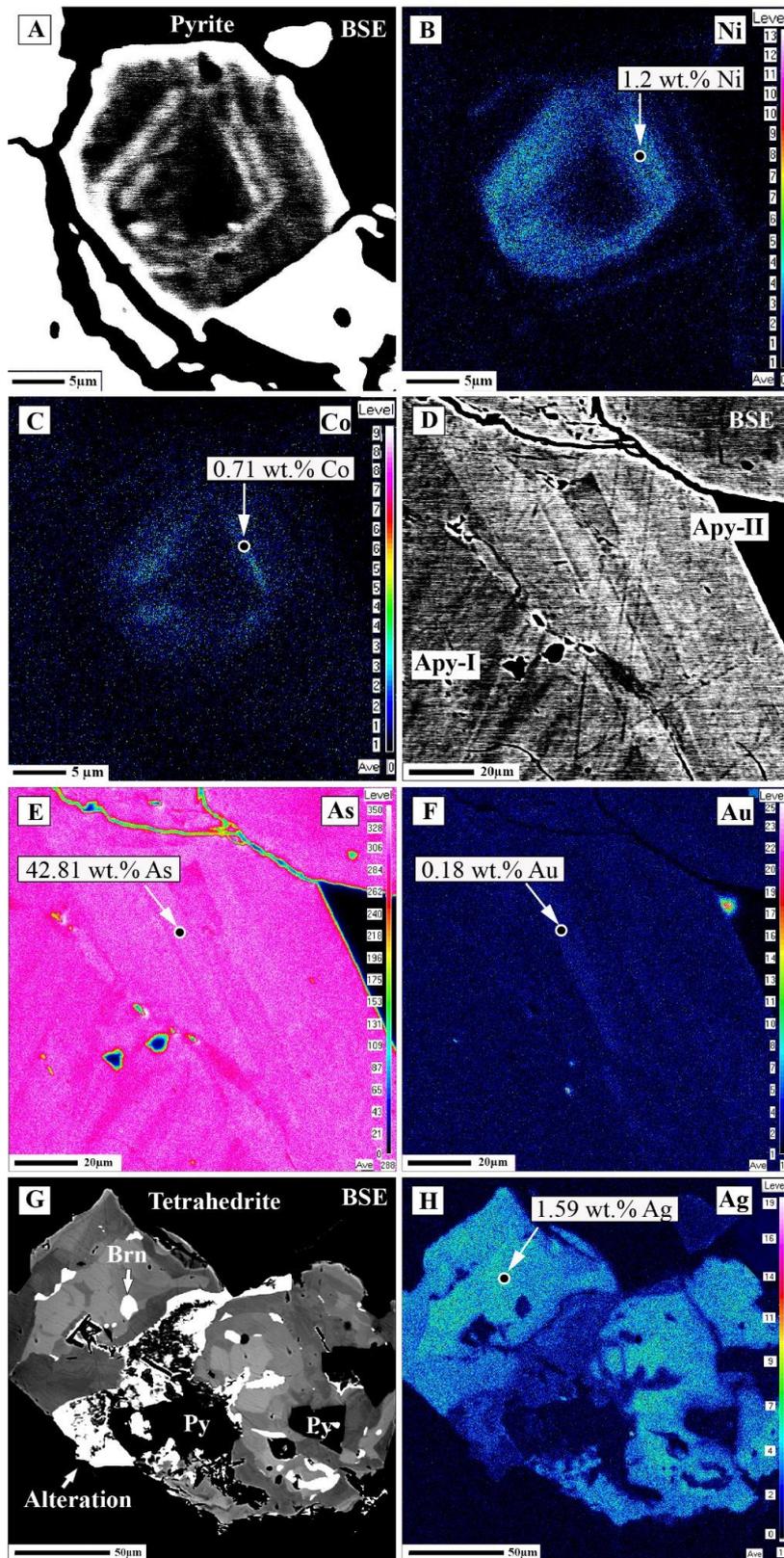
**Fig. 20** Backscattered electron (BSE) images and X-ray maps showing compositional differences and zonations of pyrite, arsenopyrite and tetrahedrite in the disseminated and

71

stockwork ores and in the auriferous quartz vein ores. (A) Euhedral pyrite showing oscillatory zoning. (B) Nickel distribution map in pyrite with oscillatory zoning. (C) Cobalt distribution map in pyrite with oscillatory zoning. (D) Later stage arsenopyrite-II rimming early stage arsenopyrite-I. (E) Arsenic distribution map in arsenopyrite. (F) Gold distribution map in arsenopyrite. (G) Tetrahedrite showing variable zoning, and textural relation with bournonite. (H) Silver distribution map in tetrahedrite.

Bournonite and boulangerite compositions almost match their ideal formulae of $PbCuSbS_3$ and $Pb_5Sb_4S_{11}$, but regularly contain trace amounts of Bi ( $< 0.71$ wt%), As ( $< 0.74$ wt%), and Cd ( $< 0.24$ wt%) (Tables 5 and 6).

Geerite often occurs in the rims of tetrahedrite and chalcopyrite, but it is difficult to obtain precise chemical data. The best analysis showed an atomic ratio of Cu:S = 8.57:5 (Table 5).

Alloclasite is rich in Ni, with contents ranging from 9.70 to 18.38 wt%. Co contents are negatively correlated with Ni content, and fall as low as 5.14 wt%, suggesting Ni ↔ Co substitution. Such compositional variation is observed in solid solutions occurring in the Fe-Co-Ni-As-S system (Hem and Makovicky, 2004).

Native gold in the disseminated and stockwork ores has Au and Ag contents ranging between 85.22 and 92.82 wt% and from 13.47 to 7.77 wt%, respectively. In contrast, Au and Ag contents in native gold in the auriferous quartz vein ores range between 93.29 and 96.56 wt% and 7.68 and 4.88 wt%, respectively (Tables 5 and 6). The Au/Ag ratio of native gold varies significantly between grain sizes, with low ratios in coarse grained gold, and higher ratios in finer grains. However, native gold does not show

72

any zonation caused by Ag contents. Native gold contains small amounts of Te 0.59-1.73 wt% and Cd 0.61 wt%.

Electrum contains 52.9 to 77.2 wt% Au, 22.93 to 42.69 wt% Ag, 0.15 to 0.76 wt% Te, and up to 2.03 wt% Cd.

### 5.2.3  Mineral chemistry of the Ulaanbulag deposit

Most pyrite grains exhibit chemical zoning. Early generation pyrite-I rarely contains Ni up to 0.12 wt% and Co reaches up to 3.17 wt%, whereas later generation pyrite-II contains constantly As up to 4.9 wt%, and shows concentric chemical zoning with As.

Arsenopyrite has also a strong chemical zonation due to As-deficiency. Compositional difference was detected between early and later generation arsenopyrite. Pyrite-II and arsenopyrite-II in both ore types contain Au up to 0.09 and 0.13 wt%, respectively. Such Au contents are attributed to "invisible" gold, because native gold grains were not observed under the ore microscope and EPMA analyses.

Sphalerite in the disseminated and stockwork ores contains up to 4.42 wt% Fe, and shows no compositional zoning in either ore type. Sphalerite in the siliceous ores contains less than 1.08 wt% Fe. Manganese, Co, Cd, Bi, As and Au were detected as trace metals in sphalerite, with maximum values of 0.03, 0.03, 0.22, 0.20, 0.17 and 0.07 wt%, respectively.

Galena in both the ore types consistently contains Cd, Bi and Ag in a range between 0.04 - 0.16, 0.24 - 1.41, and 0.05 – 0.49 wt%, respectively.

Chalcopyrite in both ore types has almost ideal chemical composition of $Cu_{0.97}Fe_{1.02}S_2$.

Bournonite and boulangerite have same compositions their ideal formulae of $PbCuSbS_3$ and $Pb_5Sb_4S_{11}$, and there is not detected any elevated compositions of other metals.

Native gold grains contain 86.67-87.97 wt% Au, 15.09-16.27 wt% Ag and 0.59-1.73 wt% Te. Au:Ag ratios of native gold in the both ore types are constant.

## 5.3    Wall rock alteration analysis in the Gatsuurt deposit

Sericite, quartz, albite and microcline gangue minerals were identified by X-ray powder diffraction in the disseminated and stockwork ores, whereas only quartz was identified in the quartz vein ores and silicified ores. In the disseminated and stockwork ores, sericite and quartz are regarded as alteration minerals produced by the reaction of $2H^+ + 2NaAlSi_3O_8$ (albite) $+ KAlSi_3O_8$ (microcline) $\rightarrow KAl_3Si_3O_{10}(OH)_2$ (muscovite) $+ 2Na^+ + 6SiO_2$ (quartz). These alteration minerals indicate that the Gatsuurt deposit was subjected to both sericitic and siliceous alteration. Sericitic alteration occurs with significant sulfidization in the disseminated and stockwork ores, and siliceous alteration is also common. The assemblage of gangue minerals in the Gatsuurt deposit suggests circulation of a weekly acidic pH hydrothermal fluid.

**Table 7** Hydrothermal alteration minerals in each ore type of the Gatsuurt deposit.

| Ore types | Alteration minerals |
|---|---|
| Intrusion hosted ore | sericite, K-feldspar, albite, quartz |
| Discrete quartz vein hosted ore | quartz |
| Silicified zone hosted ore | quartz |

## 5.4 Fluid inclusion analysis

### 5.4.1 Fluid inclusion study on the Gatsuurt deposit

In the disseminated and stockwork ores, fluid inclusions occur within quartz as clusters and as two- or three-dimensional arrays. Three types of fluid inclusions were recognized using optical microscopy, based on constituent phases in the fluid inclusions at room temperature, following the criteria outlined by Roedder (1984). In this study, only the homogenization temperatures of fluid inclusions were measured, as other microthermometric data could not be determined due to decrepitation and the small size of the inclusions. Type I fluid inclusions are defined by the three-phase assemblage of aqueous liquid phase + liquid $CO_2$ + $CO_2$ gas, and the two-phase assemblage of aqueous liquid phase + liquid $CO_2$ (Fig. 21A) at room temperature. Type I assemblages are the most abundant among all types of fluid inclusions. Type I inclusions are subdivided into two types: Type Ia is characterized by a larger $CO_2$ liquid phase than aqueous liquid (>50% of the volume by visual estimate); Type Ib contains is more than 50 vol% aqueous liquid. Most type I fluid inclusions occur as isolated clusters showing three dimensional arrays, and are interpreted to be primary fluid inclusions. Type I inclusions vary from 10 to 30 μm in size, and have rounded, irregular, and rectangular shapes. Type II aqueous fluid inclusions are defined by two-phase assemblages of aqueous liquid and vapor at room temperature (Fig. 21B). The volume of vapor is <50 % of the total volume of the inclusion. These inclusions have round to negative shapes, and are 5-15 μm in size. Primary fluid inclusions have particular shapes elongated to the growth direction of the host quartz crystal. Secondary fluid inclusions trapped by healing of micro-fractures typically occur on micro-fracture planes or on curved surfaces that cut the growth zonation of the host mineral (Fig. 21C). Type III fluid inclusions consist of aqueous

liquid, halite and liquid $CO_2$ phases (Fig. 21D). These inclusions are irregular to rounded in shape, 25-30 μm in size, and are classified as primary. Sample AM-7 from the disseminated and stockwork ores in the Main zone contains type I, II and III fluid inclusions with homogenization temperatures of 194 – 327°C, 194 – 282°C and 208 – 240°C, respectively. Sample GT-172a from the disseminated and stockwork ores in the Central zone contains type I and II fluid inclusions with homogenization temperatures of 289 – 355°C and 254 – 292°C, respectively (Fig. 22).
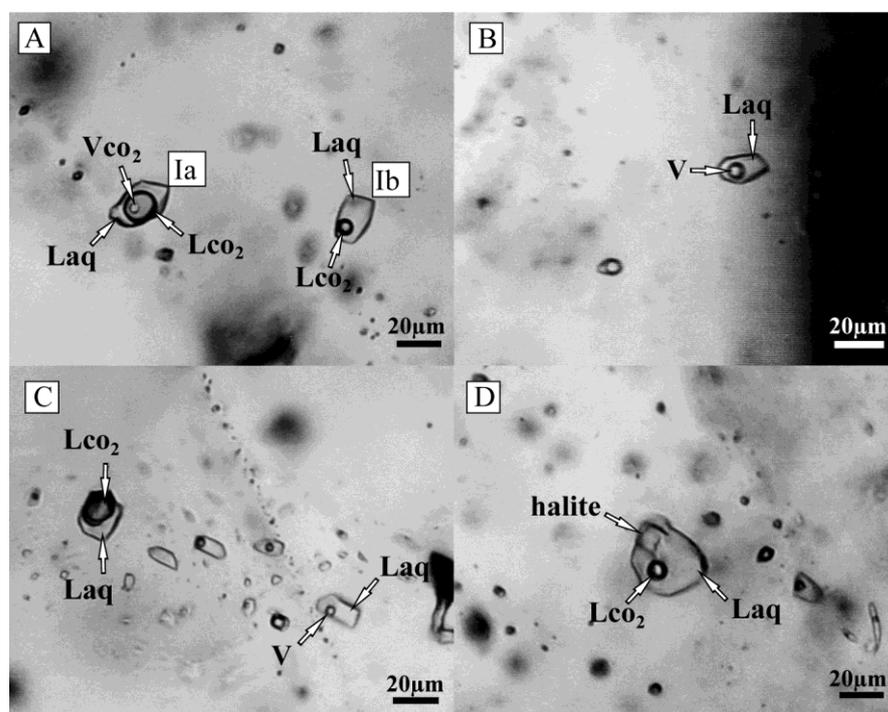


**Fig. 21** Photomicrographs of fluid inclusions in quartz of the disseminated and stockwork ores from the Main and Central zones in the Gatsuurt deposit. (A) $CO_2$-rich type I inclusions: $CO_2$-bearing three-phase ($V_{CO_2}$-$L_{CO_2}$-Laq) inclusions (Ia); $CO_2$ volume less than aqueous liquid inclusions (Ib). (B) Aqueous type II inclusion. (C) Secondary aqueous and $CO_2$-bearing fluid inclusions. (D) Halite-bearing type III inclusion. $V_{CO_2}$, $CO_2$ gas; $L_{CO_2}$, liquid $CO_2$; Laq, aqueous liquid; V, vapor.
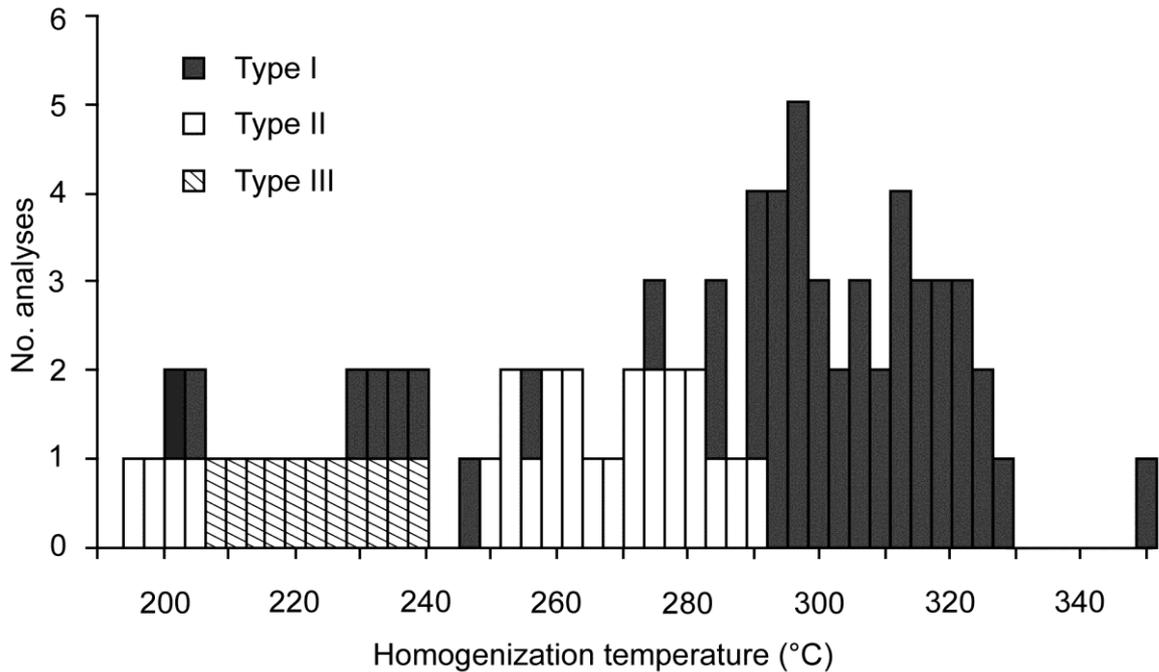
**Fig. 22** Histogram of homogenization temperatures of the primary fluid inclusions in quartz of the disseminated and stockwork ores of the Main and Central zones.

### 5.4.2 Fluid inclusion study on the Boroo deposit

Two generations of quartz veins, which are narrow quartz veins and discrete quartz veins in granite have been selected for fluid inclusion study. Two types of primary fluid inclusions are identified: (I) $CO_2$-rich inclusions and (II) aqueous inclusions (Fig. 23). Type I inclusions are abundant in veins with variable sizes (5-30 μm) hosted in granite, and subdivided into three types: (Ia) $Laq+Lco_2+Vco_2$, (Ib) $Laq+Lco_2$ and (Ic) $Lco_2$. Type II inclusions are small in size (5-15 μm), and common in discrete quartz vein. Homogenization temperatures of type I and II were at 317 to 362ºC and 237 to 305ºC, and corresponding salinities were 3 to 6 wt% and 3.6 to 5.4 wt% (NaCl equiv.), respectively (Fig. 23).
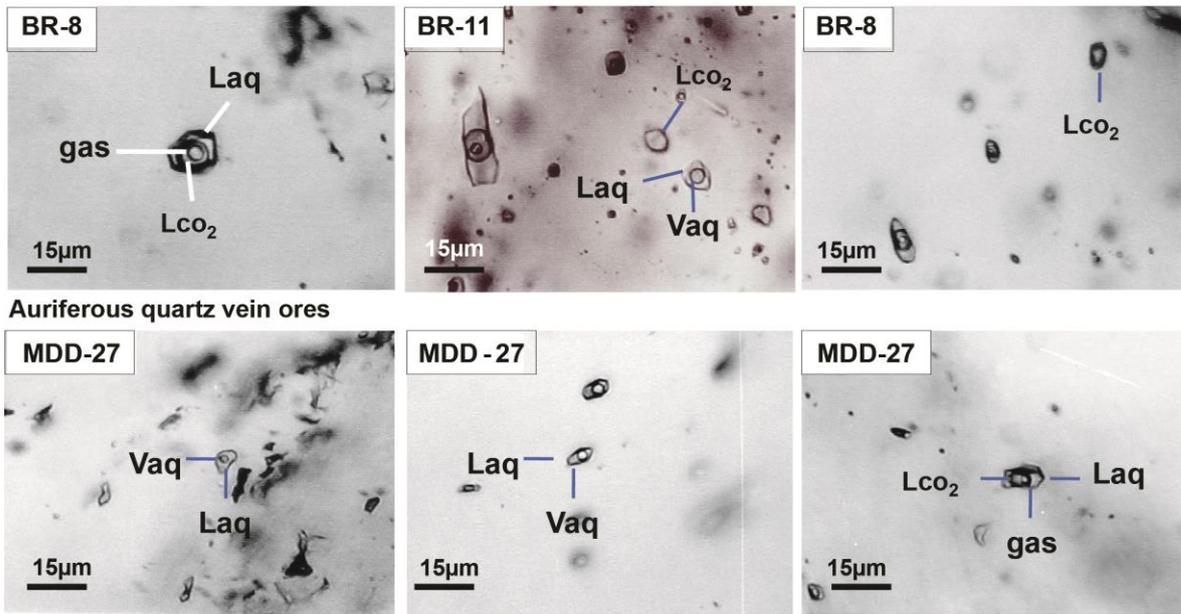
**Fig. 23** Photomicrographs of fluid inclusions in quartz of the disseminated and stockwork ores and auriferous quartz vein ores from the Boroo deposit. $Lco_2$, liquid $CO_2$; Laq, aqueous liquid; V, vapor.

## 5.5 Age dating analysis

### 5.5.1 Zircon LA-ICP-MS U-Pb age dating in the Boroo deposit

U-Pb dating of twelve, ten and thirteen zircon grains of granite near the Boroo deposit, granite in the ore zone 3 of Boroo deposit, and diorite dike in the ore zone 5, respectively, were determined by analyzing Pb and U contents at 14, 10 and 12 positions for zircons using LA-ICP-MS (Tables 8, 9, 10 and Figs. 24, 26, 28). Concordia diagrams are shown in Figures 25, 27 and 29. Two samples are granite (KH-01, BR-16), and another one is diorite (BR-19).

Zircon grains from granite (KH-01) show very strong magmatic oscillatory zoning in backscattered electron (BSE) images (Fig. 24). Zircons are prismatic in shape, and core domain carries some mineral inclusions. The weighted mean age ($^{206}$Pb/$^{238}$U) of all points is 467.5 ± 5.1 Ma (95% conf.). Th/U-ratios are 0.22 - 0.75 > 0.1. These ages correlate with 467.5 ± 5.1 Ma that corresponds to the timing of the igneous event of the granite.

Cathodoluminescence (CL) images of zircons from granite (BR-19) show also magmatic oscillatory zoning in the rims (Fig. 25). Zircons are prismatic in shape. Determined $^{206}$Pb/$^{238}$U ages denote contemporary rims and cores of the zircons within error. The weighted mean age ($^{206}$Pb/$^{238}$U) of all points is 472.5 ± 6.9 Ma (95% conf.). Th/U-ratios are 0.30 - 0.57 > 0.1.

Zircon grains from diorite (BR-19) show irregular and weakly igneous oscillatory zoning, as shown by CL and BSE images (Fig. 26). Zircons are needles in shape. The analyzed spot $^{206}$Pb/$^{238}$U ages present 465.4 ± 3.0 Ma (95 % conf.). Th/U-ratios are 0.75 – 5.24 > 0.1.

**Table 8** Summary of age dating LA-ICP-MS analysis in zircons from granite, near the Boroo deposit.

| Spot Label | $^{206}Pb/^{238}U$ age | err 6/8 age | $^{207}Pb/^{235}U$ age | err 7/5 age | $^{207}Pb/^{206}Pb$ age | err 7/6 age | Th/U | disc. |
|---|---|---|---|---|---|---|---|---|
| 1KH-01-A | 439.6 | 14.0 | 438.4 | 20.5 | 432.2 | 105.9 | 0.661 | -0.3% |
| 2KH-01-A | 474.2 | 13.7 | 474.7 | 17.2 | 477.4 | 74.7 | 0.278 | 0.1% |
| 3KH-01-A | 458.2 | 14.2 | 448.6 | 18.3 | 399.6 | 87.5 | 0.458 | -2.1% |
| 4KH-01-A | 472.5 | 15.1 | 485.6 | 16.7 | 548.3 | 60.1 | 0.402 | 2.8% |
| 5KH-01-A | 476.3 | 13.8 | 478.8 | 17.3 | 491.3 | 74.5 | 0.223 | 0.5% |
| 6KH-01-A | 474.1 | 13.3 | 474.3 | 14.9 | 475.3 | 58.5 | 0.360 | 0.0% |
| 7KH-01-A | 461.7 | 16.5 | 461.9 | 21.4 | 463.0 | 98.2 | 0.745 | 0.0% |
| 8KH-01-A | 468.8 | 14.5 | 486.7 | 23.9 | 572.2 | 117.3 | 0.453 | 3.8% |
| 9KH-01-A | 459.3 | 15.5 | 471.5 | 19.8 | 531.0 | 85.4 | 0.657 | 2.7% |
| 10KH-01-A | 470.4 | 15.0 | 471.5 | 16.3 | 477.0 | 60.9 | 0.366 | 0.2% |
| 11KH-01-A | 443.0 | 18.0 | 447.0 | 47.4 | 468.2 | 293.1 | 0.426 | 0.9% |
| 12KH-01-A | 470.7 | 15.5 | 486.0 | 18.7 | 558.7 | 75.9 | 0.224 | 3.3% |
| 13KH-01-A | 466.4 | 16.7 | 481.1 | 18.2 | 551.9 | 64.6 | 0.341 | 3.2% |
| 14KH-01-A | 469.1 | 15.4 | 470.9 | 17.9 | 479.4 | 74.7 | 0.270 | 0.4% |
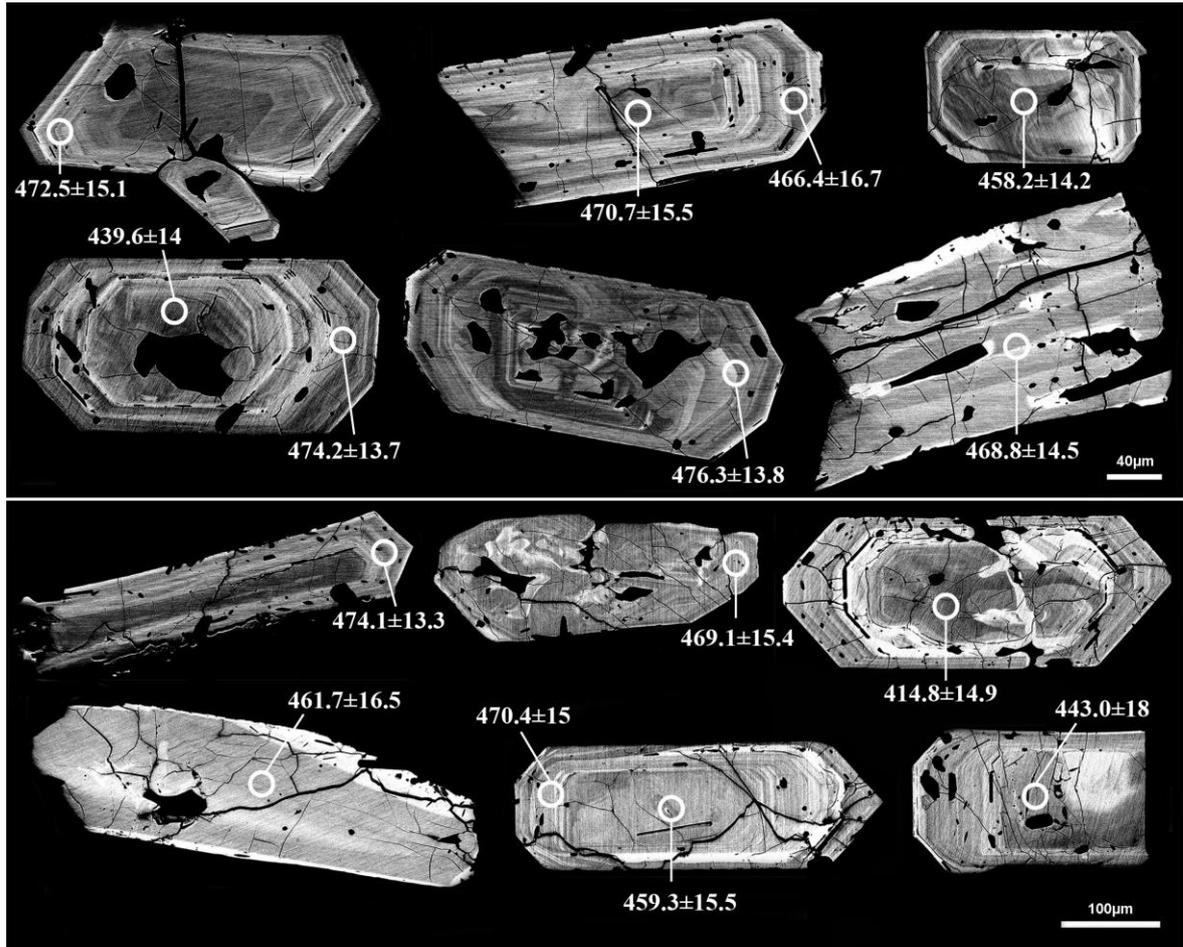
**Fig. 24** Backscattered electron (BSE) images of zircon grains, and their analyzed positions with age values from granite of near the Boroo deposit.
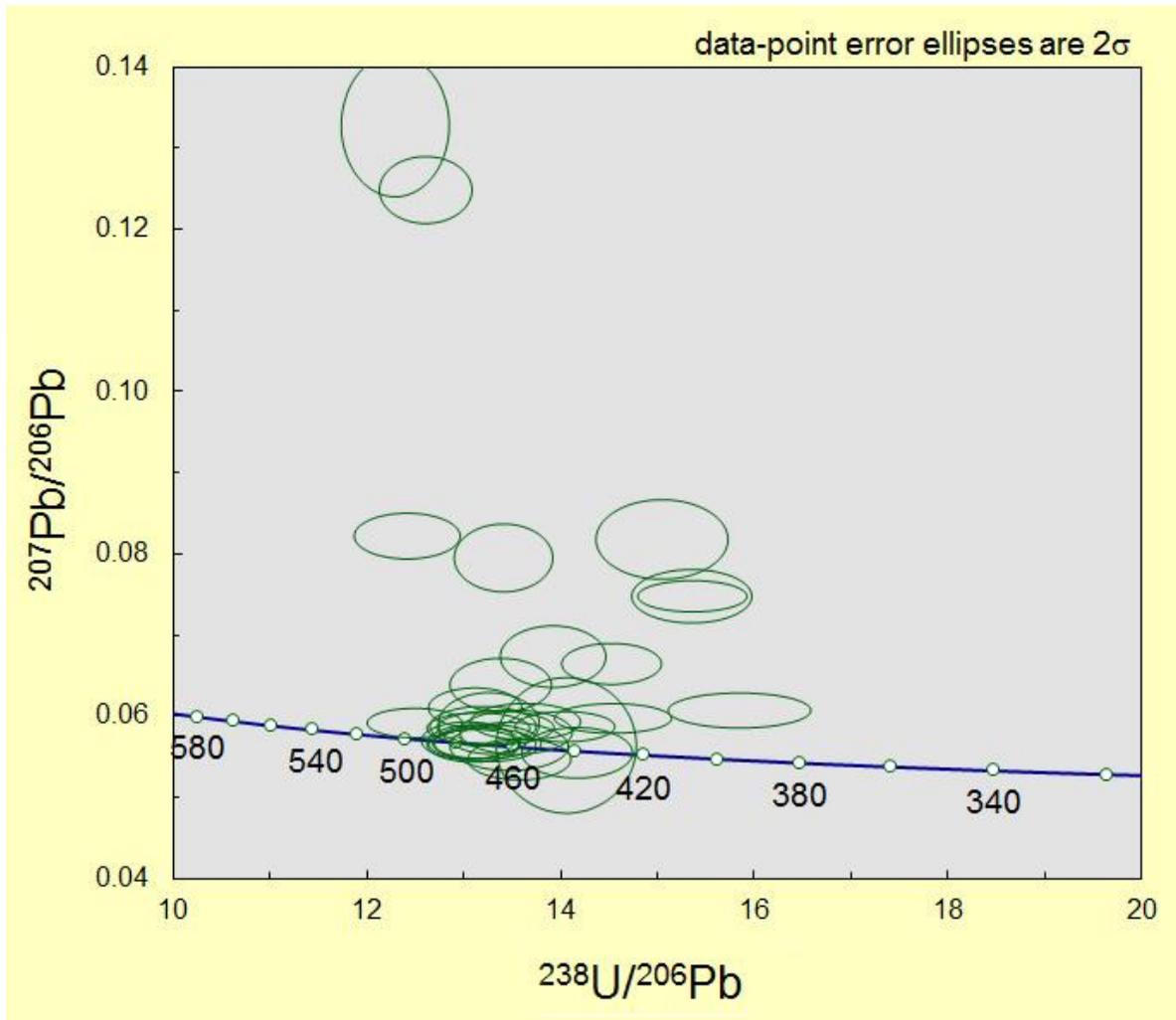
**Fig. 25** Concordia diagram showing LA-ICP-MS analysis in zircons from granite in near the Boroo deposit.

**Table 9** Summary of age dating LA-ICP-MS analysis in zircons from granite in the ore zone 3, Boroo deposit.

| Spot Label | $^{206}Pb/^{238}U$ age | err 6/8 age | $^{207}Pb/^{235}U$ age | err 7/5 age | $^{207}Pb/^{206}Pb$ age | err 7/6 age | Th/U | disc. |
|---|---|---|---|---|---|---|---|---|
| 1BR-16.csv | 488.3 | 15.5 | 494.4 | 15.8 | 522.8 | 51.3 | 0.431 | 1.2% |
| 2BR-16.csv | 466.8 | 15.3 | 475.7 | 19.2 | 518.9 | 81.1 | 0.304 | 1.9% |
| 3BR-16.csv | 470.6 | 13.6 | 469.9 | 15.9 | 466.3 | 67.8 | 0.471 | -0.1% |
| 4BR-16.csv | 461.6 | 14.3 | 459.4 | 17.1 | 448.1 | 75.0 | 0.479 | -0.5% |
| 5BR-16.csv | 472.6 | 17.3 | 468.0 | 20.5 | 445.7 | 89.1 | 0.385 | -1.0% |
| 6BR-16.csv | 469.7 | 15.0 | 482.3 | 17.8 | 542.8 | 71.5 | 0.312 | 2.7% |
| 7BR-16.csv | 463.2 | 14.8 | 470.6 | 17.5 | 506.7 | 71.9 | 0.565 | 1.6% |
| 8BR-16.csv | 486.8 | 17.8 | 500.5 | 22.0 | 563.8 | 89.6 | 0.375 | 2.8% |
| 9BR-16.csv | 469.6 | 20.0 | 485.9 | 25.4 | 563.1 | 108.2 | 0.563 | 3.5% |
| 10BR-16.csv | 483.9 | 17.3 | 473.7 | 17.6 | 424.8 | 63.7 | 0.312 | -2.1% |
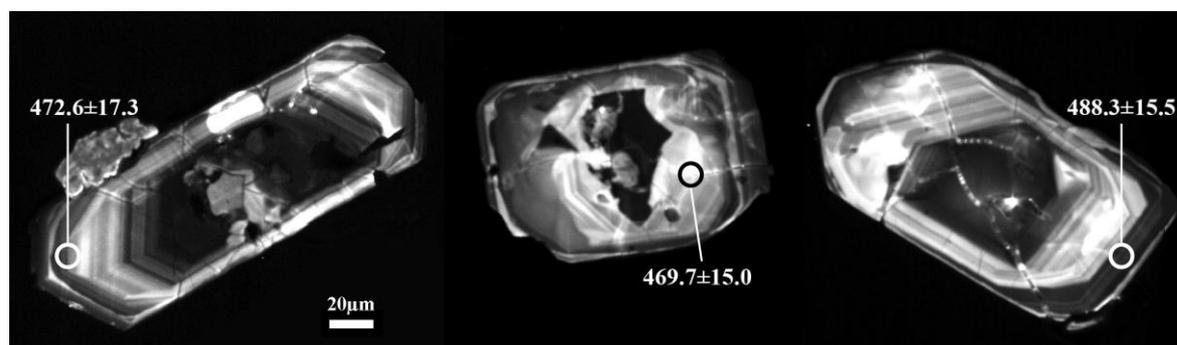


**Fig. 26** Cathodoluminescence (CL) images of zircon grains, and their analyzed positions with age values from granite in the ore zone 3 of the Boroo deposit.
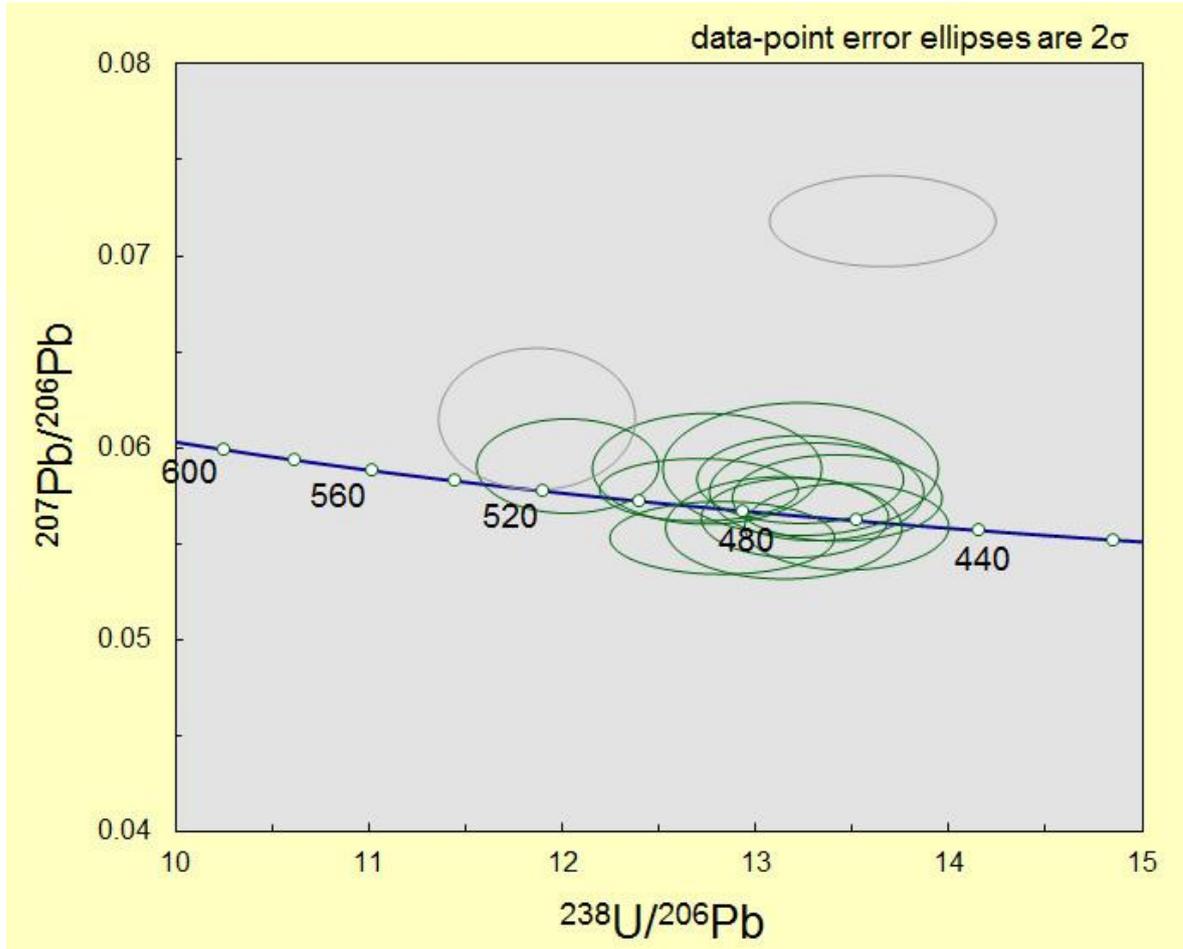
**Fig. 27** Concordia diagram showing LA-ICP-MS analysis in zircons from granite in the ore zone 3 of the Boroo deposit.

**Table 10** Summary of age dating LA-ICP-MS analysis in zircons from diorite dike in the

ore zone 5, Boroo deposit.

| Spot Label | $^{206}Pb/^{238}U$ age | err 6/8 age | $^{207}Pb/^{235}U$ age | err 7/5 age | $^{207}Pb/^{206}Pb$ age | err 7/6 age | Th/U | disc. |
|---|---|---|---|---|---|---|---|---|
| 1BR-19.csv | 469.0 | 14.0 | 474.7 | 19.9 | 502.8 | 95.2 | 1.262 | 1.2% |
| 2BR-19.csv | 468.7 | 14.5 | 466.6 | 27.3 | 456.5 | 148.7 | 0.758 | -0.4% |
| 3BR-19.csv | 466.5 | 13.1 | 463.3 | 14.2 | 447.7 | 54.2 | 0.901 | -0.7% |
| 4BR-19.csv | 469.9 | 13.6 | 462.2 | 14.2 | 424.0 | 52.1 | 0.937 | -1.6% |
| 5BR-19.csv | 470.7 | 13.2 | 478.6 | 14.2 | 516.3 | 51.3 | 2.053 | 1.7% |
| 6BR-19.csv | 478.3 | 15.7 | 482.9 | 15.1 | 504.7 | 44.6 | 1.596 | 1.0% |
| 7BR-19.csv | 471.3 | 17.7 | 472.2 | 40.8 | 476.7 | 235.2 | 0.749 | 0.2% |
| 8BR-19.csv | 466.5 | 13.5 | 458.9 | 16.8 | 421.2 | 75.4 | 2.244 | -1.6% |
| 9BR-19.csv | 470.6 | 13.6 | 490.4 | 16.5 | 584.0 | 66.5 | 1.909 | 4.2% |
| 10BR-19.csv | 457.8 | 12.8 | 459.8 | 25.8 | 469.5 | 145.9 | 1.029 | 0.4% |
| 11BR-19.csv | 463.3 | 12.1 | 473.8 | 14.9 | 525.2 | 62.6 | 1.181 | 2.3% |
| 12BR-19.csv | 461.7 | 11.6 | 463.2 | 15.7 | 470.8 | 74.7 | 1.184 | 0.3% |
| 13BR-19.csv | 473.2 | 13.7 | 473.1 | 15.2 | 472.5 | 58.5 | 3.190 | 0.0% |
| 14BP-19.csv | 462.2 | 12.9 | 460.9 | 15.3 | 454.0 | 65.7 | 0.745 | -0.3% |
| 15BP-19.csv | 470.4 | 13.6 | 458.3 | 14.1 | 397.9 | 52.4 | 5.238 | -2.6% |
| 16BP-19.csv | 463.9 | 13.4 | 468.0 | 14.3 | 488.0 | 53.9 | 1.590 | 0.9% |
| 17BP-19.csv | 464.0 | 14.3 | 482.5 | 16.7 | 571.6 | 62.1 | 1.631 | 4.0% |
| 18BP-19.csv | 454.0 | 13.6 | 461.7 | 14.6 | 499.8 | 51.4 | 1.288 | 1.7% |
| 19BP-19.csv | 456.9 | 12.4 | 454.6 | 14.0 | 442.8 | 56.5 | 1.134 | -0.5% |
| 20BP-19.csv | 456.2 | 19.0 | 453.7 | 43.7 | 440.7 | 262.8 | 0.711 | -0.5% |
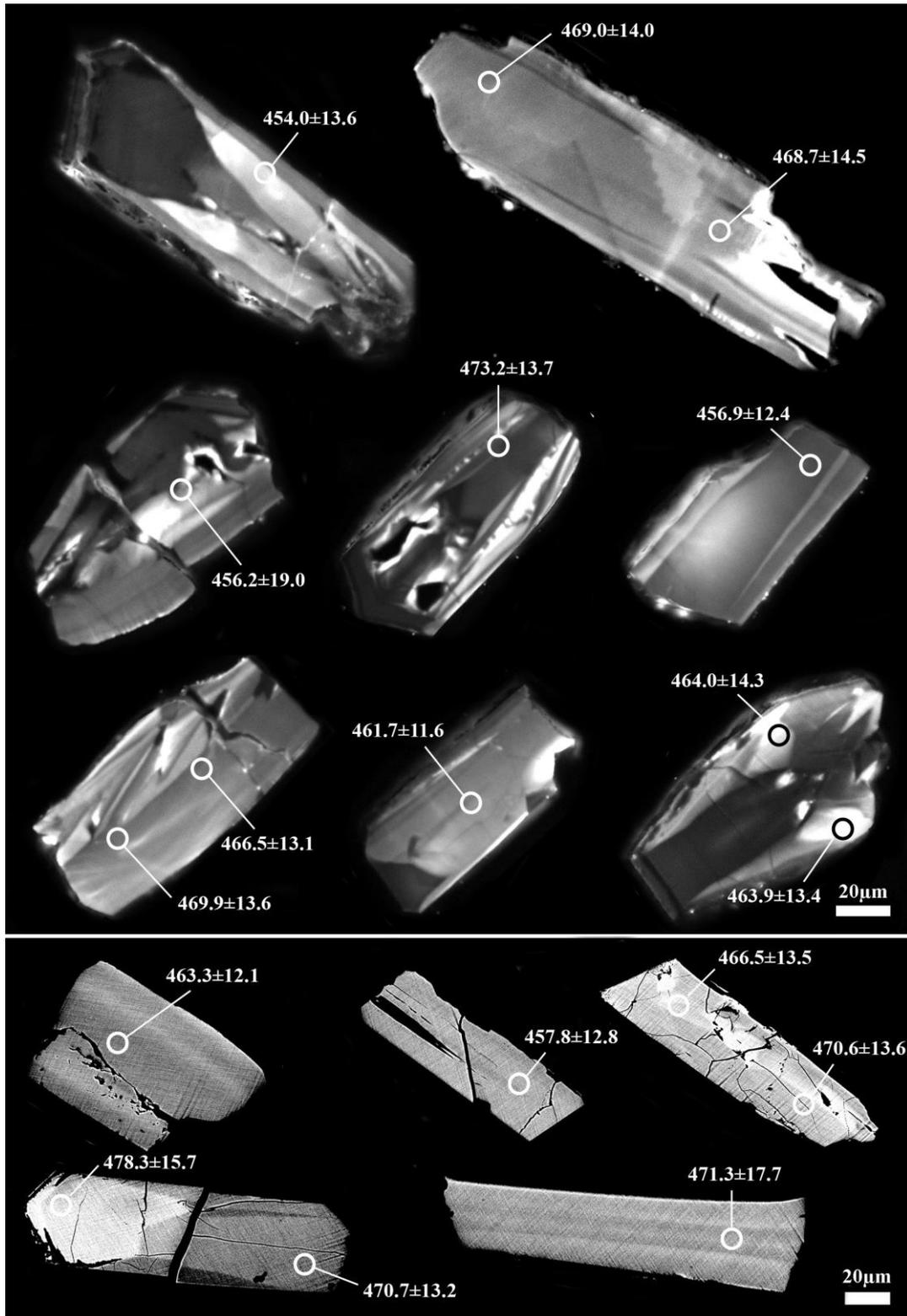
**Fig. 28** Cathodoluminescence (CL) and backscattered electron (BSE) images of zircon grains, and their analyzed positions with age values from diorite in the ore zone 5 of the Boroo deposit.
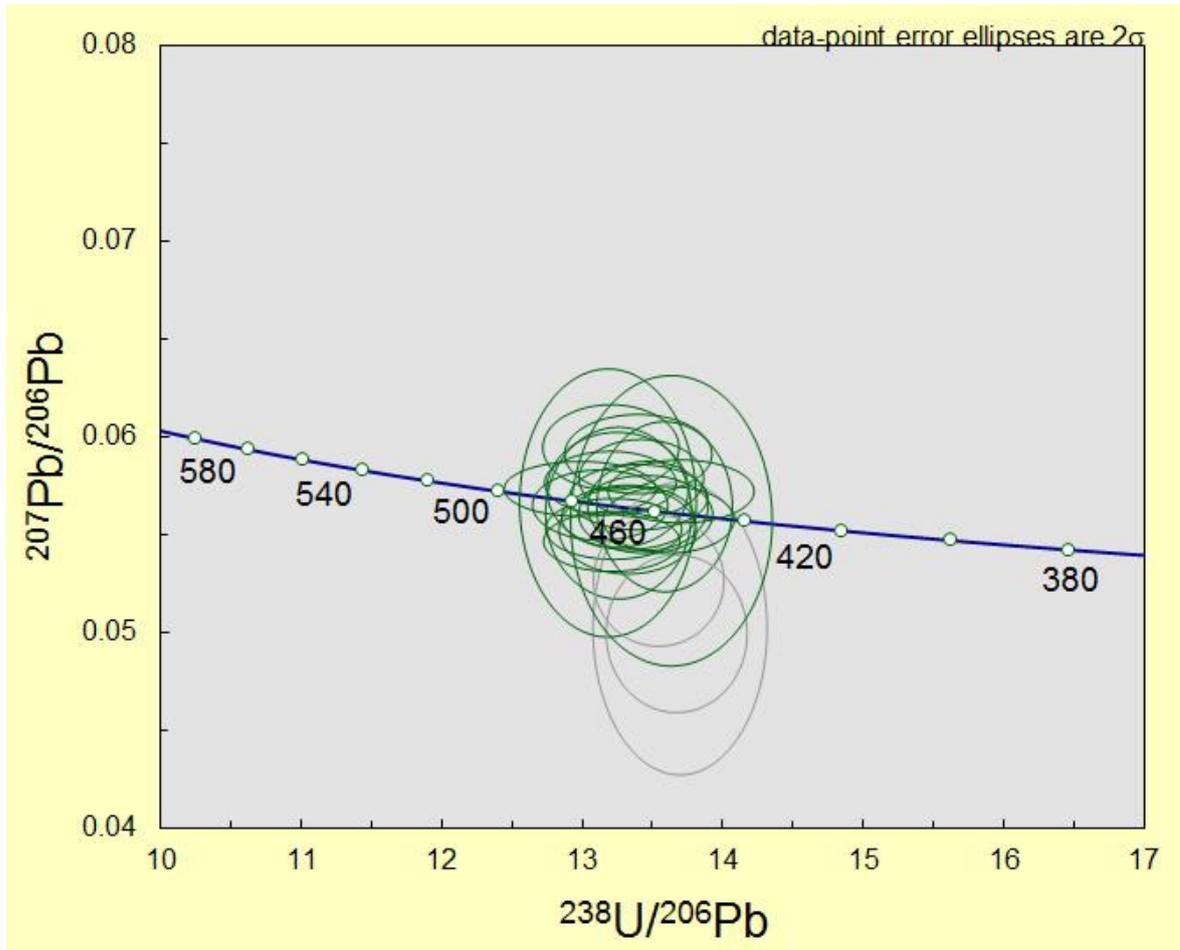
**Fig. 29** Concordia diagram showing LA-ICP-MS analysis in zircons from diorite dike in the ore zone 5 of the Boroo deposit.

**5.5.2 Zircon LA-ICP-MS U-Pb age dating in the Khadat copper deposit**

U-Pb contents at the positions of ten zircon grains in the granodiorite were analyzed using LA-ICP-MS (Table 11, Fig. 30).

Zircon grains from granodiorite (KHDT-20) show igneous oscillatory zoning from core to rim. High-U mantle domain is bright part in the BSE images, and low-U rim domain is dark (Fig. 30). However, LA-ICP-MS $^{206}Pb/^{238}U$ spot ages denote contemporary cores, mantles, and rims of zircon within the error. The weighted mean age ($^{206}Pb/^{238}U$) of all analyses is 274.2 ± 1.7 Ma (95% conf.), and all data are close to a Concordia of ca. 270 Ma (Fig. 31). Th/U-ratios of all data lies between 0.20 and 5.33.

**Table 11** Summary of age dating LA-ICP-MS analysis in zircons from granodiorite in the Khadat copper deposit.

| Spot Label | $^{206}Pb/^{238}U$ age | err 6/8 age | $^{207}Pb/^{235}U$ age | err 7/5 age | $^{207}Pb/^{206}Pb$ age | err 7/6 age | Th/U | disc. |
|---|---|---|---|---|---|---|---|---|
| 1KDT-20.csv | 274.7 | 8.6 | 275.8 | 20.0 | 285.2 | 183.8 | 0.312 | 0.4% |
| 2KDT-20.csv | 272.3 | 9.1 | 270.3 | 31.6 | 252.8 | 252.7 | 0.242 | -0.7% |
| 3KDT-20.csv | 280.1 | 8.5 | 276.6 | 22.0 | 247.5 | 205.9 | 0.237 | -1.2% |
| 4KDT-20.csv | 273.1 | 9.4 | 277.3 | 32.8 | 312.7 | 312.6 | 0.199 | 1.5% |
| 5KDT-20.csv | 265.0 | 7.8 | 275.7 | 29.1 | 367.4 | 282.4 | 0.237 | 4.0% |
| 6KDT-20.csv | 273.7 | 9.1 | 261.4 | 30.6 | 152.4 | 152.3 | 0.285 | -4.5% |
| 7KDT-20.csv | 279.3 | 8.2 | 277.7 | 18.4 | 264.7 | 166.6 | 0.443 | -0.6% |
| 8KDT-20.csv | 272.4 | 7.7 | 260.2 | 18.1 | 151.5 | 151.4 | 0.318 | -4.5% |
| 9KDT-20.csv | 273.7 | 7.8 | 266.0 | 14.9 | 198.7 | 135.5 | 0.308 | -2.8% |
| 10KDT-20.csv | 276.5 | 8.4 | 266.4 | 16.1 | 178.6 | 146.2 | 0.344 | -3.7% |
| 11KDT-20.csv | 269.9 | 6.9 | 282.9 | 14.4 | 392.2 | 121.1 | 0.378 | 4.8% |
| 12KDT-20.csv | 282.2 | 8.0 | 277.8 | 15.7 | 241.6 | 136.9 | 0.446 | -1.6% |
| 13KDT-20.csv | 277.5 | 7.6 | 275.8 | 13.4 | 261.8 | 111.6 | 0.460 | -0.6% |
| 14KDT-20.csv | 277.2 | 7.6 | 281.2 | 18.1 | 314.7 | 160.0 | 0.263 | 1.4% |
| 15KDT-20.csv | 279.0 | 7.1 | 276.3 | 13.1 | 253.3 | 111.8 | 0.523 | -1.0% |

| | | | | | | | |
|---|---|---|---|---|---|---|---|
| 16KDT-20.csv | 270.0 | 8.2 | 264.2 | 25.4 | 213.2 | 213.1 | 0.391 | -2.1% |
| 17KDT-20.csv | 269.6 | 7.9 | 268.2 | 20.5 | 256.1 | 197.7 | 0.270 | -0.5% |
| 18KDT-20.csv | 271.9 | 8.0 | 273.5 | 21.1 | 287.2 | 199.2 | 0.360 | 0.6% |
| 19KDT-20.csv | 273.5 | 7.8 | 262.3 | 13.5 | 163.5 | 121.3 | 0.503 | -4.1% |
| 20KDT-20.csv | 272.9 | 8.6 | 277.6 | 33.3 | 317.2 | 317.1 | 0.256 | 1.7% |
| 21KDT-20.csv | 273.4 | 8.6 | 263.0 | 13.8 | 171.4 | 121.1 | 0.533 | -3.8% |
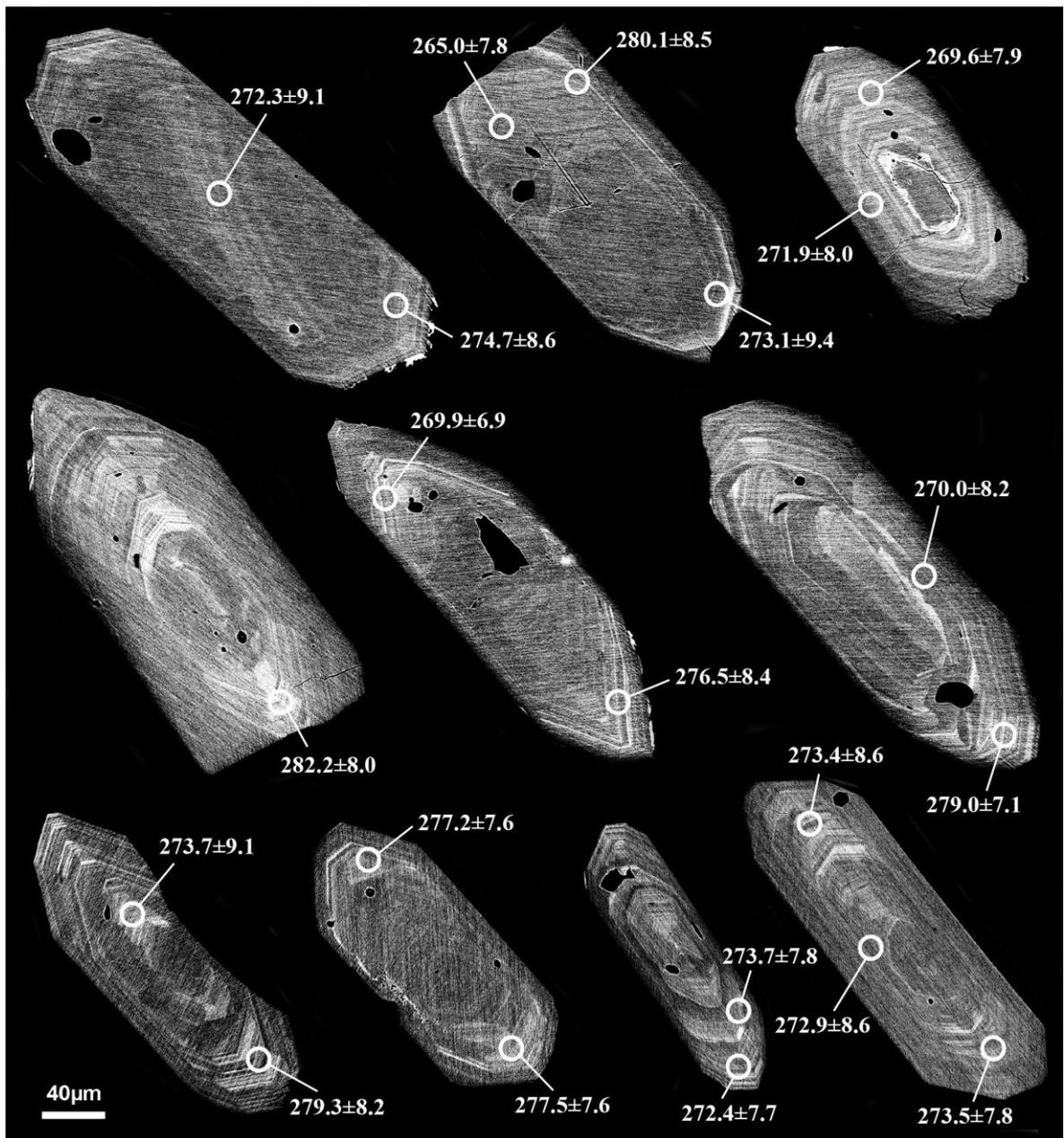
**Fig. 30** Backscattered electron (BSE) images of zircon grains, and their analyzed positions with age values from granodiorite of the Khadat deposit.
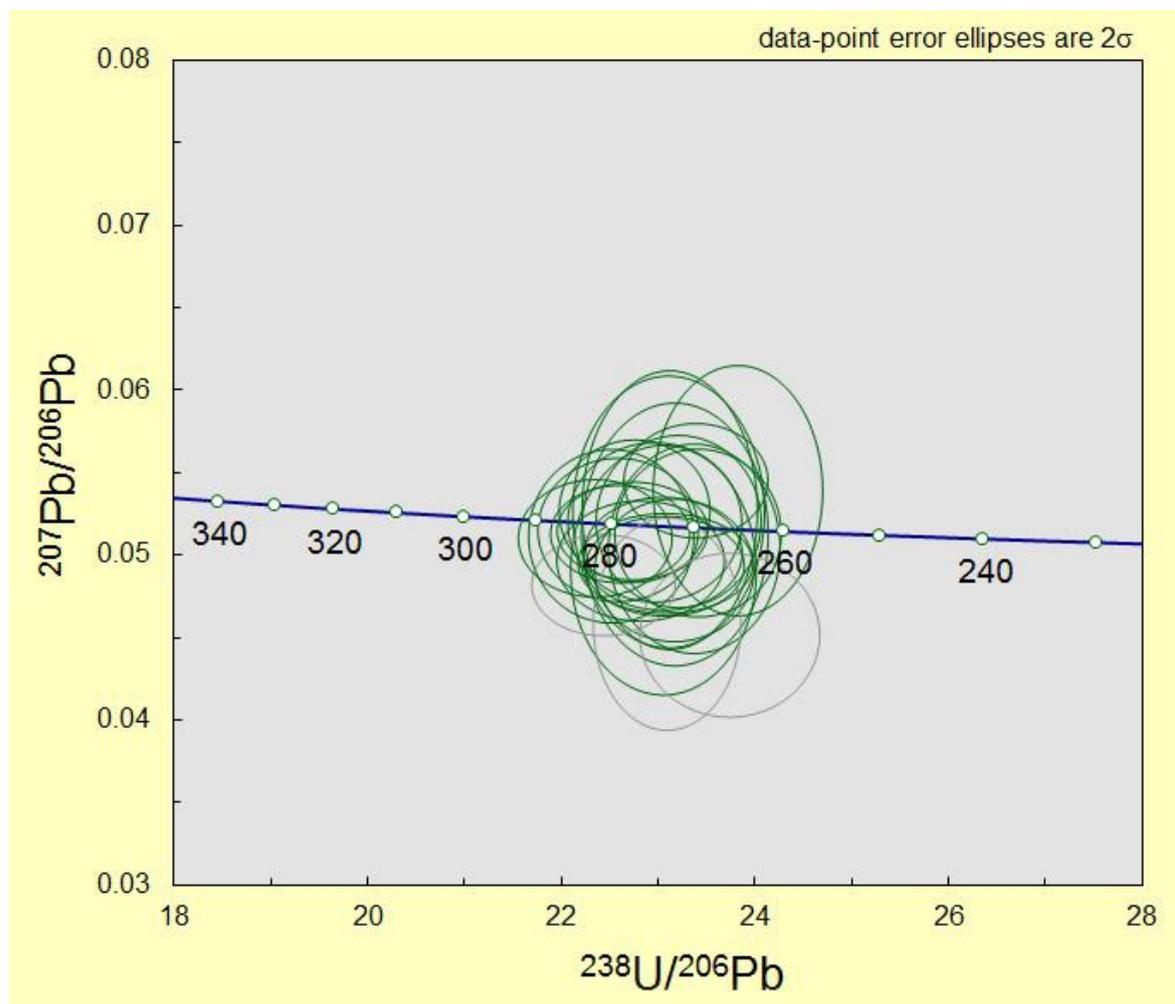


**Fig. 31** Concordia diagram showing LA-ICP-MS analysis in zircons from granodiorite of the Khadat deposit.

# Chapter VI

# 6  DISSCUSION

## 6.1  Mineralization of the Gatsuurt deposit

### 6.1.1  Mineralization stages and gold deposition

Three types of gold mineralization are defined in this study, based on the occurrence of the ores and their ore mineral assemblages: disseminated and stockwork ores, quartz vein ores, and silicified ores. According to their mineral assemblages and compositional changes of ore minerals and textures, each ore type can be sub-divided into several mineralization stages (Fig. 32). The disseminated and stockwork mineralization is divided into four stages (I, II, III and IV), as defined by assemblages of pyrite-I + arsenopyrite-I; pyrite-II + arsenopyrite-II; galena + tetrahedrite + sphalerite + chalcopyrite + jamesonite + bournonite + scheelite; and boulangerite + native gold, respectively.

Four stages are also recognized in the quartz vein mineralization: stage I is characterized by pyrite-I; stage II by the assemblage pyrite-II + arsenopyrite + galena + Ag-rich tetrahedrite-tennantite + sphalerite + chalcopyrite + bournonite; stage III by geocronite + geerite + native gold; and stage IV by native gold. The mineralization of the silicified ores comprises stage I, as defined by the assemblage pyrite + arsenopyrite + tetrahedrite + chalcopyrite; and stage II, characterized by sphalerite + galena + native gold. As described above, pyrite-I and arsenopyrite-I in the disseminated and stockwork ores and quartz vein ores have nearly ideal compositions, whereas pyrite-II, arsenopyrite-II and other sulfides contain detectable amounts of Au and minor elements (As in pyrite-II; Bi and Pb in arsenopyrite-II), and exhibit chemical zoning. Moreover, in contrast to the

simple mineral assemblages of stage I disseminated and stockwork ores and quartz vein ores, the assemblages of stage III disseminated and stockwork ores and stage II and III quartz vein ores consist of eight phases at maximum, and variable. These features indicate that stages II and III in the disseminated and stockwork and quartz vein ores represent the main phase of economic ore deposition, in which the ore minerals were produced by hydrothermal activity. The stage I event defined by pyrite-I and arsenopyrite-I in the disseminated and stockwork ores and quartz vein ores can thus be regarded as a precursor stage of the main ore mineralization stages. It is clear that the silicified zone ores were produced by hydrothermal activity, and the mineral assemblages of the stages I and II of the silicified zone mineralization are similar to those in the stages II and III of the disseminated and stockwork mineralization and quartz vein mineralization types. Gold was precipitated as "invisible" gold in pyrite-II and arsenopyrite-II during the stage II event in the disseminated and stockwork type mineralization, and in As-rich growth bands in pyrite within the silicified ores.

At the same time, stage IV of the disseminated and stockwork mineralization and quartz vein mineralization and stage II in the silicified zone mineralization are also important in terms of the gold deposition, because visible native gold was formed in these stages. In the disseminated and stockwork ores, the main gold deposition event occurred in stage IV, with mostly micronscale native gold occurring within sulfides or at grain boundaries, especially as fillings in pyrite and arsenopyrite. In the quartz vein ore type, coarse-grained or visible native gold was deposited with sulfides or as free grains in a matrix of quartz in stages III and IV, whereas in the silicified ores, microscopic inclusions of native gold were deposited within pyrite and arsenopyrite.

| Mineral | Disseminated and stockwork ores | | | | Quartz vein ores | | | | Silicified ores | |
|---|---|---|---|---|---|---|---|---|---|---|
| | Stage | | | | Stage | | | | Stage | |
| | I | II | III | IV | I | II | III | IV | I | II |
| Pyrite | ▅▅▅▅▅ | ▅▅▅▅ | | | ▅▅▅ | ▅ | | | ▅▅▅ | |
| Arsenopyrite | ▅▅▅▅▅ | ▅▅▅▅ | | | | ── | | | ▅▅▅ | |
| Galena | | | ── | | | ▂▂▂ | | | | ── |
| Tetrahedrite | | | ▂▂▂ | | | ▂▂▂ | | | ▂▂▂ | |
| Tennantite | | | | | | ─ | | | | |
| Sphalerite | | | ▂▂▂ | | | ▂▂▂ | | | | ── |
| Chalcopyrite | | | ── | | | ▂▂▂ | | | ── | |
| Jamesonite | | | ▪▪▪▪ | | | | | | | |
| Bournonite | | | ▪▪▪▪ | | | ── | | | | |
| Boulangerite | | | | ▪▪▪▪ | | | | | | |
| Geocronite | | | | | | | ▪▪▪▪ | | | |
| Scheelite | | | ▪▪▪▪ | | | | | | | |
| Geerite | | | | | | | ▪▪▪ | | | |
| Native gold | | | | ── | | | | ── | | ── |
| Zircon | | ▪▪▪▪ | | | | | | | | |
| Quartz | ▅▅▅▅▅▅▅▅▅▅ | | | | ▅▅▅▅▅▅▅▅▅▅ | | | | ▅▅▅▅▅ | |

▅▅ Abundant,　── common,　── occasional,　▪▪▪▪ rare

**Fig. 32** Paragenetic sequence of ore minerals at the Gatsuurt deposit.

93

## 6.1.2 General process of ore mineralization

The Au-rich quartz vein and silicified zone ore mineralization is surrounded by or is included within the disseminated and stockwork Au-mineralization region (Fig. 4). This arrangement suggests that the disseminated and stockwork mineralization was emplaced first, and the quartz vein and silicified zone type mineralization followed. The maximum homogenization temperatures of the type I fluid inclusions in the disseminated and stockwork ores reach 355°C, significantly greater than those of types II and III, although the homogenization temperatures in this study do not mean real temperature of mineralization because of non-compensation of pressure. Ag-rich tetrahedrite tennantite in the stage II of the quartz vein suggests its low temperature crystallization from hydrothermal ore fluids, because crystallization temperatures of Ag-rich tetrahedrite and Ag-minerals in quartz vein have been reported to be less than 300°C (Gallego Hernández & Akasaka, 2010). The model that the disseminated and stockwork type mineralization occurred earlier and the quartz vein and silicified zone mineralization followed thus seems to be reasonable. The lode gold deposits in the NKGB have been classified as either of mesothermal or orogenic type (Kotlyar et al., 1999; Hendry et al., 2006; Goldfarb et al., 2013). The textures of the ores, the mineral assemblages present, the mineralization sequences and the fluid inclusion data determined here are consistent with orogenic classification (cf. Groves et al., 1998) for the Gatsuurt deposit.

## 6.2 Gold mineralization of the Boroo deposit

### 6.2.1 Mineralization stages and gold deposition

Two distinct types of ores were defined, based on the geological relation that the disseminated and stockwork ore bodies are crosscut by the auriferous quartz vein ores, the ore occurrences in the host rocks, and distributions and assemblages of ore minerals. The disseminated and stockwork ores were produced by early stage mineralization, and the auriferous quartz vein ores by later stage mineralization. Four modes of gold occurrence are recognized in these two ore types: i) "invisible" gold in pyrite and arsenopyrite in both ore types; ii) microscopic native gold, 3 to 100 μm in diameter, that occurs as grains filling fine cavities or as an interstitial phase in sulfides in both ore types; iii) visible native gold grains, up to 1 cm in diameter, in the auriferous quartz vein ores; and iv) electrum in the auriferous quartz vein ores.

In accordance of the mineral assemblages, textures and compositional changes of ore minerals of the disseminated and stockwork ores and auriferous quartz vein ores, several mineralization stages were identified (Fig. 33).

The disseminated and stockwork mineralization is divided into four stages (I, II, III and IV), as defined by assemblages of pyrite-I + arsenopyrite-I; pyrite-II + arsenopyrite-II; sphalerite + galena + chalcopyrite + tetrahedrite + bournonite + boulangerite + alloclasite + native gold; and native gold, respectively. In the auriferous quartz vein ores, five mineralization stages are recognized: stage I is characterized by pyrite-I; stage II by pyrite-II + arsenopyrite; stage III by the assemblage sphalerite + galena + chalcopyrite; stage IV by Ag-rich tetrahedrite-tennantite + bournonite + geerite + native gold; and stage V by electrum.

The stage I event in the disseminated and stockwork ores defined by pyrite-I and

95

arsenopyrite-I can be regarded as a precursor stage of the main gold mineralization stages. Gold mineralization is distinct in stage II, where pyrite-II and arsenopyrite-II in the disseminated and stockwork ores contain trace amounts of "invisible" Au up to 0.19 and 0.22 wt% respectively (Table 5). The Au enrichment in these phases is strongly correlated with As-rich bands in pyrite-II and arsenopyrite-II (Fig. 20D, E, F). In stage III, micron-scale native gold formed along micro-fractures in sulfides or at grain boundaries, especially in pyrite and arsenopyrite. Stage IV is also a major gold crystallization event in the disseminated and stockwork ores, and native gold formed as a free phase in gangue minerals. This indicates the final stage of native gold crystallization in the hydrothermal ore fluids (Mikucki, 1998).

In the auriferous quartz vein ores, stages I and III lack significant gold mineralization. Pyrite-II and arsenopyrite in stage II commonly contain up to 0.16 and 0.20 wt% Au (Table 6), but gold minerals are not observed. This Au occurrence in pyrite-II and arsenopyrite is nearly the same as that in stage II in the disseminated and stockwork ores. The stage IV event is the most significant for gold deposition in the auriferous quartz vein ores. Native gold crystallized in this stage is coarse grained, and is characterized by higher silver contents than the micro-scale native gold grains. Furthermore, Ag-rich tetrahedrite-tennantite formed in this stage. These features indicate an increase in the Ag content in the hydrothermal ore fluids, or depletion of Au concentration due to the crystallization of native gold during stage IV. Finally, electrum was deposited in stage V.

The mineral assemblages and crystallization sequences in the paragenetic sequences from stages I to IV in both ore types are very similar, except for stage V in the auriferous quartz vein ores. Gold mineralization in the disseminated and stockwork ores and auriferous quartz vein ores also show common features. These characteristics imply that gold was deposited repeatedly in the two mineralization stages.

| Mineral \ Stage | Disseminated and stockwork ores | | | | Auriferous quartz vein ores | | | | |
|---|---|---|---|---|---|---|---|---|---|
| | I | II | III | IV | I | II | III | IV | V |
| Pyrite | Py-I | Py-II | | | Py-I | Py-II | | | |
| Arsenopyrite | Apy-I | Apy-II | | | ▬▬▬ | ▬▬▬ | | | |
| Sphalerite | | | ▬ | | | | ▬ | | |
| Galena | | | ▬ | | | | ▬ | | |
| Chalcopyrite | | | ▬ | | | | ▬ | | |
| Tetrahedrite | | | ▬ | | | | | ▬ | |
| Tennantite | | | | | | | | ▬ | |
| Bournonite | | | ···· | | | | | ▬ | |
| Boulangerite | | | ···· | | | | | | |
| Geerite | | | | | | | | ▬ | |
| Alloclasite | | | ········ | | | | | | |
| Native gold* | | ········ | ············· | | | ········ | | ▬▬▬ | |
| Electrum | | | | | | | | | ········ |
| Quartz | ▬▬▬▬▬▬▬▬▬▬▬ | | | | ▬▬▬▬▬▬▬▬▬▬▬▬▬ | | | | |

▬▬ abundant,  ▬▬ common,  ▬ occasional,  ····· rare
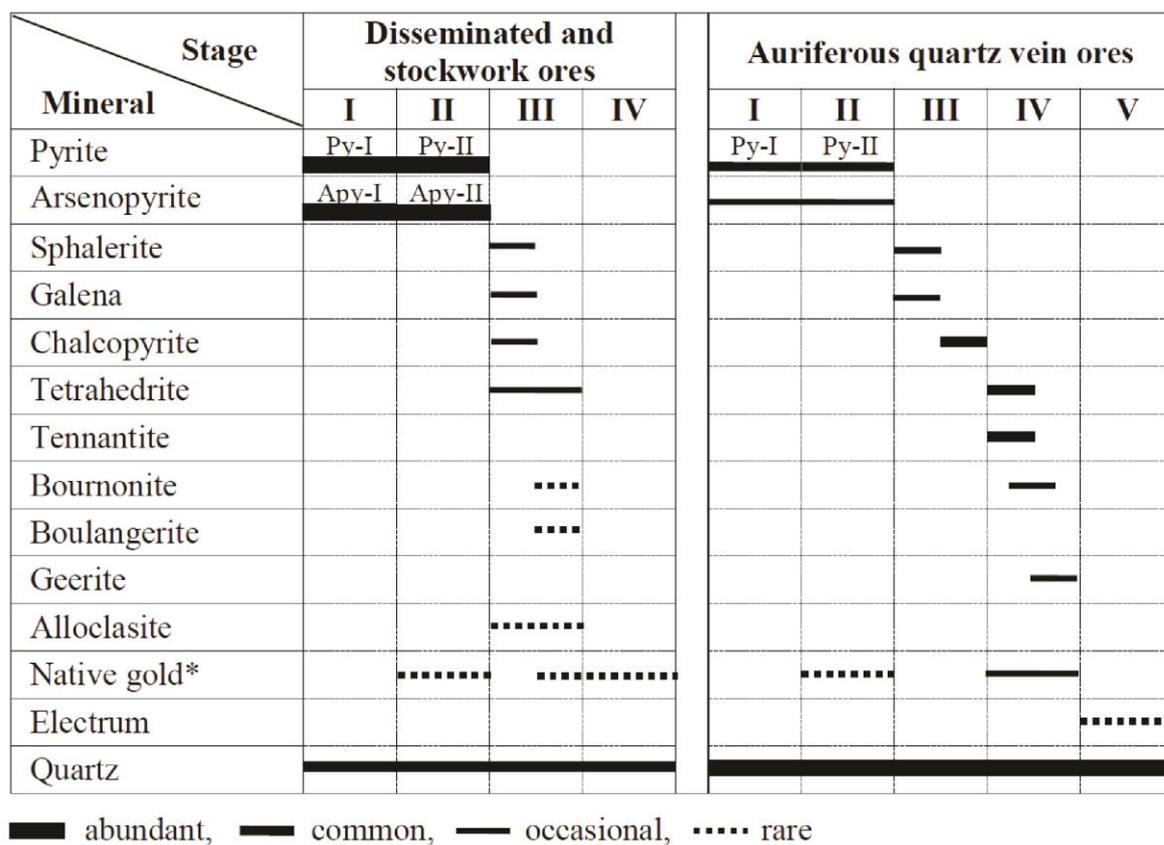
**Fig. 33** Paragenetic sequence of ore minerals at the Boroo deposit.

### 6.2.2 Mineralization condition

Gold mineralization in the Boroo deposit is closely associated with crystallization of pyrite and arsenopyrite. Arsenic-Au relations in pyrite and arsenopyrite are an indicator of the gold solubility in As-bearing pyrite and arsenopyrite (Reich et al., 2005). Based on the As-Au relations observed in this study, "invisible" gold is attributed to $Au^{+1}$ in pyrite-II and arsenopyrite, because most of the 501 EMPA analyses determined here fall below the solubility limit of gold in pyrite and arsenopyrite (Fig. 34). It is also notable that some data plot above the solubility limit of gold in pyrite, suggesting the existence of nanoparticles of gold. This result suggests that gold ions were mainly incorporated within pyrite and arsenopyrite as a trace constituent in the period of stage-II.
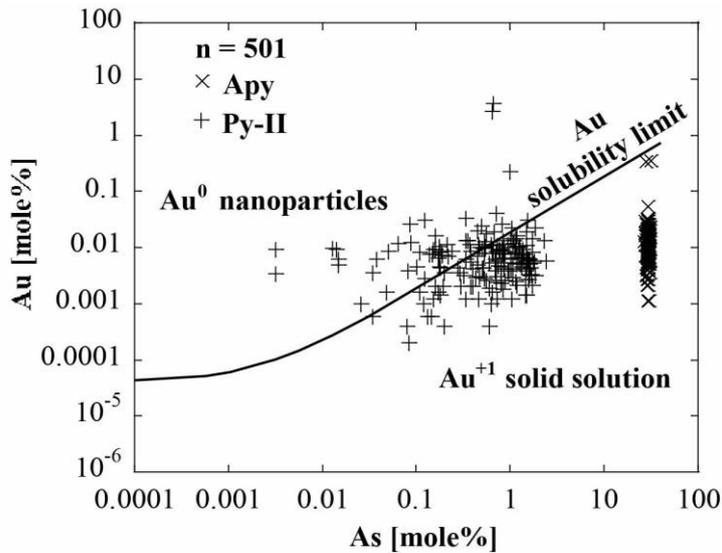


**Fig. 34** Au-As (mol%) relation diagram by Reich et al. (2005) and plots of pyrite-II and arsenopyrite from the Boroo deposit. The inferred solubility limit for gold is approximated by the line $C_{Au} = 0.02 \times C_{As} + 4 \times 10^{-5}$, where $C_{Au}$ and $C_{As}$ represent the concentrations of Au and As in mole percent (mol%) (Reich et al., 2005). Below this line, Au is present in solid solution ($Au^{+1}$), whereas above it a significant amount of Au is contained as nanoparticles of native Au ($Au^0$).

On the basis of the above, the arsenopyrite geothermometer (Clark, 1960; Krestchmar and Scott, 1976; Sharp et al., 1985) was applied to estimate the temperature-$fs_2$ conditions of the gold mineralization. For this purpose, data for coexisting arsenopyrite and As-rich pyrite were employed, because the coexistence of arsenopyrite and As-rich pyrite is the most important criterion for the estimation of equilibrium condition in the arsenopyrite-bearing assemblage (Sharp et al., 1985). Arsenopyrite-I in the disseminated and stockwork ores does not satisfy this criterion, because it is commonly rimmed by arsenopyrite-II (Figs. 14D; 18D). The low As contents (27.2-29.5 As atom%; 0.816-0.885 atoms per 1.0S) of arsenopyrite-I also show non-equilibrium features reflecting the kinetics of growth of arsenopyrite and local fluctuations in the $fS_2/fAs_2$ ratio (Kretschmar and Scott, 1976). Thus, arsenopyrite-II in the disseminated and stockwork ores was used in the arsenopyrite geothermometer.

As shown in Figure 35, arsenopyrite-II with As contents ranging from 29.5 to 31.0 atom% (0.885-0.930 atoms per 1.0S) plots in the arsenopyrite + pyrite field. The estimated temperatures vary from 365 to 300°C, and log$fS_2$ falls in the range of -7.5 to -10.1 (Fig. 35). The results suggest that sulfur fugacity in the hydrothermal ore fluids decreased with decreasing temperature, which led to precipitation of later stage visible gold as fine grains in pyrite and arsenopyrite, or as a filling phase in their micro-fractures. This proposed gold mineralization process seems to be consistent with the results that the gold contents in pyrite-II exceed the solubility limit of gold in pyrite (Fig. 33), because gold saturation during the crystallization of later stage pyrite and arsenopyrite from the hydrothermal ore fluids causes precipitation of gold nanoparticles.

Mobilization of gold ions has also been regarded as a typical mechanism for gold mineralization in orogenic gold deposits dominant in pyrite and arsenopyrite (e.g.,

Mumin et al., 1994; Morey et al., 2008; Bigot & Jébrak, 2015). According to this model, $Au^{+1}$ ions in pyrite and arsenopyrite formed at an early stage are extrapolated into fluids at temperatures above 450ºC (Morey et al., 2008), and visible native gold grains crystallize from the fluid near the alteration rims of pyrite and arsenopyrite (cf. Mumin et al., 1994; Morey et al., 2008). However, as discussed above, the estimated formation temperature of pyrite and arsenopyrite-bearing assemblage of the disseminated and stockwork ores of the Boroo deposit are 365ºC at maximum, which is considerably lower than the 450ºC critical temperature for the mobilization of $Au^{+1}$ ions. Therefore, gold mineralization based on the gold remobilization mechanism was not considered for the Boroo deposit in this study.

In the case of the auriferous quartz vein ores, pyrite and arsenopyrite mostly occur as individual grains, and their equilibrium assemblage is not recognized. Therefore, the formation temperature of the pyrite and arsenopyrite in this ore type could not be estimated using the arsenopyrite geothermometer. However, coarse native gold grains and low sulfide contents in this ore type suggest that they were formed by a later stage gold mineralization. Electrum may also have precipitated from the gold-saturated ore fluids during gradual cooling at the latest stage.
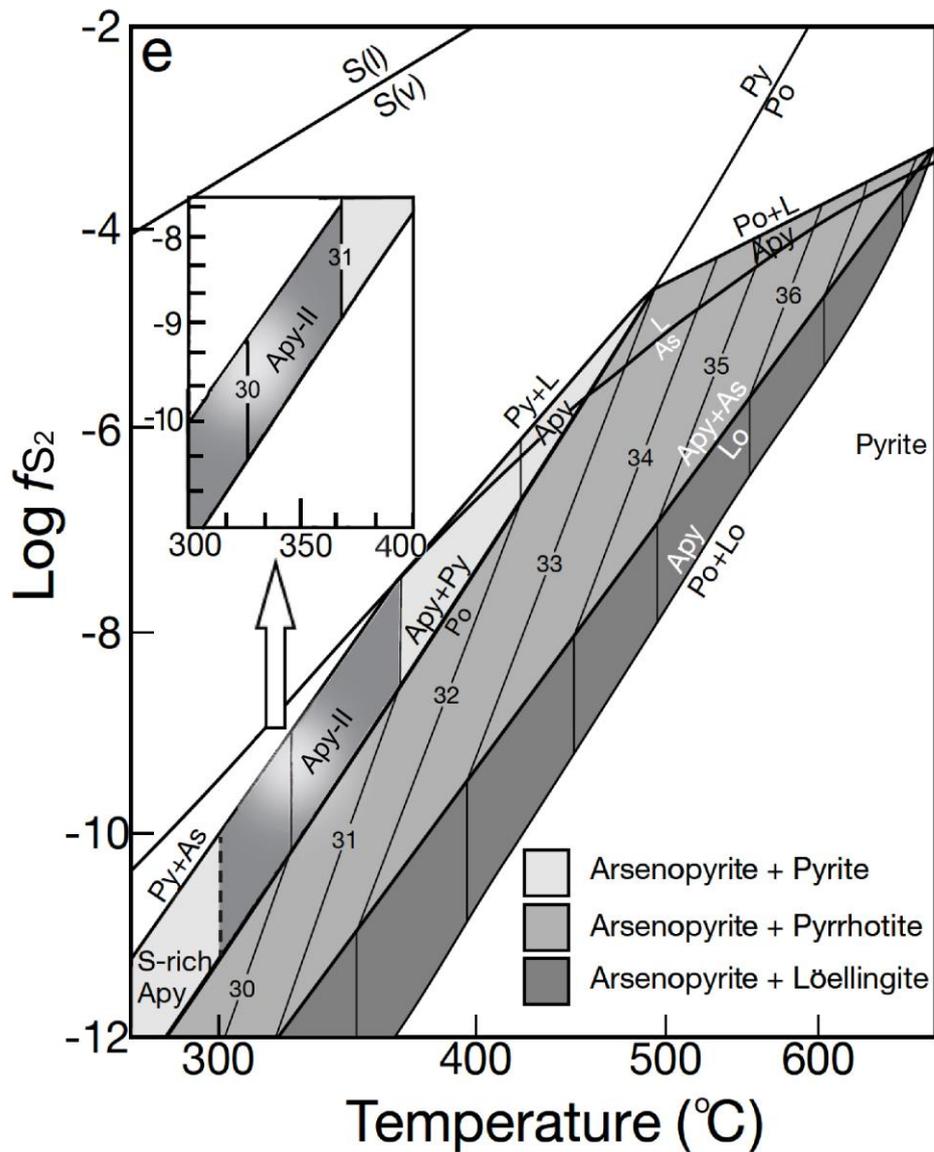
**Fig. 35** Temperature-logfs$_2$ diagram showing arsenopyrite stability field with atomic% arsenic in the system Fe-As-S after Clark (1960), Kretschmar and Scott (1976) and Sharp et al. (1985). The average As contents (29.5 to 31.0 As atomic%) of arsenopyrite-II (Apy-II) in the disseminated and stockwork ores are plotted. Apy, arsenopyrite; Lö, löellingite; Py, pyrite; Po, pyrrhotite; As, arsenic; L, sulfur-arsenic liquid.

## 6.3 Gold mineralization of the Ulaanbulag deposit

Two types of gold mineralization are defined in the deposit, based on the occurrence of the ores and their host rocks, and ore mineral assemblages: disseminated and stockwork ores and siliceous ores. According to their mineral assemblages and compositional changes of ore minerals and textures, each ore type can be sub-divided into four crystallization stages (Fig. 36).

The disseminated and stockwork mineralization is divided into four stages (I, II, III and IV): stage I is characterized by pyrite-I + arsenopyrite-I; stage II by pyrite-II + arsenopyrite-II; stage III consisted by assemblage of sphalerite + galena + chalcopyrite; and stage IV by native gold, respectively. Four stages are also recognized in the siliceous type ores: stage I by pyrite-I + arsenopyrite; stage II by pyrite-II + arsenopyrite; stage III by assemblage of sphalerite + galena + chalcopyrite + bournonite + boulangerite; and stage IV by native gold. Thus, the mineralization stages in the disseminated and stockwork ores and siliceous type ores are characterized by similar ore mineral assemblages and crystallization stages, although, a rare sulfides such as bournonite and boulangerite occurring in the siliceous type ores are not found in the disseminated and stockwork ores.

The stage I is defined by only Fe-sulfides in the both ore types, and not significant for gold deposition.

The stage II is essential for gold mineralization in the disseminated and stockwork ores and siliceous ores, because "invisible gold" is often detected in pyrite and arsenopyrite. Especially, arsenopyrite-II is relatively rich in Au which attains up to 0.13 wt%. In the stage III, only small amounts of sulfides crystallized, and gold mineral is not deficient.

102

The stage IV is the most significant for gold crystallization in the disseminated and stockwork ores and siliceous ores, as shown by the occurrence of fine native gold in the both ore types. The chemical composition of native gold in the ore types is characterized by higher silver contents ranging from 12.62 to 19.26 wt% Ag.

According to paragenetic sequence of ore minerals and their chemical compositions, disseminated and stockwork ores and siliceous ores in the deposit were formed at the same time. However, cross cutting or fault relations on the structure of the siliceous type ores indicate that the mineralization of the siliceous ores is the later event than or immediately followed to the mineralization of the disseminated and stockwork ores.

| Stage / Mineral | Disseminated and stockwork ores | | | | Siliceous ores | | | |
|---|---|---|---|---|---|---|---|---|
| | I | II | III | IV | I | II | III | IV |
| Pyrite | Py-I | Py-II | | | Py-I | Py-II | | |
| Arsenopyrite | Apy-I | Apy-II | | | | | | |
| Sphalerite | | | ▬ | | | | ▬ | |
| Galena | | | ▬ | | | | ▬ | |
| Chalcopyrite | | | ▬ | | | | ▬ | |
| Bournonite | | | | | | | ····· | |
| Boulangerite | | | | | | | ····· | |
| Native gold* | | ····· | ······· | | | | | ····· |
| Quartz | ▬▬▬ | | | | ▬▬▬ | | | |

▬▬▬ abundant,   ▬▬ common,   ▬ occasional,   ····· rare
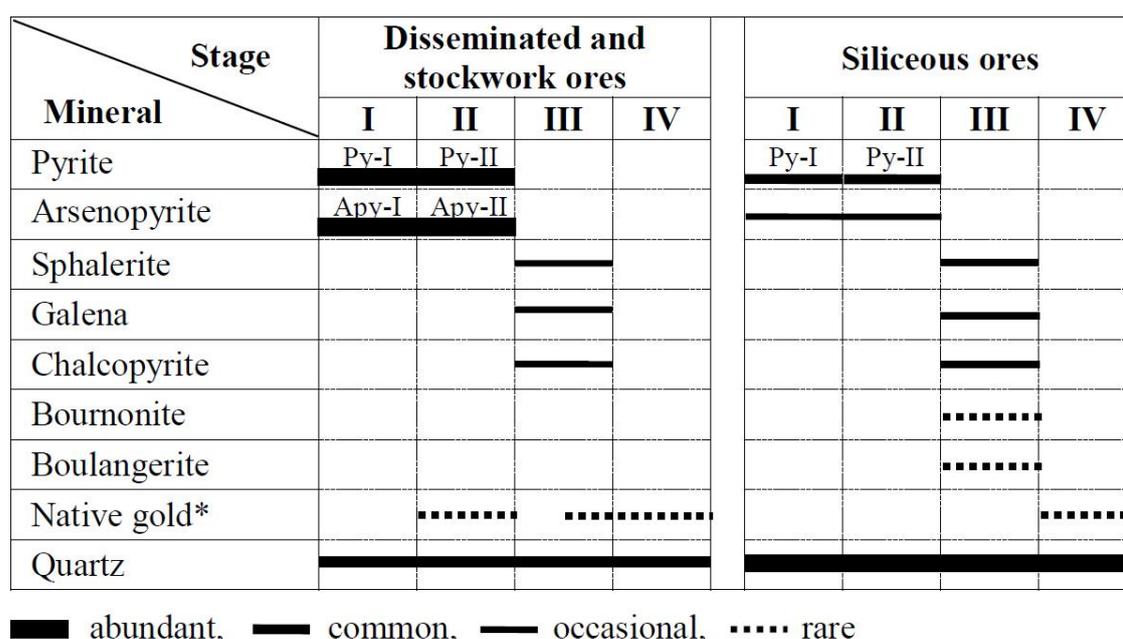
**Fig. 36** Paragenetic sequence of ore minerals at the Ulaanbulag deposit.

103

## 6.4   Copper mineralization of the Khadat deposit

The ore body in shallow part of the Khadat copper deposit, which is from surface to 200 meters depth, consists of the vein type ores, but ores in deeper part of the deposit from 200 to 250 meters in depth show signature of the disseminated and stockwork mineralization (Fig. 11C). However, the samples collected from deeper part of the deposit are not sufficient for the identification of the ore types. Thus, only the vein type of mineralization is defined in the deposit.

Based on mineral assemblages, five crystallization stages (I, II, III, IV and V) (Fig. 37) are recognized for the vein-type copper mineralization: stage I is characterized by pyrite-I, stage II by pyrite-II + arsenopyrite-I, stage III by pyrite-III + arsenopyrite-II, stage IV by assemblage of pyrrhotite + sphalerite + galena, and stage V by chalcopyrite.

As shown by the dominance of chalcopyrite from surface to 100 meters in depth, common mineral assemblages of sphalerite, galena, pyrite, arsenopyrite, pyrrhotite and chalcopyrite in the ores from 100 to 200 meters in depth, and dissemination of pyrite, arsenopyrite and chalcopyrite below 200 meters, metal zoning from surface to deep is observed in the deposit, which is common feature in the porphyry deposits (Sillitoe, 2010). The copper mineralization occurring at 250 m depth in the metasedimentary rocks (Fig. 11C) suggests that the copper mineralization may continuing to deep in the deposit, because host metasediments should have covered intrusive stock that associated with copper mineralization. The age of intrusive stock determined in this study is 274.2 ± 1.7 Ma.

The arsenopyrite geothermometer (Clark, 1960; Krestchmar and Scott, 1976; Sharp et al., 1985) was also applied to estimate the temperature-$fs_2$ conditions of the copper mineralization, because the coexistence of arsenopyrite and pyrrhotite can be the

important criterion for the estimation of equilibrium condition in the arsenopyrite-bearing assemblage (Sharp et al., 1985). Based on this geothermometer, arsenopyrite with As contents ranging from 31.6 to 33.0 atom% (0.948-0.990 atoms per 1.0S) plots in the arsenopyrite + pyrrhotite field. The estimated temperatures vary from 400 to 495°C, and $\log f\mathrm{S}_2$ falls in the range of -6.8 to -5 (Fig. 38).

Thus, the Khadat copper deposit is expected one of the porphyry deposit in the NKGB, in terms of geologic setting, mineral assemblages and high temperatures of ore mineral crystallization.

| Stage / Mineral | Copper ores | | | | |
|---|---|---|---|---|---|
| | I | II | III | IV | V |
| Chalcopyrite | | | | | ▬▬ |
| Pyrite | Py-I | Py-II | Py-III | | |
| Arsenopyrite | | Apy-I | Apy-II | | |
| Pyrrhotite | | | | ·········· | |
| Sphalerite | | | | ▬▬ | |
| Galena | | | | ▬▬ | |

▬▬ abundant,  ▬ common,  rare ·····

**Fig. 37** Paragenetic sequence of ore minerals at the Khadat deposit.

## 6.5 Relation of ore types in the gold deposits, and tectonic significance

The gold mineralization of the Gatsuurt, Boroo and Ulaanbulag deposits in the North Khentei gold belt is related to the Yeroogol fault. The fault and related fractures played roll as pathways for hydrothermal fluid into wall rocks. Granitic body was fractured by this fault, whereas volcanic and metasedimentary rocks are less fractured due to the massive textures (Hendry et al., 2006).
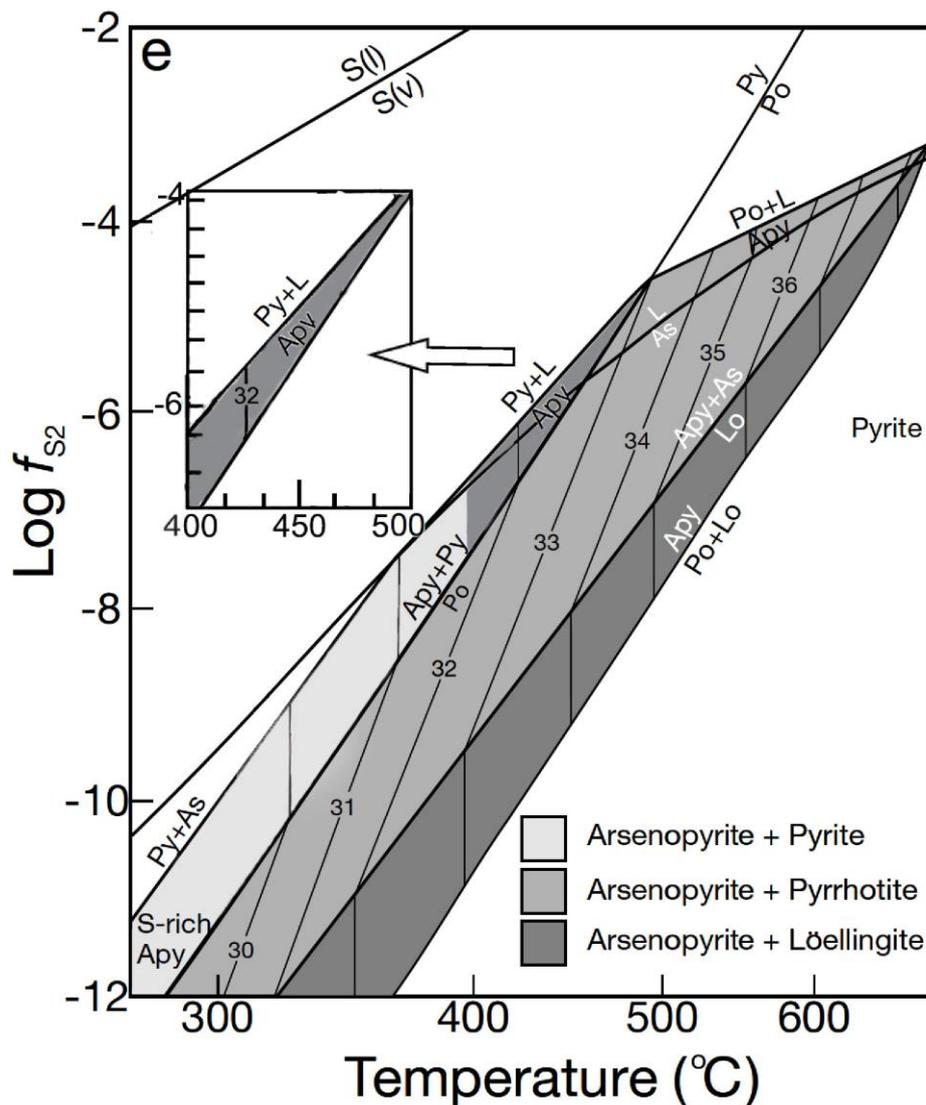
**Fig. 38** Temperature-logfs₂ diagram showing arsenopyrite stability field with atomic% arsenic in the system Fe-As-S after Clark (1960), Kretschmar and Scott (1976) and Sharp et al. (1985). The average As contents (31.6 to 33.0 As atomic%) of arsenopyrite (Apy) in the ores hosted in granodiorite are plotted. Apy, arsenopyrite; Lö, löellingite; Py, pyrite; Po, pyrrhotite; As, arsenic; L, sulfur-arsenic liquid.

Thus, the auriferous quartz vein type ores developed in granite, and the volume of quartz vein or vein type ores in volcanic and metasedimentary rocks is less than that of the auriferous quartz vein type ore in granite.

The disseminated and stockwork mineralization of the deposit can be interpreted by interaction between the hydrothermal ore fluids and wall rock alteration (McCuaig and Kerrich, 1998). The disseminated and stockwork ores are regarded to have been formed at the highest temperatures than other type of ores. This interpretation is supported by the homogenization temperatures of the fluid inclusions up to 355 to 365 ºC in the Gatsuurt and Boroo deposits. However, the silicified ores in the Gatsuurt deposit are different from the disseminated and stockwork ores, the auriferous quartz vein ores and siliceous type ores in the Ulaanbulag deposit, in terms of the ore mineral assemblages and distributions, strong siliceous alteration, high Au grade, host rock that consists of fine to micron sized quartz grains, ore body shape and localization. According to these characteristics, the silicified ores is considered to have been formed by later hydrothermal fluid activity along the major structure. The separated two ore zones in the Gatsuurt deposit also indicate that structure was active after then mineralization (Hendry et al., 2006).

## 6.6 Classification of the gold deposits in the North Khentei gold belt

Gold deposits in the NKGB have been previously classified as intrusion-related vein-type gold mineralization by Dejidmaa (1996). However, the lithology-controlled mineralization types consisting of low-grade disseminated and stockwork ores and moderate to high grade auriferous quartz vein and silicified type ores in the Gatsuurt, Boroo and Ulaanbulag deposits do not fit the intrusion-related gold deposit model as defined by Lang and Baker (2001), Hart (2005, 2007), and Mair et al. (2011). Intrusion-related gold deposits occur in a very restricted tectonic setting (post-orogenic), are associated with reduced ilmenite-bearing magmas, and are characterized by low-grade disseminated sulfide ore bodies with Mo and Bi anomalies, and localized in restricted

zones of the causative intrusion. In, addition, they are small ore systems unrelated to major regional structures, and gold has a magmatic origin.

By recent studies, the lode gold deposits in the study area have been classified as both mesothermal and orogenic types (Goldfarb et al., 2013).

The orogenic type is the most common and most significant type of gold deposit which is introduced by Groves et al. (1998) (Fig. 39). This type of deposits are typically developed in terranes that have experienced moderate to high-T low to moderate-P metamorphism (Groves et al., 1998, 2003), with consequent generation of large volumes of granitic stocks. Hence, a distal spatial relationship with certain intrusions is also expected for these deposits, and there is a possibility of genetic connection.

The NKGB is considered to have formed by granitoid intrusive activity during the final closure of the Mongol-Okhotsk Ocean by the collision along the Mongol-Okhotsk belt in the middle Triassic to middle Jurassic (Zorin et al., 2001; Gordienko et al., 2012; Hara et al., 2013). The NKGB is hosted in the Haraa terrane, which is interpreted as accretionary to collisional, subduction-related orogen region (Badarch et al., 2002). Thus, the NKGB has very similar geology and geotectonic settings with the model of orogenic type deposit by Groves et al. (1998). Moreover, structure controls, geochemistry of alteration, ore mineral association, and fluid inclusion of the gold deposits in the NKGB correspond to the overall features of the orogenic classification.

Also, Groves et al. (1998) defined the unifying term "orogenic gold deposit" to include those deposits widely referred to as mesothermal in the past few decades. Therefore, the gold deposits in the NKGB, which were previously recognized as mesothermal type by Kotlyar et al. (1998, 1999), are classified into orogenic type.
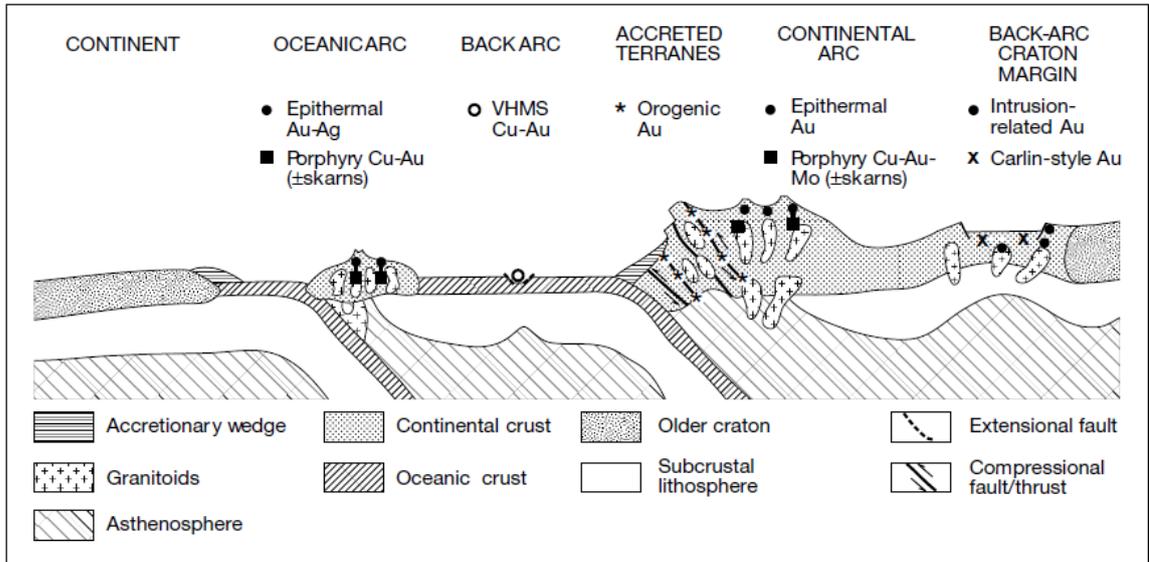
**Fig. 39** Tectonic settings of gold-rich epigenetic mineral deposits. Adapted from Groves et al. (1998). Abbreviations: VHMS, Volcanic Hosted Massive Sulfide.

## 6.7 Implication to gold mineralization in the North Khentei gold belt

Based on the present study on the Gatsuurt, Boroo and Ulaanbulag, the gold mineralization process in the NKGB can be generalized. The geological settings of the Gatsuurt, Boroo and Ulaanbulag deposits are similar to each, and the deposits are related to the major fault structure (Fig. 2). The deposits mainly consist of the disseminated and stockwork type and vein type ores, such as the auriferous quartz vein ores in the Boroo deposit, the quartz vein and silicified type ores in the Gatsuurt deposit and siliceous type ores in the Ulaanbulag deposit. The Gatsuurt, Boroo and Ulaanbulag deposits show common geological relations that the quartz vein ores, auriferous vein ores and siliceous type ores are localized along the thrust fault, and cut across disseminated and stockwork ores hosted in granite, volcanics and metasedimentary rocks. They have almost identical ore mineral assemblages and mineralization stages (Fig. 40). The main sulfides (pyrite and arsenopyrite) in these deposits formed in two stages, and exhibit the same chemical features, such as arsenic enrichment and the presence of "invisible" gold in pyrite-II and arsenopyrite-II. Furthermore, Ag-rich tetrahedrite-tennantite occurs in the auriferous quartz vein ores in the Boroo deposit and in the quartz vein ores in the Gatsuurt deposit. The occurrences of native gold in these deposits are also very similar to each other. Moreover, the estimated maximum mineralization temperature of 365ºC for pyrite-II and

110

| Mineral \ Stage | Disseminated-stock. | | | | Auriferous quartz-vein | | | | | Silicified | |
|---|---|---|---|---|---|---|---|---|---|---|---|
| | Ia | Ib | II | III | Ia | Ib | II | III | IV | I | II |
| Pyrite ($FeS_2$) | | | | | | | | | | | |
| Arsenopyrite (FeAsS) | | | | | | | | | | | |
| Chalcopyrite ($CuFeS_2$) | | | | | | | | | | | |
| Tetrahedrite $(Cu,Fe)_{12}Sb_4S_{13}$ | | | | | | | | | | | |
| Tennantite $(Cu,Fe)_{12}As_4S_{13}$ | | | | | | | | | | | |
| Sphalerite $(Zn,Fe)S$ | | | | | | | | | | | |
| Galena (PbS) | | | | | | | | | | | |
| Bournonite ($CuPbSbS_3$) | | | | | | | | | | | |
| Boulangerite ($Pb_5Sb_4S_{11}$) | | | | | | | | | | | |
| Jamesonite ($Pb_4FeSb_6S_{14}$) | | | | | | | | | | | |
| Geocronite $Pb_{14}(Sb,As)_6S_{23}$ | | | | | | | | | | | |
| Geerite ($Cu_8S_5$) | | | | | | | | | | | |
| Scheelite ($CaWO_4$) | | | | | | | | | | | |
| Alloclasite (Co,Fe)AsS | | | | | | | | | | | |
| Native gold (Au) | | | | | | | | | | | |
| Electrum (Au:Ag) | | | | | | | | | | | |
| Temperatures ($T_h$) | 254-355°C | | 317-362 °C | | 237-305 °C | | | | | | |

**Fig. 40** Comparison of the paragenetic sequence of the Gatsuurt, Boroo and Ulaanbulag deposits.

arsenopyrite-II in the disseminated and stockwork ores of the deposits is comparable with homogenization temperatures of up to 355°C for fluid inclusions in quartz from the disseminated and stockwork ores in the Gatsuurt and Boroo deposits (Khishgee et al., 2014). These are considered as common features of the gold mineralization in the NKGB. However, the Boroo and Ulaanbulag deposits lack the silicified ores that occur in the Gatsuurt deposit, and native gold in the Boroo and Ulaanbulag deposits is finer than that in the Gatsuurt deposit, showing some local difference among these deposits. Khishgee et al. (2014) characterized the silicified ores in the Gatsuurt deposit by their restricted linear distribution along a fault, their occurrence within the disseminated and stockwork ore

111

region, high Au grades, and presence of very fine grained quartz and dispersed sulfides, and concluded that the silicified ores were one of the later stage products.

The common features of the deposits described above strongly indicate that these deposits formed from the same source of the hydrothermal activity in this region (Fig. 41). Therefore, the gold mineralization of the Gatsuurt, Boroo and Ulaanbulag deposits is classified into orogenic type, and other deposits distributing in the NKGB, such as the Baavgait, Ereen, Sujigtei, Urt and Tsagaanchuluut deposits, are also regarded to belong to the same type as that of the Gatsuurt, Boroo and Ulaanbulag deposits, because those deposits are situated in the same tectonic settings (Figs. 1, 2, 41).
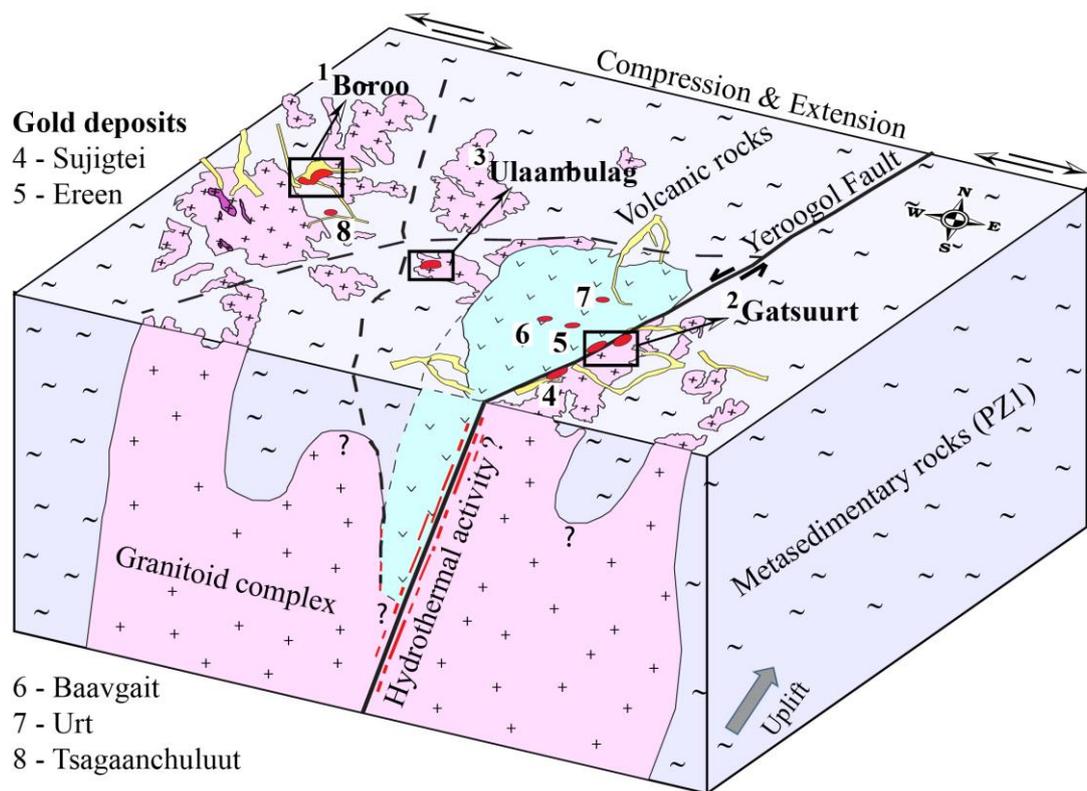


**Fig. 41** Genetic model of gold mineralization in the Gatsuurt, Boroo, Ulaanbulag and other gold deposits in the North Khentei gold belt.

# Chapter VII

## 7. CONCLUSIONS

The Boroo, Gatsuurt and Ulaanbulag deposits consist of the disseminated and stockwork ores and the vein type ores which includes the auriferous quartz vein ores, quartz vein ores, siliceous ores and silicified ores. The disseminated and stockwork mineralization in gold deposits consists of four stages, separately. The vein type mineralization consists of four and two, five, and four mineralization stages in the quartz vein ores and silicified ores for the Gatsuurt deposit, auriferous quartz vein ores for the Boroo deposit, and siliceous type ores for the Ulaanbulag deposit, respectively.

In the early stages of both types of gold mineralization, gold was deposited as "invisible gold" in pyrite and arsenopyrite. In the later stages, gold was deposited as (i) microscopic native gold within sulfides or at grain boundaries in the disseminated and stockwork ores; (ii) coarse-grained or visible native gold in matrix quartz in the vein type ores; and (iii) very narrow electrum veinlets within coarse-grained native gold in the vein ores.

In the Gatsuurt and Boroo deposits, both ore types contain coexisting $CO_2$-rich and aqueous fluid inclusions. The inclusions in quartz of the disseminated and stockwork ores homogenized at temperatures between 254–362ºC, whereas inclusions in the auriferous quartz vein ores of the Boroo homogenized at 237–305ºC. Fluid salinities in both ore types range from 3–6 wt% (NaCl equiv.).

Chemical compositions of arsenopyrite-II (29.5-31.0 As atom%; 0.885-0.930 atoms per 1.0S) in the Boroo deposit suggest crystallization temperatures between 365 and 300°C and sulfur fugacity of $10^{-7.5}$ to $10^{-10.1}$ atm, indicating that sulfur fugacity in the

hydrothermal ore fluids decreased critically with cooling. Consequently, sulfide contents are lower in the vein type ores than in the stockwork and disseminated type ores. These interpretation is also applicable to the Gatsuurt and Ulaanbulag deposits, because of comparable mineral assemblages and mineralization stages.

In the case of Khadat deposit, the copper mineralization occurs as vein type ores, and only chalcopyrite is recognized as copper-bearing sulfide. However, the metal zoning is defined from surface to deeper part of the deposit.

The U-Pb age of zircons from the Boroo host granites of 472.5 ± 6.9 Ma is much older than previously defined alteration minerals ages (ca. 210 Ma). U-Pb age of zircons in host granodiorite of the Khadat deposit presents 274.2 ± 1.7 Ma.

According to the paragenetic sequences in the Gatsuurt, Boroo and Ulaanbulag deposits, gold mineralization can be formed from the same source of the hydrothermal activity in this region. Thus, the gold deposits can be classified as contiguous orogenic type mineralization.

Similar features on the mineral assemblages and mineralization stages would hold for other deposits in the NKGB, and illustrate the general properties of gold mineralization in this belt.

The Khadat copper deposit could be expected to be one of the porphyry systems in this orogenic gold belt, in terms of geologic setting, mineral assemblages and high temperatures of ore mineral crystallization.

# Acknowledgements

# References

Alekseichik, S. N. (1943) Report of geological mapping at scale 1:200 000 Khentei area. Geological Information Center, Ulaanbaatar, Report No. 385 (in Russian).

Baasandolgor, L. (2003) Geologic and geochemical peculiarities of the Zuunmod ore district. M.Sc. Thesis, Mongolian Technical University, Ulaanbaatar, 1-101 (in Russian).

Badarch, G., Gunningham, W. D. and Windley, B. F. (2002) A new terrane subdivision for Mongolia: implications for the Phanerozoic crustal growth of Central Asia. J. Asian Earth Sci., 21, 87-110.

Bigot, L. and Jébrak, M. (2015) Gold mineralization at the syenite-hosted Beattie gold deposit, Duparquet, Neoarchean Abitibi belt, Canada. Econ. Geol., 110, 315-335.

Blanchard, M., Alfredsson, M., Brodholt, J., Wright, K. and Catlow, C. R. A. (2007) Arsenic incorporation into $FeS_2$ pyrite and its influence on dissolution: A DFT study. Geochim. Cosmochim. Acta, 71, 624-630.

Claoué-Long, J. C., Compston, W., Roberts, J., Fanning, C. M. (1995) Two Carboniferous ages: a comparison of SHRIMP zircon dating with conventional zircon ages and $^{40}Ar/^{39}Ar$ analysis. In: Berggren, W. A., Kent, D. V., Aubrey, M. P., Hardenbol, J. (eds.), Geochronology Time Scales and Global Stratigraphic Correlation: SEPM (Society for Sedimentary Geology). Special Publication, 54, 3–21.

Clark, L. A. (1960) The Fe-As-S system: phase relations and applications. Econ. Geol., 55, 1345-1381.

Cluer, J. K., Kotlyar, B., Gantsetseg, O., Togtokh, D., Wood, G. and Ullrich, T. (2005) Geology of the Boroo gold deposit, northern Mongolia. *In* Seltmann, R., Gerel, O.

and Kirwin, D. J. (eds.) Geodynamics and metallogeny of Mongolia with a special emphasis on copper and gold deposits. International Association on the Genesis of Ore Deposits, London, 105-117.

Dejidmaa, G. (1996) Gold metallogeny of Mongolia. Mongolian Geosci., 1, 6-29.

Dejidmaa, G. and Badarch, G. (1999) Summary of pre-accretionary and accretionary metallogenic belts of Mongolia. *In* Nokleberg, W. J., Naumova, V. V., Kuzmin, M. I. and Bounaeva, T. V. (eds.) Preliminary publications book 1 from project on mineral resources, metallogenesis, and tectonics of Northeast Asia: U.S. geological survey open-file report. U.S. Department of the Interior, U.S. Geological Survey, 99-165, CD-ROM. http://pubs.usgs.gov/of/1999/of99-165/.

Dril, S., Khanchuk, A. I., Obolenskiy, A. A., Ogasawara, M., Rodionov, S. M., Sotnikov, V. I., Spiridonov, A. M., Seminsky, Z. V., Prokopiev, A. V., Timofeev, V. F. and Nokleberg, W. J. (2010) Late Carboniferous through early Jurassic metallogenesis and tectonics of Northeast Asia. *In* Nokleberg, W. J. (ed.) Metallogenesis and Tectonics of Northeast Asia: U. S. Geological Survey Professional Paper 1765, chapter 7, 56 p. [http://pubs.usgs.gov/pp/1765/chapter_7/].

Fleet, M. E., Chryssoulis, S. L., MacLean, P. J., Davidson, R. and Weisener, C. G. (1993) Arsenian pyrite from gold deposits: Au and As distribution investigated by SIMS and EMP, and color staining surface oxidation by XPS and LIMS. Can. Mineral., 31, 1-17.

Gerel, O., Kotlyar, B., Cluer, J. K., Enkhtuvshin, K. and Bold-Erdene, B. (1999) Geology and gold mineralization in the Khentei range. Mongolian Geosci., 14, 110-115.

Goldfarb, R. J., Taylor, R. D., Collins, G. S., Goryachev, N. A. and Orlandini, O. F. (2013) Phanerozoic continental growth and gold metallogeny of Asia. Gondwana Res., 25, 48-102.

Gordienko, I. V., Medvedev, A. Ya., Gornova, M. A., Tomurtogoo, O. and Goneger, T. A. (2012) The Haraa Gol terrane in the western Hentiyn Mountains (northern Mongolia): Geochemistry, geochronology, and geodynamics. Russian Geology and Geophysics, 53, 281-292.

Groves, D. I., Goldfarb, R. J., Gebre-Mariam, M., Hagemann, S. G. and Robert, F. (1998) Orogenic gold deposits: A proposed classification in the context of their crustal distribution and relationship to other gold deposit types. Ore Geology Reviews, 13, 7-27.

Hara, H., Kurihara, T., Tsukada, K., Kon, Y., Uchino, T., Suzuki, T., Takeuchi, M., Nakane, Y., Nuramkhaan, M. and Chuluun, M. (2013) Provenance and origins of a late Paleozoic accretionary complex within the Khangai-Khentei belt in the Central Asian Orogenic Belt, central Mongolia. Journal of Asian Earth Sciences, 75, 141-157.

Hem, S. R. and Makovicky, E. (2004) The system Fe-Co-Ni-As-S. I. Phase relations in the $(Fe,Co,Ni)As_{0.5}S_{1.5}$ section at 650º and 500ºC. Can. Mineral., 42, 43-62.

Hendry, J. W., Roscoe, W. E. and Ross, D. A. (2006) Technical report on the Gatsuurt gold project, Northern Mongolia, prepared for Centerra Gold Inc. Roscoe Postle Associates Inc., Toronto, 6-1 to 9-1.

Hou, W., Nie, F., Jiang, S., Bai, D., Liu, Y., Yun, F. and Liu, Y. (2010) SHRIMP zircon U-Pb dating of ore-bearing granite in the Boroo large-size gold deposit, Mongolian

and its geological significance. Acta Geosci. Sin., 31, 331-342 (in Chinese with English abstract).

Kampe, A. and Gottesmann, V. (1966) Report on Results of 1:50 000 Scale Geological Mapping and General Prospecting Carried out in South-western Khentei Gold-bearing District. Geological Information Center, Ulaanbaatar, Report No. 1836 (in Russian).

Khanchuk, A. J. (eds.) (2006) Geodynamics, Magmatism and Metallogeny of the Russian East, 1. Dalnauka, Vladivostok, 572 (in Russian).

Khishgee, C., Akasaka, M., Ohira, H. and Sereenen, J. (2014) Gold mineralization of the Gatsuurt deposit in the North Khentei gold belt, central northern Mongolia. Resource Geol., 64, 1-16.

Khishgee, C. and Akasaka, M. (2015) Mineralogy of the Boroo deposit in the North Khentei gold belt, central northern Mongolia. Resource Geol., (in press).

Kolokol'nikov, V. V. (1933) Report on results of bedrock gold exploration in Yeroo, Sujigtei, Khargana deposits. Geological Information Center, Ulaanbaatar, Report No. 0038 (in Russian).

Kotlyar, B., Gantsetseg, O., Tungalag, F. and Burentugs, J. (1999) Location and variations in mesothermal Au mineralization in the North Khentei gold trend. Mongolian Geosci., 14, 107-110.

Kotlyar, B., Drown, T., Tungalag, F. and Gantsetseg, O. (1998) Two types of mineralization in the North Khentei gold trend. Mongolian Geosci., 11, 10-13.

Kretschmar, U. and Scott, S. D. (1976) Phase relations involving arsenopyrite in the system Fe-As-S and their application. Can. Mineral., 14, 364-386.

Ludwig, K. R. (2003) User's Manual for Isoplot 3.00. Berkeley Geochronology Center, Berkeley, CA.

McCuaig, T. C. and Kerrich, R. (1998) P-T-t-deformation-fluid characteristics of lode gold deposits: evidence from alteration systematics. Ore Geol. Rev., 12, 381-453.

Mikucki, E. J. (1998) Hydrothermal transport and depositional processes in Archean lode-gold systems: A review. Ore Geol. Rev., 13, 307-321.

Morey, A. A., Tomkins, A. G., Bierlein, F. P., Weinberg, R. F. and Davidson, G. J. (2008) Bimodal distribution of gold in pyrite and arsenopyrite: Examples from the Archean Boorara and Bardoc shear systems, Yilgarn Carton, Western Australia. Econ. Geol., 103, 599-614.

Mumin, A. H., Fleet, M. E. and Chryssoulis, S. L. (1994) Gold mineralization in As-rich mesothermal gold ores of the Bogosu-Prestea mining district of the Ashanti Gold Belt, Ghana: remobilization of "invisible" gold. Miner. Deposita, 29, 445-460.

Nyamsuren, L. and Altan-Erdene, L. (1991) Report of 1:50 000 scale geological mapping and general prospecting. Geological Information Center, Ulaanbaatar, Report No. 4578 (in Mongolian).

Paces, J. B., Miller, J. D. (1993) Precise U–Pb ages of Duluth Complex and related mafic intrusions, northeastern Minnesota: geochronological insights to physical, petrogenetic, paleomagnetic, and tectonomagmatic processes associated with the 1.1 Ga midcontinent rift system. Journal of Geophysical Research, 98, 13997–14013.

Raponi, T. R. and Redmond, D. (2009) Technical report on the Boroo gold mine Mongolia, prepared for Centerra Gold Inc., Toronto, 1-121.

Reich, M., Kesler, S. E., Utsunomiya, S., Palenik, C. S., Chryssoulis, S. L. and Ewing, R. C. (2005) Solubility of gold in arsenian pyrite. Geochim. Cosmochim. Acta, 69, 2781-2796.

Roedder, E. (1984) Fluid Inclusions. Reviews in Mineralogy, 12, 644. Mineralogical Society of America, Washington, DC.

Sengör, A. M. C. and Natal'in, B. A. (1996) Paleotectonics of Asia: fragments of a synthesis. In: Yin, A., Harrison, M. (eds.) The tectonic evolution of Asia. Cambridge University Press, Cambridge, 486-640.

Sharp, Z. D., Essene, E. J. and Kelly, W. C. (1985) A re-examination of the arsenopyrite geothermometer: Pressure considerations and applications to natural assemblages. Can. Mineral., 23, 517-534.

Sillitoe, R. H. (2010) Porphyry Copper Systems. Econ. Geol., 105, 3-41.

Stacy, J. S., Kramers, J. D. (1975) Approximation of terrestrial lead isotope evolution by a two-stage model. Earth and Planetary Science Letters, 26, 207–221.

Tumur, S., Lkhagvasuren, J. and Gerelmaa, N. (1995) Report of 1:50000 scale geological mapping and general prospecting carried out in the Noyon Uul Area of the Boroo and Zuunmod District. Geological Information Center, Ulaanbaatar, Report No. 4859 (in Mongolian).

Zachariáš, J., Frýda, J., Paterová, B. and Mihaljevič, M. (2004) Arsenopyrite and As-bearing pyrite from Roudný deposit, Bohemian Massif. Mineralogical Magazine, 68, 31-46.

Zorin, Y. A., Zorina, L. D., Spiridonov, A. M. and Rutshtein, I. G. (2001) Geodynamic setting of gold deposits in eastern and central Trans-Baikal (Chita Region, Russia). Ore Geol. Rev., 17, 215-232.

Zorin, Y. A. (1999) Geodynamics of the western part of the Mongolia–Okhotsk collisional belt, Trans-Baikal region (Russsia) and Mongolia. Tectonophysics, 306, 33–56.

**Table 2** Representative electron microprobe analyses of selected ore minerals from the disseminated and stockwork ores in the Gatsuurt deposit.

| Mineral Element | Au | Py-I | Py-II | Apy-I | Apy-II | Gn | Td | Sp | Ccp | Jm | Brn | Boul | Oxide | Sch |
|---|---|---|---|---|---|---|---|---|---|---|---|---|---|---|
| Au (wt%) | 97.97 | n.d | 0.99 | 0.01 | 0.74 | n.d | n.d | n.d | 0.19 | n.d | n.d | n.d | FeO | 0.05 |
| Ag | 1.09 | n.d | 0.04 | n.d | 0.01 | 0.24 | 1.02 | n.d | 0.03 | 0.09 | n.d | n.d | MnO | 0.06 |
| Cu | n.d | 0.03 | 0.05 | 0.01 | 0.04 | 0.35 | 36.81 | 0.13 | 35.21 | 0.08 | 13.72 | 0.07 | CaO | 20.08 |
| Pb | n.d | n.d | 0.25 | 0.06 | 0.03 | 84.12 | n.d | 0.27 | 0.08 | 43.67 | 42.98 | 54.24 | WO$_3$ | 80.00 |
| Zn | n.d | 0.02 | n.d | 0.03 | n.d | n.d | 5.25 | 61.30 | 0.02 | n.d | n.d | n.d | SO$_3$ | 0.10 |
| Fe | n.d | 47.20 | 46.57 | 36.24 | 36.52 | 1.24 | 3.92 | 4.71 | 30.86 | 1.83 | 0.01 | 0.10 | Total | 100.29 |
| Bi | n.d | n.d | n.d | n.d | n.d | n.d | 0.04 | 0.03 | 0.05 | n.d | n.d | 0.32 | | |
| Mn | n.d | n.d | n.d | n.d | n.d | n.d | 0.04 | 0.03 | n.d | n.d | n.d | 0.01 | | |
| As | n.d | n.d | 0.55 | 39.65 | 38.94 | 0.01 | 3.03 | n.d | 0.23 | 0.49 | 0.50 | 1.05 | | |
| Sb | n.d | n.d | 0.03 | n.d | 0.11 | 0.02 | 24.54 | 0.14 | n.d | 31.96 | 22.82 | 25.54 | | |
| Te | n.d | 0.03 | n.d | n.d | n.d | n.d | 0.25 | n.d | 0.04 | n.d | n.d | n.d | | |
| Co | n.d | 0.05 | 0.06 | 0.05 | n.d | n.d | 0.01 | n.d | 0.01 | 0.04 | n.d | 0.02 | | |
| S | n.d | 52.69 | 51.16 | 24.30 | 22.70 | 13.28 | 25.67 | 32.77 | 34.06 | 21.94 | 19.92 | 18.63 | | |
| Total | 99.06 | 100.02 | 99.70 | 100.35 | 99.09 | 99.26 | 100.58 | 99.38 | 100.78 | 100.10 | 99.95 | 99.98 | | |
| | | S=2 | S=2 | S=1 | S=1 | S=1 | S=13 | S=1 | S=2 | S=14 | S=3 | S=11 | O=4 | |
| Au | 0.98 | - | 0.01 | - | 0.01 | - | - | - | - | - | - | - | Ca | 1.02 |
| Ag | 0.02 | - | - | - | - | 0.01 | 0.15 | - | - | 0.02 | - | - | W | 0.99 |
| Cu | - | - | - | - | - | 0.01 | 9.41 | - | 1.04 | 0.03 | 1.04 | 0.02 | Total | 2.01 |
| Pb | - | - | - | - | - | 0.98 | - | - | - | 4.31 | 1.00 | 4.96 | | |
| Zn | - | - | - | - | - | - | 1.30 | 0.92 | - | - | - | - | | |
| Fe | - | 1.03 | 1.05 | 0.86 | 0.92 | 0.05 | 1.14 | 0.08 | 1.04 | 0.67 | - | 0.03 | | |
| Bi | - | - | - | - | - | - | - | - | - | - | - | 0.03 | | |
| Mn | - | - | - | - | - | - | 0.01 | - | - | - | - | - | | |
| As | - | - | 0.01 | 0.70 | 0.73 | - | 0.66 | - | 0.01 | 0.13 | 0.03 | 0.27 | | |
| Sb | - | - | - | - | - | - | 3.27 | - | - | 5.37 | 0.91 | 3.97 | | |
| Te | - | - | - | - | - | - | 0.03 | - | - | - | - | - | | |
| Co | - | - | - | - | - | - | - | - | - | 0.01 | - | 0.01 | | |
| Total | 1.00 | 3.03 | 3.07 | 2.56 | 2.67 | 2.05 | 28.99 | 2.01 | 4.09 | 24.55 | 5.98 | 20.29 | | |

Au, native gold; Py-I, pyrite-I; Py-II, pyrite-II; Apy-I, arsenopyrite-I; Apy-II, arsenopyrite-II; Gn, galena; Td, tetrahedrite; Sp, sphalerite; Ccp, chalcopyrite; Jm, jamesonite; Brn, bournonite; Boul, boulangerite; Sch, scheelite; n.d, not detected.

**Table 3** Representative electron microprobe analyses of selected ore minerals from the

quartz vein ores in the Gatsuurt deposit.

| Mineral Element | Au | Py-I | Py-II | Apy | Gn | Td | Tn | Sp | Ccp | Brn | Gc | Gr |
|---|---|---|---|---|---|---|---|---|---|---|---|---|
| Au (wt%) | 92.73 | n.d | 0.02 | 0.02 | n.d | 0.33 | 0.23 | n.d | 0.11 | n.d | n.d | 0.06 |
| Ag | 7.45 | n.d | 0.02 | n.d | 0.14 | 6.34 | 11.39 | n.d | n.d | n.d | n.d | 0.07 |
| Cu | n.d | 0.02 | n.d | 0.01 | 0.35 | 32.37 | 32.62 | 0.50 | 35.05 | 13.43 | 0.02 | 75.98 |
| Pb | n.d | n.d | 0.33 | n.d | 85.57 | 0.15 | 0.14 | 0.20 | 0.14 | 41.27 | 68.62 | 0.26 |
| Zn | n.d | 0.06 | n.d | n.d | 0.02 | 4.00 | 7.50 | 63.98 | 0.22 | 0.04 | 0.04 | 0.05 |
| Fe | n.d | 46.24 | 45.14 | 36.12 | 0.02 | 3.38 | 2.55 | 2.20 | 29.30 | n.d | n.d | n.d |
| Bi | n.d | 0.01 | n.d | n.d | 0.63 | 0.08 | n.d | 0.28 | 0.24 | 0.11 | 0.05 | 0.28 |
| Mn | n.d | 0.02 | 0.04 | n.d | 0.05 | 0.04 | n.d | 0.01 | 0.03 | n.d | n.d | n.d |
| As | n.d | n.d | 0.94 | 39.85 | n.d | 0.75 | 11.01 | n.d | n.d | 0.33 | 1.92 | n.d |
| Sb | n.d | n.d | n.d | n.d | n.d | 28.10 | 8.55 | n.d | 0.02 | 24.19 | 12.42 | n.d |
| Te | n.d | n.d | n.d | n.d | 0.02 | n.d | n.d | n.d | n.d | n.d | n.d | n.d |
| Co | n.d | n.d | n.d | n.d | n.d | n.d | n.d | n.d | n.d | 0.01 | n.d | n.d |
| Cd | n.d | n.d | n.d | n.d | n.d | n.d | n.d | n.d | n.d | 0.21 | n.d | 0.01 |
| W | n.d | n.d | n.d | 0.03 | n.d | n.d | n.d | n.d | n.d | n.d | n.d | n.d |
| S | n.d | 53.04 | 52.69 | 23.69 | 13.44 | 24.86 | 26.21 | 33.42 | 34.86 | 20.17 | 17.27 | 23.57 |
| Total | 100.18 | 99.39 | 99.18 | 99.72 | 100.24 | 100.40 | 100.20 | 100.58 | 99.97 | 99.76 | 100.34 | 100.27 |
|  |  | S=2 | S=2 | S=1 | S=1 | S=13 | S=13 | S=1 | S=2 | S=3 | S=23 | S=5 |
| Au | 0.93 | - | - | - | - | 0.03 | 0.02 | - | - | - | - | - |
| Ag | 0.07 | - | - | - | - | 0.99 | 1.68 | - | - | - | - | - |
| Cu | - | - | - | - | 0.01 | 8.54 | 8.16 | 0.01 | 1.01 | 1.01 | 0.01 | 8.13 |
| Pb | - | - | - | - | 0.99 | 0.01 | 0.01 | - | - | 0.95 | 14.15 | 0.01 |
| Zn | - | - | - | - | - | 1.03 | 1.82 | 0.94 | 0.01 | - | 0.03 | 0.01 |
| Fe | - | - | - | 0.88 | - | 1.01 | 0.73 | 0.04 | 0.97 | - | - | - |
| Bi | - | - | - | - | 0.01 | 0.01 | - | - | - | - | 0.01 | 0.01 |
| Mn | - | - | - | - | - | 0.01 | - | - | - | - | - | - |
| As | - | - | - | 0.72 | - | 0.17 | 2.34 | - | - | 0.02 | 1.09 | - |
| Sb | - | - | - | - | - | 3.87 | 1.12 | - | - | 0.95 | 4.36 | - |
| Cd | - | - | - | - | - | - | - | - | - | 0.01 | - | - |
| Total | 1.00 | | | 2.60 | 2.01 | 28.67 | 28.88 | 1.99 | 3.99 | 5.94 | 42.65 | 13.16 |

Au, native gold; Py-I, pyrite-I; Py-II, pyrite-II; Apy, arsenopyrite;  Gn, galena; Td, tetrahedrite; Tn, tennantite; Sp, sphalerite; Ccp, chalcopyrite; Brn, bournonite; Gc, geocronite; Gr, geerite; n.d, not detected.

**Table 4** Representative electron microprobe analyses of selected ore minerals from the silicified ores in the Gatsuurt deposit.

| Mineral Element | Au | Py | Apy | Sp | Gn |
|---|---|---|---|---|---|
| Au (wt%) | 90.88 | 0.19 | 0.11 | n.d | n.d |
| Ag | 8.78 | 0.06 | 0.01 | n.d | 0.04 |
| Cu | n.d | 0.04 | n.d | n.d | 0.04 |
| Pb | n.d | 0.22 | 0.17 | 0.01 | 85.99 |
| Zn | n.d | 0.02 | 0.05 | 64.38 | n.d |
| Fe | n.d | 47.17 | 36.93 | 1.41 | 0.71 |
| Bi | n.d | n.d | n.d | 0.37 | n.d |
| Mn | n.d | n.d | 0.02 | n.d | n.d |
| As | n.d | 1.34 | 40.10 | n.d | n.d |
| Sb | n.d | n.d | n.d | n.d | n.d |
| Te | n.d | n.d | n.d | n.d | 0.02 |
| Co | n.d | 0.03 | 0.07 | n.d | n.d |
| Cd | n.d | n.d | n.d | 0.09 | n.d |
| W | n.d | n.d | 0.10 | 0.13 | n.d |
| S | n.d | 50.89 | 22.91 | 33.55 | 12.78 |
| Total | 99.66 | 99.96 | 100.47 | 99.94 | 99.58 |
| | | S=2 | S=1 | S=1 | S=1 |
| Au | 0.91 | - | - | - | - |
| Ag | 0.09 | - | - | - | - |
| Pb | - | - | - | - | 1.04 |
| Zn | - | - | - | 0.94 | - |
| Fe | - | 1.06 | 0.93 | 0.02 | 0.03 |
| As | - | 0.02 | 0.75 | - | - |
| Total | 1.00 | 3.09 | 2.68 | 1.97 | 2.08 |

Au, native gold; Py, pyrite; Apy, arsenopyrite; Gn, galena; Sp, sphalerite; n.d, not detected.

**Table 5** Representative electron microprobe analyses of selected ore minerals from the disseminated and stockwork ores in the Boroo deposit.

| | Native gold | Native gold | Py-I | Py-II | Apy-I | Apy-II | Gn | Sp | Ccp | Td | Brn | Boul | Alc |
|---|---|---|---|---|---|---|---|---|---|---|---|---|---|
| Au | 85.22 | 92.82 | 0.06 | 0.19 | 0.14 | 0.22 | n.d. | n.d. | n.d. | n.d. | n.d. | n.d. | 0.04 |
| Ag | 13.47 | 7.77 | n.d. | n.d. | n.d. | n.d. | 0.07 | n.d. | 0.04 | 0.78 | n.d. | n.d. | n.d. |
| Cu | n.d. | n.d. | n.d. | 0.01 | 0.03 | n.d. | n.d. | n.d. | 33.93 | 37.42 | 12.79 | 0.02 | n.d. |
| Pb | n.d. | n.d. | 0.22 | 0.27 | 0.07 | n.d. | 86.15 | 0.12 | 0.10 | n.d. | 41.00 | 54.23 | 0.02 |
| Zn | n.d. | n.d. | n.d. | n.d. | n.d. | n.d. | 0.06 | 65.08 | 0.23 | 7.02 | 0.07 | n.d. | n.d. |
| Fe | n.d. | n.d. | 46.69 | 44.33 | 35.33 | 34.34 | 0.06 | 0.78 | 28.47 | 0.56 | n.d. | n.d. | 3.68 |
| Bi | n.d. | n.d. | 0.10 | 0.07 | n.d. | 0.02 | 0.55 | 0.27 | 0.19 | 0.21 | 0.48 | 0.45 | 0.26 |
| Mn | n.d. | n.d. | n.d. | n.d. | n.d. | n.d. | n.d. | 0.02 | n.d. | n.d. | n.d. | n.d. | 0.04 |
| As | n.d. | n.d. | n.d. | 1.29 | 39.61 | 42.35 | n.d. | n.d. | n.d. | 1.52 | n.d. | n.d. | 44.91 |
| Sb | n.d. | n.d. | n.d. | 0.23 | n.d. | 0.02 | n.d. | n.d. | 0.08 | 27.86 | 25.72 | 25.50 | 0.56 |
| Te | 0.15 | 0.08 | n.d. | n.d. | n.d. | n.d. | 0.05 | n.d. | n.d. | n.d. | n.d. | n.d. | 0.65 |
| Co | n.d. | n.d. | 0.06 | 0.03 | 0.05 | 0.09 | n.d. | n.d. | n.d. | n.d. | n.d. | n.d. | 21.81 |
| Cd | 0.22 | 0.28 | n.d. | 0.02 | n.d. | n.d. | 0.07 | 0.07 | n.d. | 0.05 | n.d. | 0.24 | n.d. |
| Ni | n.d. | n.d. | n.d. | n.d. | n.d. | 0.27 | n.d. | n.d. | n.d. | n.d. | n.d. | n.d. | 9.70 |
| W | n.d. | n.d. | n.d. | n.d. | n.d. | n.d. | n.d. | 0.19 | n.d. | n.d. | n.d. | n.d. | n.d. |
| S | n.d. | n.d. | 53.84 | 52.31 | 23.80 | 22.45 | 13.92 | 33.65 | 35.06 | 25.66 | 19.97 | 19.05 | 19.50 |
| Total | 99.06 | 100.95 | 100.97 | 98.75 | 99.03 | 99.76 | 100.93 | 100.18 | 98.10 | 101.08 | 100.03 | 99.49 | 101.17 |
| Atoms per formula unit | | | S = 2 | S = 2 | S = 1 | S = 1 | S = 1 | S = 1 | S = 2 | S = 13 | S = 3 | S = 11 | S = 1 |
| Au | 0.77 | 0.86 | — | — | — | — | — | — | — | — | — | — | — |
| Ag | 0.22 | 0.13 | — | — | — | — | — | — | — | 0.12 | — | — | — |
| Cu | — | — | — | — | — | — | — | — | 0.98 | 9.57 | 0.97 | 0.01 | — |
| Pb | — | — | — | — | — | — | 0.96 | — | — | — | 0.95 | 4.85 | — |
| Zn | — | — | — | — | — | — | — | 0.95 | 0.01 | 1.74 | 0.01 | — | — |
| Fe | — | — | 1.00 | 0.97 | 0.85 | 0.88 | — | 0.01 | 0.93 | 0.16 | — | — | 0.11 |
| Bi | — | — | — | — | — | — | 0.01 | — | — | 0.02 | 0.01 | 0.04 | — |
| As | — | — | — | 0.02 | 0.71 | 0.81 | — | — | — | 0.33 | — | — | 0.99 |
| Sb | — | — | — | — | — | — | — | — | — | 3.72 | 1.02 | 3.88 | 0.01 |
| Te | — | — | — | — | — | — | — | — | — | — | — | — | 0.01 |
| Co | — | — | — | — | — | — | — | — | — | — | — | — | 0.61 |
| Cd | 0.01 | 0.01 | — | — | — | — | — | — | — | 0.01 | — | 0.04 | — |
| Ni | — | — | — | — | — | 0.01 | — | — | — | — | — | — | 0.27 |
| Total | 1.00 | 1.00 | 1.00 | 0.99 | 1.56 | 1.70 | 0.97 | 0.96 | 1.92 | 15.67 | 2.96 | 8.82 | 2.00 |

Py-I, early generation pyrite; Py-II, later generation pyrite; Apy-I, early generation arsenopyrite; Apy-II, later generation arsenopyrite; Gn, galena; Sp, sphalerite; Ccp, chalcopyrite; Td, tetrahedrite; Brn, bournonite; Boul, boulangerite; Alc, alloclasite; n.d., not detected; '—' nil.

**Table 6** Representative electron microprobe analyses of selected ore minerals from the auriferous quartz vein ores in the Boroo deposit.

| | Native gold | Native gold | Electrum | Py-I | Py-II | Apy | Gn | Sp | Ccp | Td | Tn | Brn | Gr |
|---|---|---|---|---|---|---|---|---|---|---|---|---|---|
| Au | 96.56 | 93.29 | 75.21 | 0.08 | 0.15 | 0.20 | n.d. | n.d. | n.d. | n.d. | n.d. | n.d. | n.d. |
| Ag | 4.88 | 7.68 | 23.24 | n.d. | n.d. | 0.01 | 0.12 | n.d. | 0.07 | 5.29 | 6.94 | n.d. | 0.09 |
| Cu | n.d. | n.d. | 0.02 | n.d. | 0.04 | 0.14 | 0.04 | 0.13 | 34.77 | 33.96 | 35.68 | 13.18 | 75.54 |
| Pb | n.d. | n.d. | n.d. | 0.27 | 0.01 | n.d. | 85.91 | 0.22 | 0.20 | n.d. | 0.22 | 41.98 | n.d. |
| Zn | n.d. | n.d. | 0.07 | n.d. | n.d. | n.d. | n.d. | 64.62 | 0.01 | 4.54 | 3.56 | n.d. | 0.11 |
| Fe | n.d. | n.d. | n.d. | 44.81 | 44.45 | 35.27 | 0.03 | 0.69 | 29.09 | 2.81 | 5.18 | n.d. | 1.39 |
| Bi | n.d. | n.d. | n.d. | 0.11 | 0.13 | n.d. | 0.34 | 0.14 | 0.35 | 0.13 | n.d. | 0.38 | 0.01 |
| Mn | n.d. | n.d. | n.d. | n.d. | n.d. | 0.01 | n.d. | n.d. | n.d. | 0.02 | n.d. | n.d. | n.d. |
| As | n.d. | n.d. | n.d. | n.d. | 2.79 | 41.81 | n.d. | 0.02 | n.d. | 4.01 | 14.83 | 0.24 | 0.15 |
| Sb | n.d. | n.d. | n.d. | n.d. | n.d. | 0.01 | n.d. | n.d. | 0.08 | 22.03 | 5.83 | 24.81 | n.d. |
| Te | 0.01 | 0.05 | 0.35 | n.d. | n.d. | n.d. | 0.03 | n.d. | n.d. | n.d. | n.d. | n.d. | n.d. |
| Co | n.d. | n.d. | n.d. | 0.06 | 0.07 | 0.06 | 0.01 | n.d. | n.d. | 0.02 | 0.01 | n.d. | n.d. |
| Cd | 0.06 | 0.61 | n.d. | n.d. | n.d. | n.d. | 0.10 | 0.01 | n.d. | n.d. | n.d. | 0.17 | n.d. |
| Ni | n.d. | n.d. | n.d. | n.d. | 0.01 | 0.11 | 0.02 | n.d. | n.d. | n.d. | n.d. | n.d. | n.d. |
| W | n.d. | n.d. | 0.19 | n.d. | n.d. | n.d. | n.d. | n.d. | n.d. | n.d. | n.d. | n.d. | n.d. |
| S | n.d. | n.d. | n.d. | 54.88 | 51.70 | 22.70 | 14.11 | 33.39 | 34.36 | 25.77 | 27.19 | 20.20 | 22.24 |
| Total | 101.51 | 101.63 | 99.08 | 100.21 | 99.35 | 100.32 | 100.71 | 99.22 | 98.93 | 98.58 | 99.44 | 100.96 | 99.53 |
| Atoms per formula unit | | | | S = 2 | S = 2 | S = 1 | S = 1 | S = 1 | S = 2 | S = 13 | S = 13 | S = 3 | S = 5 |
| Au | 0.92 | 0.86 | 0.63 | — | — | — | — | — | — | — | — | — | — |
| Ag | 0.08 | 0.13 | 0.36 | — | — | — | — | — | — | 0.79 | 0.99 | — | 0.01 |
| Cu | — | — | — | — | — | — | — | — | 1.02 | 8.64 | 8.61 | 0.99 | 8.57 |
| Pb | — | — | — | — | — | — | 0.94 | — | — | — | 0.02 | 0.96 | — |
| Zn | — | — | — | — | — | — | — | 0.95 | — | 1.12 | 0.83 | — | 0.01 |
| Fe | — | — | — | 0.94 | 0.99 | 0.89 | — | 0.01 | 0.97 | 0.81 | 1.42 | — | 0.18 |
| As | — | — | — | — | 0.04 | 0.79 | — | — | — | 0.86 | 3.04 | 0.02 | 0.01 |
| Sb | — | — | — | — | — | — | — | — | — | 2.93 | 0.73 | 0.97 | — |
| Te | — | — | 0.01 | — | — | — | — | — | — | — | — | — | — |
| Cd | — | 0.01 | — | — | — | — | — | — | — | — | — | 0.01 | — |
| Total | 1.00 | 1.00 | 1.00 | 0.94 | 1.03 | 1.68 | 0.94 | 0.96 | 1.99 | 15.15 | 15.64 | 2.95 | 8.78 |

Py-I, early generation pyrite; Py-II, later generation pyrite; Apy, arsenopyrite; Gn, galena; Sp, sphalerite; Ccp, chalcopyrite; Td, tetrahedrite; Tn, tennantite; Brn, bournonite; Gr, geerite; n.d., not detected, '—', nil.